National Institute of Electricity and Electronics
INELEC BOUMERDES
Department of Resarch

THESIS

Presented in partial fulfilment of the requirements of the

DEGREE OF MAGISTER

in Electronic Systems Engineering

by

Abderrahmane OUADI

Hybrid-mode Analysis of Microwave and Millimeter-wave Structures of Realistic Configuration

Defended on June 27, 1995 before the Jury :

President :	Dr. **A. FAREH** (Maitre de Conference -ENP)
Supervisor :	Dr. **H. BOURDOUCEN** (Maitre de Conference-INELEC)
Members :	Dr. **A. BENSEBTI** (Chargé de Cours-U.BLIDA)
	Dr. **M. DJEDDI** (Maitre de Conference-INELEC)
	Dr. **R. AKSAS** (Chargé de Cours-ENP)

Registration number : 03/95.

ACKNOWLEDGEMENTS

My sincere thanks go to my supervisor Dr. H. Bourdoucen, Maitre de Conference, at INELEC for his technical and tireless support, fruitful discussions, stimulating criticisms and helpful suggestions.

My supervisor and I feel very indebted to Prof. Dr. R. Pregla, FernUniverität Gesamthochschule Allgemeine und Theoretische Elektrotechnik , Prof. Dr. N. G. Alexópoulos, Department of Electrical Egineering, University of California, Los Angeles and Prof. Dr. J. Citerne, INSA Rennes, France, for providing us with scientific material on which this research work is based.

I am also grateful for the many helpful criticism and suggestions provided by the members of the jury composed by Dr. A. Fareh MC , Maitre de conference at Ecole National Polytechnique, Dr. A. Bensebti, Chargé de cours, at Université de Blida, Dr. M. Djeddi, Maitre de Conference, at INELEC, and Dr. R. Aksas, Chargé de cours, at Ecole National Polytechnique. I wish also to thank them for their acceptance to evaluate this work.

I wish to acknowledge INELEC research department staff and particularly Dr. K. Harriche for providing support and environment in which one can develop its ideas. I am also grateful to all INELEC secretarial staffs and particularly for the Library and Reprography staffs.

I would like to extend thanks to all colleagues at INELEC and particularly to M. Affane, A. Zitouni, M. Dehmas, A. Bentarzi, H. Dahimane, R. Bouchetta, M. Azzougui, H. Zabot and M. Kassraoui for their meaningful comments and valuable suggestions.

I would also like to take this opportunity to thank all the teachers and persons who taught me before and during this post-graduation level.

Finally, this acknowledgement will not be complete if I do not extend the most sincere thanks to my familly for the patience they have shown throughout this work.

ACKNOWLEDGEMENTS

My sincere thanks go to my supervisor Dr. H. Bourdoucen, Maitre de Conference, at INELEC for his technical and tireless support, fruitful discussions, stimulating criticisms and helpful suggestions.

My supervisor and I feel very indebted to Prof. Dr. R. Pregla, FernUniverität Gesamthochschule Allgemeine und Theoretische Elektrotechnik , Prof. Dr. N. G. Alexópoulos, Department of Electrical Egineering, University of California, Los Angeles and Prof. Dr. J. Citerne, INSA Rennes, France, for providing us with scientific material on which this research work is based.

I am also grateful for the many helpful criticism and suggestions provided by the members of the jury composed by Dr. A. Fareh MC , Maitre de conference at Ecole National Polytechnique, Dr. A. Bensebti, Chargé de cours, at Université de Blida, Dr. M. Djeddi, Maitre de Conference, at INELEC, and Dr. R. Aksas, Chargé de cours, at Ecole National Polytechnique. I wish also to thank them for their acceptance to evaluate this work.

I wish to acknowledge INELEC research department staff and particularly Dr. K. Harriche for providing support and environment in which one can develop its ideas. I am also grateful to all INELEC secretarial staffs and particularly for the Library and Reprography staffs.

I would like to extend thanks to all colleagues at INELEC and particularly to M. Affane, A. Zitouni, M. Dehmas, A. Bentarzi, H. Dahimane, R. Bouchetta, M. Azzougui, H. Zabot and M. Kassraoui for their meaningful comments and valuable suggestions.

I would also like to take this opportunity to thank all the teachers and persons who taught me before and during this post-graduation level.

Finally, this acknowledgement will not be complete if I do not extend the most sincere thanks to my familly for the patience they have shown throughout this work.

ABSTRACT

In this research work, the rigorous hybrid-mode full-wave analysis is used for an accurate characterization of planar and quasi-planar microwave and millimeter-wave structures, required by the spectacular growth of microwave technology. The method of lines is used as a mathematical tool for solving the associated eigenvalue problems, for modelling the dispersive properties of the aforementioned structures. The frequency dependent characterization of general planar multilayer multiconductor waveguiding structures based on isotropic and/or anisotropic substrates, has been established by using directly field components or suitable Hertzian potential functions formulations. This technique has also been applied for the analysis of structures with finite metallization thickness, in order to improve the modelling of planar microwave circuit structures that are of reduced size and operating at higher frequencies. Furthermore, the E-plane planar circuits, particularly finline structures, have been investigated with practical considerations. In addition to the substrate anisotropy and finite metal thickness parameters, the sidewall grooves, used in an actual realization to support mechanically the substrate, has been accounted for an efficient analysis of this kind of structures. particular interest is directed to the analysis of isolated unilateral finline configurations which are suitable for mounting semiconductor devices, where one or both fins are isolated by a gasket which allows a dc voltage to be developed across the fins. The numerical results obtained by the developed algorithm are found to agree excellently with the published data for a wide range of planar microwave and millimeter-wave structures. The effect of the technological parameters such as substrate anisotropy, strip thickness, side-wall groove depth and insulating gasket height have been also discussed.

Table of contents

introduction

The evolution of microwave engeneering in the last three decades originates from the emergence of semiconductor devices operating at microwave frequencies. A new passive microwave structure media have been developed and adapted to these semiconductor devices in a printed circuit form working at higher frequencies, in analog way as printed circuits operating at the low frequency range. Present types of Microwave Integrated Circuits (MICs) have gradually evolved to fulfill the substantial demand for very compacted microwave systems and subsystems. In hybrid forms, almost all passive elements of MICs are developed on a single or multilayer dielctrics. The Monolithic Microwave Integrated Circuits (MMICs) approach is a further technological step involved for modern microwave system designs, offering enhanced scope for the miniaturization of microwave and millimeter wave equipements. In the monolithic approach, all active and passive circuit elements are fabricated on a semi-insulating Gallium Arsenide (GaAs) substrate by some deposition shceme such as epitaxy, ion implantation, sputtering, evaporation, diffusion, or a combination of these processes and others [1].

The availability of small size semiconductor devices made it necessary to look for the transmission media compatible with these devices. For a transmission line structure to be suitable as circuit element in MICs and MMICs , one of the principal requirements is that, the structure should be planar in configuaration [2]. Fig 1 shows various forms of transmission structures, which are assembled from planar conductors or conducting strips on insulating substrates, that are essential elements in microwave, millimeter-wave hybrid, and monolthic microwave integrated circuits. Metal strips are deposited by thin-film or thick-film technology on dielectric substrates, procuring mechanical stability.

These transmission line structures have distinct advantages such as light weight, small size, improved performance, better reliability and reproducibilty and low cost.

The microstrip line is by far the most popular one, although the interest for alternative configurations such as the coplanar waveguide is recently growing. Although the microstrip has been used also at millimeter wave frequencies, E-plane circuits seem to be more viable condidates in such a frequency range. These are printed circuits placed in E-plane of a rectangular waveguide. At very high frequencies the use of thinner substrates with low dielctric constant is also usefull to avoid problems of excessive miniaturization. Low dielectric constant materials and the presence of air gap, as in the suspended microstrip, is also recommended to reduce conductor loss [3].

introduction

The evolution of microwave engeneering in the last three decades originates from the emergence of semiconductor devices operating at microwave frequencies. A new passive microwave structure media have been developed and adapted to these semiconductor devices in a printed circuit form working at higher frequencies, in analog way as printed circuits operating at the low frequency range. Present types of Microwave Integrated Circuits (MICs) have gradually evolved to fulfill the substantial demand for very compacted microwave systems and subsystems. In hybrid forms, almost all passive elements of MICs are developed on a single or multilayer dielctrics. The Monolithic Microwave Integrated Circuits (MMICs) approach is a further technological step involved for modern microwave system designs, offering enhanced scope for the miniaturization of microwave and millimeter wave equipements. In the monolithic approach, all active and passive circuit elements are fabricated on a semi-insulating Gallium Arsenide (GaAs) substrate by some deposition shceme such as epitaxy, ion implantation, sputtering, evaporation, diffusion, or a combination of these processes and others [1].

The availability of small size semiconductor devices made it necessary to look for the transmission media compatible with these devices. For a transmission line structure to be suitable as circuit element in MICs and MMICs , one of the principal requirements is that, the structure should be planar in configuaration [2]. Fig 1 shows various forms of transmission structures, which are assembled from planar conductors or conducting strips on insulating substrates, that are essential elements in microwave, millimeter-wave hybrid, and monolthic microwave integrated circuits. Metal strips are deposited by thin-film or thick-film technology on dielectric substrates, procuring mechanical stability. These transmission line structures have distinct advantages such as light weight, small size, improved performance, better reliability and reproducibilty and low cost.

The microstrip line is by far the most popular one, although the interest for alternative configurations such as the coplanar waveguide is recently growing. Although the microstrip has been used also at millimeter wave frequencies, E-plane circuits seem to be more viable condidates in such a frequency range. These are printed circuits placed in E-plane of a rectangular waveguide. At very high frequencies the use of thinner substrates with low dielctric constant is also usefull to avoid problems of excessive miniaturization. Low dielectric constant materials and the presence of air gap, as in the suspended microstrip, is also recommended to reduce conductor loss [3]

introduction

The evolution of microwave engeneering in the last three decades originates from the emergence of semiconductor devices operating at microwave frequencies. A new passive microwave structure media have been developed and adapted to these semiconductor devices in a printed circuit form working at higher frequencies, in analog way as printed circuits operating at the low frequency range. Present types of Microwave Integrated Circuits (MICs) have gradually evolved to fulfill the substantial demand for very compacted microwave systems and subsystems. In hybrid forms, almost all passive elements of MICs are developed on a single or multilayer dielctrics. The Monolithic Microwave Integrated Circuits (MMICs) approach is a further technological step involved for modern microwave system designs, offering enhanced scope for the miniaturization of microwave and millimeter wave equipements. In the monolithic approach, all active and passive circuit elements are fabricated on a semi-insulating Gallium Arsenide (GaAs) substrate by some deposition shceme such as epitaxy, ion implantation, sputtering, evaporation, diffusion, or a combination of these processes and others [1].

The availability of small size semiconductor devices made it necessary to look for the transmission media compatible with these devices. For a transmission line structure to be suitable as circuit element in MICs and MMICs , one of the principal requirements is that, the structure should be planar in configuaration [2]. Fig 1 shows various forms of transmission structures, which are assembled from planar conductors or conducting strips on insulating substrates, that are essential elements in microwave, millimeter-wave hybrid, and monolthic microwave integrated circuits. Metal strips are deposited by thin-film or thick-film technology on dielectric substrates, procuring mechanical stability. These transmission line structures have distinct advantages such as light weight, small size, improved performance, better reliability and reproducibilty and low cost.

The microstrip line is by far the most popular one, although the interest for alternative configurations such as the coplanar waveguide is recently growing. Although the microstrip has been used also at millimeter wave frequencies, E-plane circuits seem to be more viable condidates in such a frequency range. These are printed circuits placed in E-plane of a rectangular waveguide. At very high frequencies the use of thinner substrates with low dielctric constant is also usefull to avoid problems of excessive miniaturization. Low dielectric constant materials and the presence of air gap, as in the suspended microstrip, is also recommended to reduce conductor loss [3].

introduction

The evolution of microwave engeneering in the last three decades originates from the emergence of semiconductor devices operating at microwave frequencies. A new passive microwave structure media have been developed and adapted to these semiconductor devices in a printed circuit form working at higher frequencies, in analog way as printed circuits operating at the low frequency range. Present types of Microwave Integrated Circuits (MICs) have gradually evolved to fulfill the substantial demand for very compacted microwave systems and subsystems. In hybrid forms, almost all passive elements of MICs are developed on a single or multilayer dielctrics. The Monolithic Microwave Integrated Circuits (MMICs) approach is a further technological step involved for modern microwave system designs, offering enhanced scope for the miniaturization of microwave and millimeter wave equipements. In the monolithic approach, all active and passive circuit elements are fabricated on a semi-insulating Gallium Arsenide (GaAs) substrate by some deposition shceme such as epitaxy, ion implantation, sputtering, evaporation, diffusion, or a combination of these processes and others [1].

The availability of small size semiconductor devices made it necessary to look for the transmission media compatible with these devices. For a transmission line structure to be suitable as circuit element in MICs and MMICs , one of the principal requirements is that, the structure should be planar in configuaration [2]. Fig 1 shows various forms of transmission structures, which are assembled from planar conductors or conducting strips on insulating substrates, that are essential elements in microwave, millimeter-wave hybrid, and monolthic microwave integrated circuits. Metal strips are deposited by thin-film or thick-film technology on dielectric substrates, procuring mechanical stability.

These transmission line structures have distinct advantages such as light weight, small size, improved performance, better reliability and reproducibilty and low cost.

The microstrip line is by far the most popular one, although the interest for alternative configurations such as the coplanar waveguide is recently growing. Although the microstrip has been used also at millimeter wave frequencies, E-plane circuits seem to be more viable condidates in such a frequency range. These are printed circuits placed in E-plane of a rectangular waveguide. At very high frequencies the use of thinner substrates with low dielctric constant is also usefull to avoid problems of excessive miniaturization. Low dielectric constant materials and the presence of air gap, as in the suspended microstrip, is also recommended to reduce conductor loss [3]

The recent advances in microwave technology involve the previous complicated circuit configurations and structures of small size when higher frequencies are used. This engenders a number of unwanted phenomena and the approximated electrical characteristics are no longer valid. A corroloary of this, is that for MMICs design, it is difficult or virtualy impossible to tune circuits after manifacture. Clearly, there is an urgent need for accurate numerical characterization of microwave circuits and components.

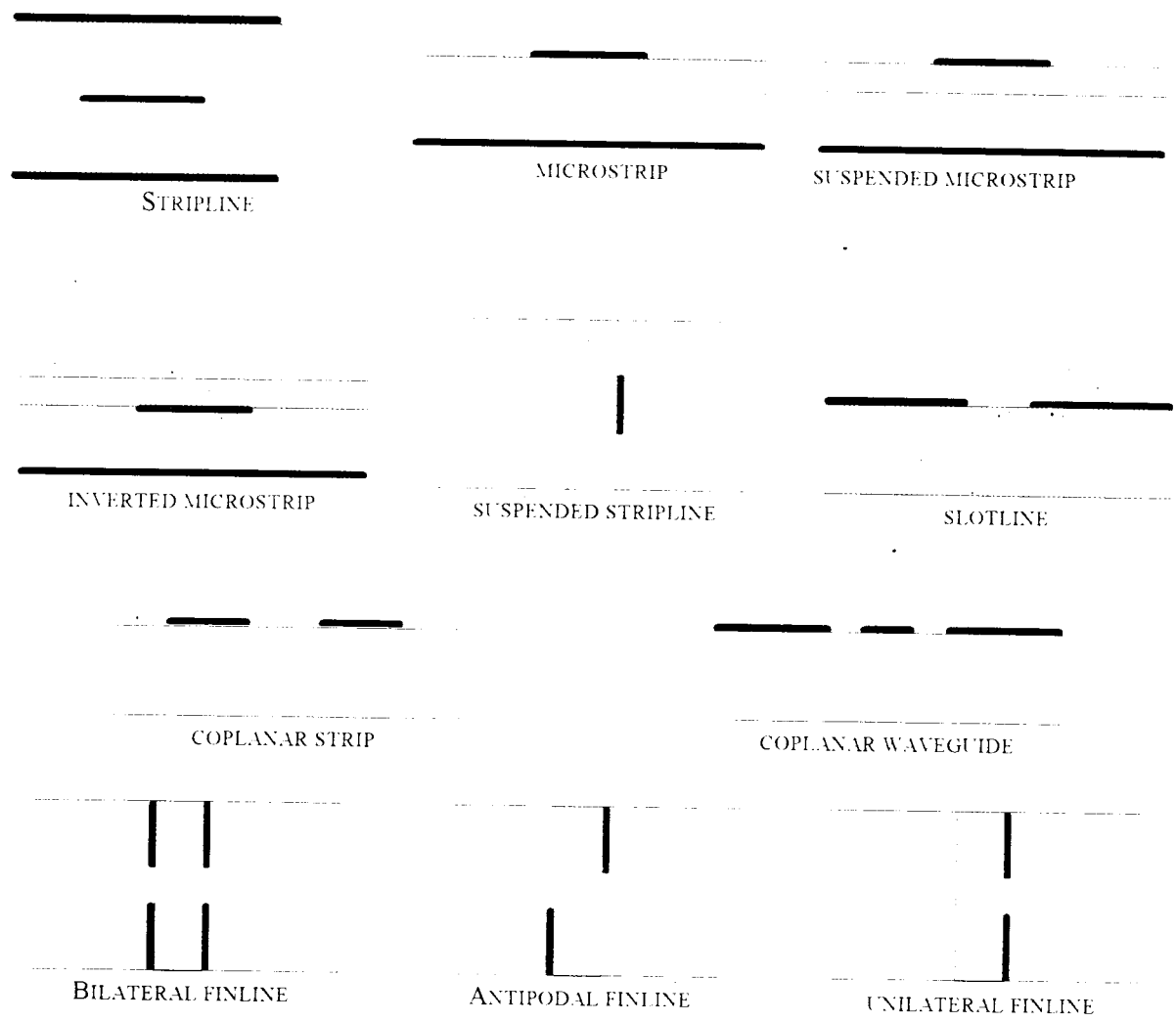

Fig. 1 Plannar transmission line structures

Two analytical approaches are principally used for an accurate characterization of transmission line structures, the quasi-static and the full-wave approaches.

The quasi-static approach is suitable for the analysis of structures supporting TEM or quasi-TEM wave mode. It is however, an approximate technique that cannot be expected

to give extremely accurate results in all practical cases, particularly in the higher frequency spectrum. According to reference [2], the microstrip transmission lines which are fully shielded and completely filled with dielectric material can propagate transverse electromagnetic, transverse electric, and transverse magnetic modes. Partially filled and fully shielded lines cannot support these modes because the boundary conditions at the interface between air and dielectric cannot be rigorously fulfilled. In addition, as it has been indicated in [2] that a hybrid mode can be found which satisfies all boundary conditions and which can be decomposed into sums of transverse electric and transverse magnetic space harmonics. It can be deduced that the hybrid mode, for planar structures supporting Quasi-TEM mode, propagates at all frequencies and it approaches the transverse electromagnetic mode at low frequencies or for sufficiently small line dimensions [2].

In order to achieve an accurate characterization of these planar transmission line structures at higher frequencies, the hybrid-mode full-wave analysis has to be adopted. Since it is inherently much more computationally expensive, it is very important to devise appropriate techniques apt to reduce or maintain at acceptable levels the computational effort. Microwave litterature provides a wide variety of numerical techniques capable of tackling the actual adressed eigenvalue problem. Among those mathematical methods provided in the litterature, the Method of Lines (MoL), which has been recently applied to the field of electromagnetic wave engineering by Pregla et al. [4] in 1980. Since then, its use with electromagnetic wave problems, continues incessantly, and it is being established as one of the powerful numerical methods for the analysis of planar microwave integrated circuits and optical structures. The most serious difficulty, as for other numerical techniques based on the discretization aspect, in using this technique for the analysis of structures having open boundaries. Consequently, the developement of this method to overcome such limitations is pressingly needed, and research on this topic has been extensive in the very recent years.

The objective of this work is to describe, discuss the MoL and illustrates its application for the characterization of planar and quasi-planar MICs and MMICs structures using the full-wave approach.

The first chapter deals with mathematical basis and concepts of the semi-analytical Method of Lines, which are established by describing the numerical algorithm and the steps required for solving a certain types of partial differential equations. This technique has been applied particularly for solving generalized Dirichlet boundary value problems but can also be used to solve Neumman problems. In order to show the method consistency and numerical accuracy, illustrative examples are undertaken, which consist of solving Laplace equation for a simple regular and curved boundary conditions cases.

[2] M. V. Schneider. " Microstrip lines for microwave integrated circuits." *The bell system technical journal*. pp. 1421-1444. june 1969

[3] R. Sorrentino. " Numerical techniques for planar and quasi-planar millimeter-wave passive components." Ann. Télécommun., vol.43. nº 7-8. pp. 392-404. 1988.

[4] U. Shulz and R. Pregla, " A New technique for the Analysis of the Dispersion Characteristics of Planar waveguides ", AEÜ, band. 34, Half 4, pp. 169-173, 1980.

[5] T. Kitazawa. " Metallization thickness effect of striplines with anisotropic media :quasi-static and hybrid-mode analysis. " *IEEE Trans. Microwave Theory and Tech.*, Vol. MTT-37. pp.769-775. Apr. 1989.

[6] R. Vahldieck. " Accurate hybrid-mode analysis of various finline configurations including multilayer dielectrics. finite metallization thickness. and substrate holding grooves. " *IEEE Trans. Microwave Theory and Tech.*, Vol. MTT-32. pp.1454-1460. Nov. 1984.

[7] P. J. Meier. " Integrated finline millimeter components." *IEEE trans. Microwave theory and Tech.*, Vol. MTT-22.pp. 1209-1216. Dec. 1974

Chapter 1

The Method of Line Mathematical Foundation

1.1 INTRODUCTION

In sight of the increasing use of mathematical analysis for applications in physics and engineering sciences, it has become evident that a great amount of researches were attached to this perspective. The study of partial differential equations (PDE), has been the major projects of mathematics for two centuries, and practically every field of modern science depends on these equations for the foundation of the quantitative aspect of its theory. The subject is vast and, in fact, many basic problems are still unsolved, but a few important equations have been solved completely and many methods have been devised to solve PDE, capable of affording an arbitrary high degree of accuracy, in a wide class of situations, if calculating devices are correspondingly high.

Among those methods available in mathematical literature, the method of lines is of interest . This method is a semi-analytical technique for solving two, or recently extended to more, variables PDE. The idea behind this method for solving PDE problems, consist on the application of the finite difference approximation for one or more variables of the PDE while leaving only one variable in its analytical form. Hence the PDE is transformed to a system of Ordinary Differential Equation (ODE), where most of time, can be solved analytically as indicated in [1,2]. This idea was first applied by R. Eothe [3] in 1930 to equations of parabolic type. Few years latter , in 1939, this method was first used as a means for numerical solution of elliptic problems in mathematical physics by M.G. Slobodianskii [3]. In 1949, steeping up this principle more conveniently, V.N.Faddeva [4] has qualified this method as the method of lines, where she developed and applied this method to boundary value problems. In one hand, to solve Laplace equation and Poisson equation, on the other hand to solve the thermal conductibility equation. The application of this method of lines has been increasingly

evolved to involve solution of large variety of PDE [1]. For further details about the evolution of this technique, we may refer to [5-7,10-12] included in [1].

The objective of this chapter is to set up the mathematical foundation of the Method of Lines by establishing the description of the discretization procedure and the steps required for deriving the solution of the partial differential equation in question. For convenience, only a certain type of two variables PDE of equilibrium problem [3], known in mathematical parlance as boundary value problems, that are invoked in physical problems, are considered. The method is applied particularly to Dirichlet boundary value problem, but may be easily extended to Neumman boundary condition as well. For simplicity, it is assumed that the unknown solution functions do not possess singularities neither in the interior of the integration domain, that is to be discussed in the next chapter, nor on the boundary contour. In addition, only a closed contour is supposed to be the domain of solution. For computation convenience and to show the method consistency, illustrative examples are undertaken, for both the simple boundary type and the curved one. This consists of solving the Laplace equation in Cartesian co-ordinate and polar co-ordinate according to the boundary type.

1.1-1 Finite Difference Approximation

To illustrate the idea about the method of lines, it is first necessary to consider the nomenclature and the fundamental concept encountered in this form of approximation theory.

In Finite Difference Method (FDM), the domain of solution of the given PDE is first divided by a finite number of mesh points. The derivative is then replaced at each point by a finite difference approximation. Thus the differential operator of the PDE is completely substituted.

The Method of Lines (MoL), is an alternative to the FDM, where the domain of solution is merely discretized according to one space variable, so that the solution is considered on straight lines (Fig. 1.1-b) rather than on nodes (Fig. 1.1-a) as in FDM. The derivative is also replaced at each line by a finite-difference approximation. Hence the differential operator of the PDE is partially substituted.

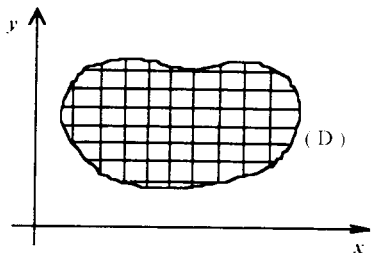

Fig. 1.1a: Discretization for FDM

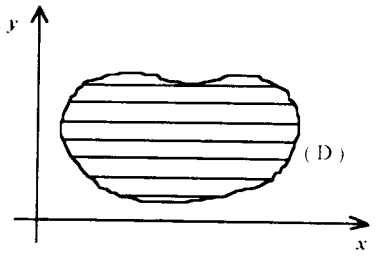

Fig. 1.1b: Discretization for MoL

To get a better distinction between the discretization scheme concept of the two methods, a generalised second order PDE case is selected where more than two space variables are used. The FDM discretize the domain of solution over all its space variables. While the MoL keeps only one space variables in its analytical form and discretizes all the remaining space variables.

1.1-2 Second-differences and derivatives relations

Consider a function u(y) within a certain interval, where its higher derivatives exist. The second order difference $\Delta^2 u = u(y+2h) + u(y+h) + u(y)$ may be approximated in terms of the second derivatives of u at points $y+2h$, $y+h$ and y with an error of order 6.
Using Taylor series expansion, we can write

$$u(y+2h) = u(y+h) + h\frac{du(y+h)}{dy} + \frac{h^2}{2!}\frac{d^2u(y+h)}{dy^2} + \frac{h^3}{3!}\frac{d^3u(y+h)}{dy^3} + \frac{h^4}{4!}\frac{d^4u(y+h)}{dy^4} + O(h^5)$$

$$u(y) = u(y+h) - h\frac{du(y+h)}{dy} + \frac{h^2}{2!}\frac{d^2u(y+h)}{dy^2} - \frac{h^3}{3!}\frac{d^3u(y+h)}{dy^3} + \frac{h^4}{4!}\frac{d^4u(y+h)}{dy^4} + O(h^5)$$

Hence

$$u(y+2h) - 2u(y+h) + u(y) = h^2\frac{d^2u(y+h)}{dy^2} + \frac{h^4}{12}\frac{d^4u(y+h)}{dy^4} + O(h^5) \qquad (1.1)$$

but we have

$$\frac{d^2u(y+2h)}{dy^2}=\frac{d^2u(y+h)}{dy^2}+h\frac{d^3u(y+h)}{dy^3}+\frac{h^2}{2!}\frac{d^4u(y+h)}{dy^4}+\cdots$$

$$\frac{d^2u(y)}{dy^2}=\frac{d^2u(y+h)}{dy^2}-h\frac{d^3u(y+h)}{dy^3}+\frac{h^2}{2!}\frac{d^4u(y+h)}{dy^4}+\cdots$$

Summing up these two equations, yields

$$h^2\frac{d^4u(y+h)}{dy^4}=\frac{d^2u(y+2h)}{dy^2}-2\frac{d^2u(y+h)}{dy^2}+\frac{d^2u(y)}{dy^2}+O(h^4)$$

Substituting these last expressions into equation (1.1), we get

$$\Delta^2u=u(y+2h)-2u(y+h)+u(y)=\frac{5}{6}h^2\frac{d^2u(y+h)}{dy^2}+\frac{h^2}{12}\frac{d^2u(y+2h)}{dy^2}-\frac{h^2}{12}\frac{d^2u(y)}{dy^2}+O(h^6)\cdot \tag{1.2}$$

1. 2 Quantitative description of the MoL

1.2-1 Equations of Elliptic type

As an introductory description of the method, an illustrative simplified example, namely the Dirichlet boundary value problem, where the function to be find, has to satisfy the following equation:

$$\frac{\partial^2u(x,y)}{\partial x^2}+\frac{\partial^2u(x,y)}{\partial y^2}=0 \tag{1.3}$$

Subject to boundary condition $u = 0$ along the closed contour of the domain of solution D.The contour is assumed convex, that is each straight line parallel to the x- axis, crosses it in only two points.

Let us first uniformly discretize the domain of solution by straight equidistant lines, parallel to the x-axis as shown in Fig. 1.2, at $y=y_1, y=y_2, \ldots, y=y_n$
If we designate $u_k(x)=u(x,y_k)$, then each function of $u_{k+1}(x)$, $u_k(x)$ and $u_{k-1}(x)$ satisfies the relation (1.2)

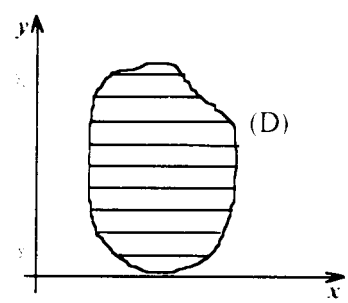

Fig. 1.2 Discretization of the solution domain

In this case , at each line we have:

$$u_{k-1}(x)-2u_k(x)+u_{k-1}(x)=\frac{5}{6}h^2\left.\frac{\partial^2 u(x,y)}{\partial y^2}\right|_{y=y_k}+\frac{h^2}{12}\left.\frac{\partial^2 u(x,y)}{\partial y^2}\right|_{y=y_{k+1}}$$
$$+\frac{h^2}{12}\left.\frac{\partial^2 u(x,y)}{\partial y^2}\right|_{y=y_{k-1}}+O(h^6) \qquad (1.4)$$

from equation (1.3) we have :

$$\left.\frac{\partial^2 u(x,y)}{\partial y^2}\right|_{y=y_k}=-u_k''(x)$$

Substituting this last expression into equation (1.4), where the truncation error of the infinite series is of order 6, the following system is then obtained:

$$\frac{5}{6}u_k''(x)+\frac{1}{12}\left[u_{k-1}''(x)+u_{k+1}''(x)\right]+\frac{1}{h^2}\left[u_{k-1}(x)-2u_k(x)+u_{k+1}(x)\right]=0 \qquad (1.5)$$
$$k=1,2\cdots N$$

The system (1.5) which is a set of ODEs, is independently established from the contour delimiting the domain of solution. The solution $u(x,y)$ is now described by n functions $u_k(x)\ \{k=1,2,\cdots,n\}$ that may be easily obtained by solving the system (1.5) when associated with the boundary conditions.

At each border of the contour (D) (see Fig. 1.3), the limit functions $u_0(x)$ and $u_{n+1}(x)$ have to be evaluated according to the boundary type. Two shapes of boundaries are considered and are of particular interest in our main investigation.

Regular boundaries :

The limits of the domain (top and bottom borders) are represented by straight lines, which are parallel to the x-axis (Fig. 1.3-a). In such a case, the functions $u_0(x)$ and $u_{n+1}(x)$ are regularly constant.

Curved boundaries :

The limits of the domain are not represented by straight lines as shown in Fig.(1.3-b).

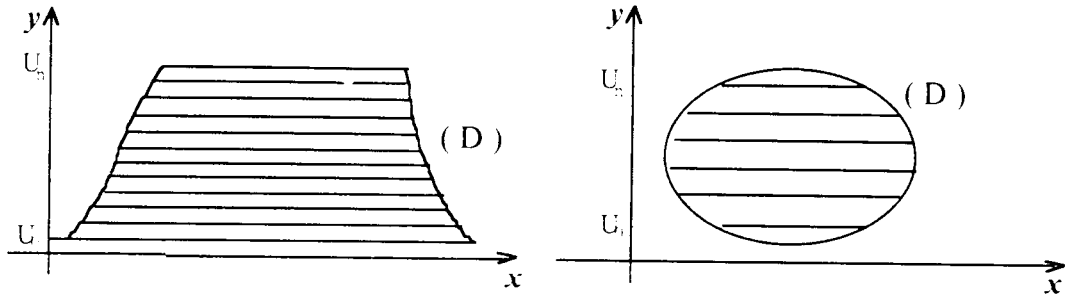

a - Regular boundaries b- Curved boundaries

Fig. 1.3 illustration of line positions at boundary limits

The above treatment may also be used for non homogenous PDE, as shown for the following Poisson's equation:

$$\frac{\partial^2 u(x,y)}{\partial x^2}+\frac{\partial^2 u(x,y)}{\partial y^2}=f(x,y) \tag{1.6}$$

Subject to boundary conditions $u(x,y)=0$ over the border of the closed domain of solution.

Equation (1.6) may be restated, at a given position y_k, as follows :

$$\frac{\partial^2 u(x,y)}{\partial y^2}\Big|_{y=y_k}=-u_k(x)+f_k(x) \tag{1.7}$$

Where $f_k(x)=f(x,y_k)$. After applying the foregoing procedure, the system of ODE will have the following form :

$$\frac{5}{6}u_k(x)+\frac{1}{12}\left[u_{k-1}(x)+u_{k+1}(x)\right]+\frac{1}{h^2}\left[u_{k-1}(x)-2u_k(x)+u_{k+1}(x)\right]$$
$$-f_k(x)-\frac{f_{k-1}(x)-2f_k(x)+f_{k+1}(x)}{12}=0 \qquad ; k=1,2,\cdots,n$$

Which can be reduced to :

$$\frac{5}{6}u_k(x)+\frac{1}{12}\left[u_{k-1}(x)+u_{k+1}(x)\right]+\frac{1}{h^2}\left[u_{k-1}(x)-2u_k(x)+u_{k+1}(x)\right]$$
$$-\frac{5}{6}f_k(x)-\frac{f_{k-1}(x)+f_{k+1}(x)}{12}=0 \qquad k=1,2,\cdots N \tag{1.8}$$

Note that, once the functions $u_0(x)$, $u_{n-1}(x)$, $u_0''(x)$ and $u_{n-1}''(x)$ are evaluated according to appropriate boundary conditions (for Dirichlet condition $u_0(x) = u_{n-1}(x) = u_0''(x) = u_{n-1}''(x) = 0$), the system (1.8) is completely determined.

In this way, the solution $u(x,y)$ is approximated by a set of n functions $u_k(x)$, which in turn are obtained from this last system. this compels us now, to solve this system by taking each type of boundary in turn.

1.2-2 Regular boundaries

In this section, the solution of the boundary value problem is considered in a deeper analysis through examples of Dirichlet problems, particularly for Poisson and Laplace equations, constrained by regular boundaries. The boundary conditions are regular when the limits of such boundaries are only represented by straight lines.

For simplicity, let's take back the Poisson's equation:

$$\frac{\partial^2 u(x,y)}{\partial x^2} + \frac{\partial^2 u(x,y)}{\partial y^2} = f(x,y)$$

Subject to Dirichlet boundary condition $u(x,y) = 0$ over the closed contour. This means that at both limits of the domain of solution $u_0(x) = u_{n-1}(x) = u_0''(x) = u_{n-1}''(x) = 0$.

The established system is rewritten as:

$$\frac{5}{6}u_k''(x) + \frac{1}{12}\left[u_{k-1}''(x) + u_{k+1}''(x)\right] + \frac{1}{h^2}\left[u_{k-1}(x) - 2u_k(x) + u_{k+1}(x)\right] - F_k(x) = 0 \qquad (1.9)$$

$$k = 1, 2, \cdots, n$$

Where $$F_k(x) = \frac{5}{6}f_k(x) + \frac{f_{k-1}(x) + f_{k+1}(x)}{12} \qquad (1.10)$$

In order to arrange the system (1.9) of ODE in a vectorial form, we designate:

$$U = \left[u_1(x), u_2(x) \cdots u_n(x)\right]^t \; ; \; F = \left[f_1(x), f_2(x) \cdots f_n(x)\right]^t$$

$$A = \begin{bmatrix} \frac{5}{6} & \frac{1}{12} & & & \\ \frac{1}{12} & \frac{5}{6} & \ddots & & \\ & \ddots & \ddots & \frac{1}{12} & \\ & & \frac{1}{12} & \frac{5}{6} & \frac{1}{12} \\ & & & \frac{1}{12} & \frac{5}{6} \end{bmatrix} \; ; \; M = \begin{bmatrix} -2 & 1 & & & \\ 1 & -2 & \ddots & & \\ & \ddots & \ddots & 1 & \\ & & 1 & -2 & 1 \\ & & & 1 & -2 \end{bmatrix} \qquad (1.11)$$

Using eq.(1.11), the system (1.9) may then have the following form:

$$AU'' + \frac{1}{h^2} MU - F = 0 \qquad (1.12)$$

Yet, a direct solution of the system (1.12) is not possible, since three components of which are coupled to each other. To decouple this system, the matrices A and M must be diagonalized by suitable transformations. As these matrices are symmetric, an orthogonal transformation matrices are possible, for a suitable normalization of their eigenvectors. This allows in fact to avoid the matrix inversion task. Moreover, it is worth to note that :

$$A = I + \frac{1}{12} M$$

Where I is the identity matrix. It is evident that from this relation , to disregard the transformation matrix of A and carrying out only the transformation matrix of M. Indeed, let T be this orthogonal transformation matrix that transforms M into a diagonal form :

$$T^{-1} M T = \lambda \quad ; \quad \lambda = diag(\lambda_k) \qquad k = 1, 2, \cdots, n$$

and

$$T^{-1} A T = \lambda \quad ; \quad \lambda = diag(1 + \frac{\lambda_k}{12}) \qquad k = 1, 2, \cdots n$$

The elements λ_k of the matrix λ are the eigenvalues of M, and the column vectors t_k of the transformation matrix T be the eigenvectors belonging to the matrix M. To determine λ_k and t_k, the following eingenvalue problem has to be solved:

$$(M - \lambda_k I) t_k = 0 \qquad \text{k} = 1, 2, \cdots, n \qquad (1.13)$$

As M is a symmetric tridiagonal matrix, we obtain a second order difference equation:

$$t_{i+1}^k + (2 + \lambda_k) t_i^k + t_{i-1}^k = 0 \qquad k = 1, 2, \cdots, n \qquad (1.14)$$

Note that, only the first and the last equation of the system (1.13) are different from this last form. The general solution of the system (1.14) is given by :

$$t_i^k = A_k e^{j i \varphi_k} + B_k e^{-j i \varphi_k} \qquad (1.15)$$

Substituting equation (1.15), into equation (1.14) gives

$$\lambda_k = 2(1-\cos\varphi_k) = 4\sin^2 \varphi_k/2 \qquad (1.16)$$

Equation (1.14) is the general form of the eigenvalue problem established independently from boundary conditions. A complete determination of the constants α_k, A_k and B_k is achieved by merely extending the solution (1.16) to the first and the last equation using fictitious quantities and appropriate boundaries as well. Thus equation (1.15) is also fulfilled.

For the Dirichlet-Dirichlet (upper and lower limits) boundary conditions, which is the case of the current problem, the number of lines is n. Then, the first and the last equations run as follows :

$$t_0^k = 0$$
$$t_{n+1}^k = 0$$

Using eq.(1.16) we have:

$$\begin{bmatrix} 1 & 1 \\ e^{j(n+1)\varphi_k} & e^{-j(n+1)\varphi_k} \end{bmatrix} \begin{bmatrix} A_k \\ B_K \end{bmatrix} = 0 \qquad (1.17)$$

For nontrivial solution, the following conditions must hold:

$$e^{j(N+1)\varphi_k} - e^{j(N+1)\varphi_k} = 0 \qquad (1.18)$$

It is easy to show that $\varphi_k = \dfrac{k\pi}{n+1}$ $\quad$ k = 1, 2, ..., n.

Using this last fact, the eigenvalues λ_k are then, given by :

$$\lambda_k = 4\sin^2 \frac{k\pi}{2n+2} \qquad \text{k} = 1, 2, \ldots, \text{n} \qquad (1.19)$$

It can be seen from equation (1.17) that $A_k = -B_k$, and eq. (1.16) gives :

$$t_i^k = A_k \sin i\varphi_k \qquad \text{k} = 1, 2, \ldots, \text{n} \qquad (1.20)$$

In order to normalise the elements of the matrix T with respect to its column vectors, the coefficients A_k must be suitably chosen such that :

$$\sum_{i=1}^{n} (A_k t_{ik})^2 = 1$$

$$A_k^2 \sum_{i=1}^{n} t_{ik}^2 = A_k^2 \sum_{i=1}^{n} \sin^2 \frac{ik\pi}{n+1} = 1 \qquad (1.21)$$

From the orthogonal property of the Sine function, it is easy to show that :

$$\sum_{i=1}^{n} \sin^2 \frac{ik\pi}{n+1} = \frac{n+1}{2}$$

Using equation (1. 21), the coefficients A_k are such that:

$$A_k = \sqrt{\frac{2}{n+1}}$$

Substitution of A_k and φ_k by their corresponding expressions and from eq.(1.20), the eigenvectors t_i^k, elements of the matrix T, are therefore, given by :

$$t_i^k = T_{ik} = \sqrt{\frac{2}{n+1}} \sin \frac{ik\pi}{n+1} \qquad k = 1, 2, \cdots, n \qquad (1.22)$$

Since the vectors t_i^k, components of T are orthogonal then it follows that :

$$T^t T = I \qquad \text{and} \qquad T^{-1} = T^t$$

After premultiplying equation (1.12) by T^{-1}, the system is entirely decoupled and gets the following form :

$$(I + \frac{\lambda}{12}) T^t U'' + \frac{1}{h^2} \lambda T^t U - T^t F = 0 \qquad (1.23)$$

For a convenient formulation, we designate the following transformed vectors:

$$T^t U = \overline{U} = \left[\overline{u}_1(x), \overline{u}_2(x) \ldots \overline{u}_n(x)\right]^t ,$$

$$T^t F = \overline{F} = \left[\overline{f}_1(x), \overline{f}_2(x) \ldots \overline{f}_n(x)\right]^t$$

Hence, the system is simplified to :

$$(I + \frac{\lambda}{12}) \overline{U}'' + \frac{1}{h^2} \lambda \overline{U} - \overline{F} = 0 \qquad (1.24)$$

Since this system is entirely decoupled, it is equivalent to a set of n independent ODEs

$$(I+\frac{\lambda_k}{12})\overline{u_k}'' + \frac{\lambda_k}{h^2}\overline{u_k} - \overline{f_k} = 0 \qquad k = 1,2,\cdots,n \tag{1.25}$$

If we introduce the following designations:

$$\alpha_k^2 = -\frac{\lambda_k}{h^2(1+\frac{\lambda_k}{12})} \quad ; \quad \psi_k = \frac{\overline{f_k}}{1+\frac{\lambda_k}{12}} \tag{1.26}$$

The system (1.24) is reduced to the set of ODEs:

$$\overline{u_k}''(x) + \alpha_k^2 \overline{u_k}(x) - \psi_k(x) = 0 \qquad k = 1,2,\cdots,n \tag{1.27}$$

The solution of this system is given by :

$$\overline{u_k}(x) = A_k\, sh\, \alpha_k x + B_k\, ch\, \alpha_k x + \upsilon_k(x) \qquad k = 1,2,\cdots,n \tag{1.28}$$

Where $\upsilon_k(x)$ is the particular solution of the system (1.26).

In the case of quite simple form of $\psi_k(x)$, the particular solution $\upsilon_k(x)$ may be found using the method of variation of parameters where it is easy to show that this particular solution has the form :

$$\upsilon_k(x) = \frac{1}{\alpha_k}\int_{x_0}^{x} sh\alpha_k(x-t)\,\psi_k(t)dt \tag{1.29}$$

where the limit x_o is the left limit of the domain of solution as shown in Fig. 1.4.

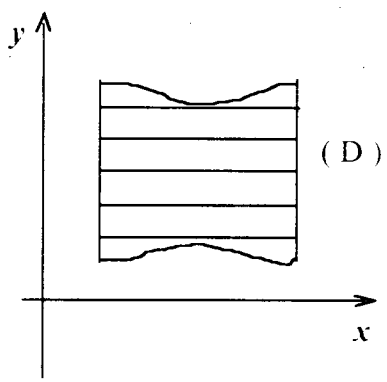

Fig. 1.4 : illustration of left limit condition x_0

However, a simplified form of the solution may be acquired when the solution domain is symmetric with respect to x-axis. This situation may be realised by judiciously positioning the axis-co-ordinate, if the domain of solution has the property of symmetry for both its shape and its boundary limits. Therefore, the solution is simplified to odd function of x, that is:

$$\overline{u_k}(x) = c_k ch\alpha_k x + \overline{v_k}(x) \qquad k = 1,2,\cdots,n \tag{1.30}$$

and

$$\overline{v_k}(x) = \frac{1}{\alpha_k}\int^{x} sh\ \alpha_k(x-t)\,\psi_k(t)dt \tag{1.31}$$

This solution was obtained in the transformed domain, and has to be transformed back to the original domain such that:

$$U = T^{-1}\overline{U} = T'\overline{U}$$

In other word:

$$u_k(x) = \sum_{i=1}^{n} t_{ki}\,\overline{u_k}(x)$$

Thus the solution in the original domain, when using the elements of the T^{-1}, may be written as :

$$\begin{aligned} u_k(x) &= \sum_{i=1}^{n} t_{ki} c_i\ \mathrm{ch}\,\alpha_i x + \sum_{i=1}^{n} t_{ki}\,\overline{v_i}\,(x) \\ &= \sum_{i=1}^{n}\sqrt{\frac{2}{n+1}}\ c_i\ \sin\frac{ik\pi}{n+1}\ \mathrm{ch}\,\alpha_i x + \\ &\int^{x}\sum_{i=1}^{n}\sqrt{\frac{2}{n+1}}\ c_i\ \frac{1}{\alpha_i}\ \sin\frac{ik\pi}{n+1}\mathrm{sh}\,\alpha_i(x-t)dt \qquad k = 1,2,\cdots,n \end{aligned} \tag{1.32}$$

It is important to notice, that the solution of (1.32) is established independently of the contour type, i.e. its shape. The constants $c_1, c_2, \ldots, c_n$ are evaluated from the algebraic system obtained from equation (1.31) after substituting the boundary conditions at the extremity, of both right and left sides, of the considered domain limits. Similarly, for a non symmetric domain, the solution in the original domain is given by:

$$\begin{aligned} u_k(x) &= \sum_{i=1}^{n} t_{ki}\,(A_i sh\alpha_i x + B_i\ ch\alpha_i x) - \sum_{i=1}^{n} t_{ki}\,\overline{v_i}\,(x) \\ &= \sum_{i=1}^{n}\sqrt{\frac{2}{n+1}}\ \sin\frac{ik\pi}{n+1}(A_i sh\alpha_i x + B_i\ ch\alpha_i x)\ + \\ &\int^{x}\sum_{i=1}^{n}\sqrt{\frac{2}{n+1}}\ \frac{1}{\alpha_i}\ \sin\frac{ik\pi}{n+1} sh\alpha_i(x-t)\,\psi_i(t)dt \qquad k = 1,2,\cdots,n \end{aligned} \tag{1.33}$$

The constants $A_1, B_1, A_2, B_2 \cdots, A_n, B_n$ are evaluated from the algebraic system obtained from equation (1.33) after substituting the boundary conditions at both left and right extremities of the domain of solution.

A widespread case used along the present work is illustrated, where the boundary limits of the solution domain is represented by straight lines parallel to their axis (boxed-contour) as shown in Fig. (1.5).

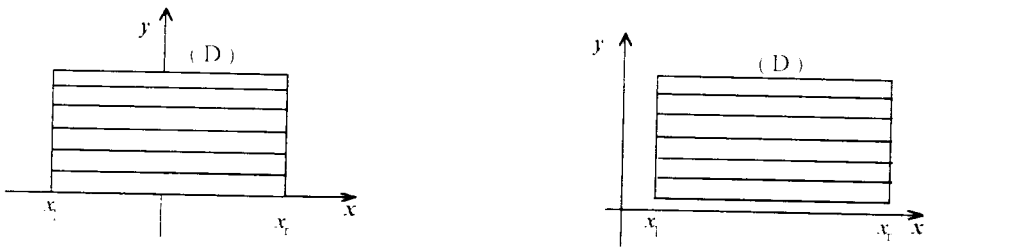

a -symmetric domain

b-non symmetric domain

Fig. 1.5 Symmetric and non symmetric Domain of solutions

In the first situation of symmetric domain of solution (Fig. 1.5-a), the constants c_i are determined in a formal analytical way from the following system:

$$\begin{bmatrix} u_1(x_r) \\ u_2(x_r) \\ \vdots \\ u_n(x_r) \end{bmatrix} = T \begin{bmatrix} c_1 \operatorname{ch} \alpha_1 x_r + \upsilon_1(x) \\ c_2 \operatorname{ch} \alpha_2 x_r + \upsilon_2(x) \\ \vdots \\ c_n \operatorname{ch} \alpha_n x_r + \upsilon_n(x) \end{bmatrix} = \begin{bmatrix} 0 \\ 0 \\ \vdots \\ 0 \end{bmatrix} \tag{1.34}$$

Where

$$c_i = -\frac{\upsilon_i(x_r)}{\operatorname{ch} \alpha_i x_r} \qquad i = 1, 2, \ldots, n \tag{1.35}$$

Similarly, in the case of non-symmetrical domain of solution, the constants A_i and B_i are also directly obtained from the following two systems :

$$\begin{bmatrix} u_1(x_{l,r}) \\ u_2(x_{l,r}) \\ \vdots \\ u_n(x_{l,r}) \end{bmatrix} = T \begin{bmatrix} A_1 \operatorname{sh} \alpha_1 x_{l,r} + B_1 \operatorname{ch} \alpha_1 x_{l,r} + \upsilon_1(x_{l,r}) \\ A_2 \operatorname{sh} \alpha_2 x_{l,r} + B_2 \operatorname{ch} \alpha_2 x_{l,r} + \upsilon_2(x_{l,r}) \\ \vdots \\ A_n \operatorname{sh} \alpha_n x_{l,r} + B_n \operatorname{ch} \alpha_n x_{l,r} + \upsilon_n(x_{l,r}) \end{bmatrix} = \begin{bmatrix} 0 \\ 0 \\ \vdots \\ 0 \end{bmatrix} \tag{1.36-a}$$

Where l,r stands for either left and right boundary condition. These two systems of equations, when gathered, may be abbreviated in the following form :

$$\begin{cases} A_i \operatorname{sh} \alpha_i x_l + B_i \operatorname{sh} \alpha_i x_l + \upsilon_i (x_l) = 0 \\ A_i \operatorname{sh} \alpha_i x_r + B_i \operatorname{sh} \alpha_i x_r + \upsilon_i (x_r) = 0 \end{cases} \quad k = 1, \cdots, n \tag{1.36b}$$

Where, the unknowns A_i and B_i are then independently obtained from this latter system.

1.2-3 CURVED BOUNDARIES

The foregoing treatment is also applied to this curved type domain of solution, where the boundary limits are not supported by straight lines. When this boundary limits are represented by straight lines, the solution is affected with an error due to the curvature shape. An attempt was made [4] to obtain more accurate results but its validity is still constrained for a particular type of PDE cases, in which the limit functions $u_0(x)$ and $u_{n+1}(x)$ are approximated with functions according to the shape boundary limits. The generalized numerical solution proposed to solve this problem is to use a non equidistant discretization scheme, when the contour shape is revealed to brusque or sensitive variation e.g. wedges and sharps. The main idea of non uniform discretization is to shorten the discretization intervals when a considerable shape variation occur, and widen these intervals as long as the shape of the boundary contour is smooth. Another easy and obvious way is to reduce this error by increasing the number of discretizations as long as the round off error is negligible, depending thus on the computation capabilities. This latter approach is briefly considered in this section. The unique distinction over the former procedure to be noted, is that the boundary conditions are situated at a moved x-position, and the following system is valid for a symmetric domain of solution case (see Fig. 1.5-a):

$$u_k(x) = \sum_{i=1}^{n} t_{ki} c_i \operatorname{ch} \alpha_i x + \sum_{i=1}^{n} t_{ki} \overline{\upsilon_i}(x) \qquad k = 1, 2, \cdots, n$$

Thus, we have:

$$\Gamma \begin{bmatrix} c_1 \\ \vdots \\ c_n \end{bmatrix} = T \begin{bmatrix} \upsilon_1 \\ \vdots \\ \upsilon_n \end{bmatrix} \tag{1.36-a}$$

Where,

$$\Gamma_{ik} = t_{ik} \operatorname{ch} \alpha_k x_k \tag{1.36-b}$$

Therefore, the coefficients c_i are determined after inverting Γ matrix and the solution is entirely derived over all the domain of solution.

1.3 DIRICHLET - NEUMMAN BOUNDARIES

Besides the case of Dirichlet boundary value problems, the Neumman and/or the mixed Neumman-Dirichlet boundary conditions are also of great importance. In order to keep valid the former procedure for these new boundaries, another approximation approach is used. We only emphasis on changes that occur with regard to that firstly used approach.

The partial derivatives with respect to x and y are now approximated by:

$$\frac{\partial^2 u(x,y)}{\partial y^2} = \frac{u_{k-1}(x) - 2u_k(x) + u_{k+1}(x)}{h^2} + O(h^2) \qquad (1.37\text{-a})$$

$$\left.\frac{\partial^2 u(x,y)}{\partial x^2}\right|_{y=y_k} = u_k''(x) \qquad (1.37\text{-b})$$

These approximations, when introduced into a non homogenous PDE, the following system of ODE is established for Poisson's equation (1.6) such as:

$$u_k''(x) + \frac{1}{h^2}\left[u_{k-1}(x) - 2u_k(x) + u_{k+1}(x)\right] - F_k(x) = 0 \quad ; \quad k = 1,2,\ldots,n \qquad (1.38)$$

Where ,

$$F_k(x) = \frac{5}{6} f_k(x) + \frac{f_{k-1}(x) - f_{k+1}(x)}{12}$$

The system (1.38) is as yet obtained independently of the boundary conditions, to which the following boundary conditions may be introduced:

- Dirichlet condition : $u = 0$ on the boundary contour,
- Neumman condition : $\frac{\partial u(x,y)}{\partial n} = 0$ on the boundary contour.

In order to fulfil these boundaries for both the top and bottom boundary sides, the discretization lines must lay along the selected axis at propitious positions. The Dirichlet condition is satisfied when $u_0(x)$ and $u_{n-1}(x)$ are aligned at both the contour's limits. However, to realise the Neumman condition $\frac{\partial u(x,y)}{\partial n} = \frac{u_{1-1} - u_1}{h} = 0$, fictitious functions u_0 and u_{n-2} are taken outside, at respectively both bottom and top of the contour. For $u_0 = u_1$ and $u_{n-1} = u_{n-2}$, the Neumman boundary condition is accomplished as depicted in Fig. 1.6

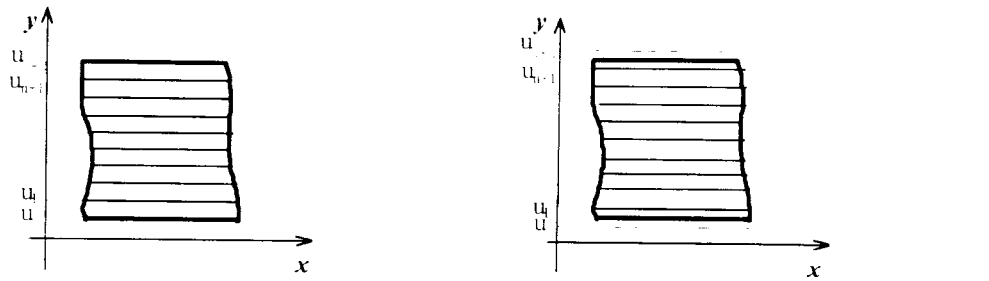

Dirichlet boundary condition Neumman boundary condition

Fig. 1.6 illustration of line positions at boundary limits

For Neumman boundary conditions , a set of $n-1$ number of lines as shown in Fig. 1.6 are held and the matrix M defined by eq.(1.11) for Dirichlet condition, becomes :

$$M = \begin{bmatrix} -1 & 1 & & & \\ 1 & -2 & \ddots & & \\ & \ddots & \ddots & \ddots & \\ & & \ddots & -2 & 1 \\ & & & 1 & -1 \end{bmatrix}$$

Where its corresponding eigenvalues λ_{NN} and the transformation matrix T_{NN} are given in appendix 1. Needless to follow up the analysis, the same procedure is expected.

In the other hand, other practical boundary conditions may be supported, namely the dual Dirichlet-Neumman and Neumman-Dirichlet conditions located at the limits, top and bottom of the contour. Their corresponding eigenvalues together with their transformation matrices are also given in appendix 1.

1.4 GENERALIZED DIRICHLET CONDITION

The Dirichlet problem as yet, was only considered for the simple boundary condition case $u = 0$ on the boundary of the solution domain . A generalised Dirichlet condition concept to any continuous space boundary function $u = g(x, y)$ is also conceivable. Indeed, a new function $F_k(x)$ of system (1.39) is reconsidered, that takes into account the limit functions $u_1(x)$ and $u_{n-1}(x)$, which are evaluated from the space-boundary function $g(x, y)$ at $y = y_0$ and $y = y_{n-1}$.

To clarify this generalised Dirichlet condition, the following Poisson's equation is reconsidered.

$$\frac{\partial^2 u(x,y)}{\partial x^2} + \frac{\partial^2 u(x,y)}{\partial y^2} = f(x,y) \tag{1.39}$$

Subject to $u = g(x,y)$ on the boundary contour of the domain of solution. The limit boundaries $u_0(x)$ and $u_{n-1}(x)$ at $y = y_0$ and $y = y_{n-1}$ are :

$$\begin{aligned} u_0(x) &= g_0(x) \\ u_{n-1}(x) &= g_{n-1}(x) \end{aligned} \tag{1.40}$$

The previously obtained eigenvalues λ and their corresponding transformation matrix T are no longer valid since these only hold for the special boundary condition $u_0(x) = u_{n-1}(x) = 0$. A hard and intricate task raised for solving this new eigenvalue problem, in which the actual boundary functions are taken into account. This may be avoided by adopting new functions, where old functions $F_k(x)$ are added to the evaluated boundary functions $u_0(x) = g_0(x)$ and $u_{n-1}(x) = g_{n-1}(x)$, whereas the functions $u_0(x)$ and $u_{n-1}(x)$ are afterward resettled to fictitious values $u_0(x) = u_{n-1}(x) = 0$. This allows to preserve the same eigenvalue problem that has been solved previously in sec. 2.2. Furthermore, the system (1.8) or (1.9) is mainly kept to solve this generalized Dirichlet boundary condition, except that some slight changes are introduced. For instance to solve the actual problem governed by eqs. (1.40) and (1.41), the corresponding generated system is principally eq. (1.39) with the following modifications :

$$u_k''(x) + \frac{1}{h^2}\left[u_{k-1}(x) - 2u_k(x) + u_{k+1}(x)\right] - F_k(x) = 0 \quad ; \quad k = 1,2,\cdots n$$

Where,

$$\begin{aligned} F_1(x) &= \frac{1}{h^2} g_0(x) + \frac{5}{6} f_1(x) + \frac{f_2(x) - f_0(x)}{12} \\ F_k(x) &= \frac{5}{6} f_k(x) + \frac{f_{k-1}(x) - f_{k+1}(x)}{12} \qquad k = 2,3,\ldots,n-1 \\ F_k(x) &= \frac{1}{h^2} g_{n-1}(x) + \frac{5}{6} f_n(x) + \frac{f_{n-1}(x) - f_{n-1}(x)}{12} \end{aligned} \tag{1.41}$$

Similarly, the treatment of a generalized Neumman condition is straightforward which may be bypassed, since it looks like that of a generalized Dirichlet condition procedure.

1.5 Hyperbolic, Parabolic and Other types of PDE's

Likewise, the recent availability of sophisticated and reliable algorithms and computer programs for automatic numerical computation of complicated systems of ODEs [13] makes extension of the method of lines to many other PDEs. For instance, let's consider a more general linear second order two space variable PDE, such as, the following equation:

$$a_1\frac{\partial^2 u}{\partial x^2}+a_2\frac{\partial^2 u}{\partial y^2}+a_3\frac{\partial^2 u}{\partial y\,\partial x}+a_4\frac{\partial u}{\partial x}+a_5\frac{\partial u}{\partial y}=f(x,y) \qquad (1.42)$$

Subject to Dirichlet conditions $u=g(x,y)$ on the boundary of the solution domain.

Applying the last procedure to this PDE, a coupled system of ODEs is obtained. A numerical sophisticated algorithm is invoked in the situation where the coefficients a_1, a_2, a_3, a_4 are functions of the space variables x and y. However, when those coefficients are constant or function of one space variable, the system of ODE may be solved analytically. Indeed, Let x be this space variable, the discretization is done with respect to the remaining space variable, the obtained system is properly arranged in a Vector form as :

$$a_1\overline{U}''+h^{-1}(a_3\delta+a_4)\overline{U}'-h^{-2}(a_2\lambda\,\overline{U}+a_5\delta)\,\overline{U}=\overline{F_k}(x) \qquad (1.43)$$

Where:

$$\overline{U}=T^{-1}U,\qquad \lambda=T^{-1}MT,\qquad \delta=T^{-1}DT$$

and

$$D=\begin{bmatrix}-1 & & \\ 1 & \ddots & \\ & \ddots & 1\\ & & -1\end{bmatrix},\qquad \delta=diag(\sqrt{\lambda_i})\quad i=1,2,\ldots,n.$$

This is an uncoupled system of ODE where each equation may be solved separately as:

$$a_1(x)\overline{u_k}''(x)+h^{-1}(a_3\delta+a_4(x))\overline{u_k}'(x)+\left(\frac{a_2(x)}{h^2}\lambda_k+\frac{a_5(x)}{h}\delta_k\right)\overline{u_k}(x)=h^{-2}\overline{f_k}(x)$$

$$k=1,2,\ldots,n.$$

Where $u_k(x)$ and $f_k(x)$ are respectively the k-th vector of $\overline{U}$ and $\overline{F}$.

A general outlook of how the Method of Lines can be extended to other types of PDEs is done heretofore, and there are still researches that are currently under work, trying to

widen this technique to a widespread type of PDE's even for non homogenous boundary conditions [1].

1.6 Verifications and Numerical computations

In order to show the MoL consistency and its efficiency, it is convenient to test the developed procedure by applying it to problems for both regular and curved boundary conditions, for which precise data are available. For this purpose, two problems are undertaken which have known analytical solutions. This allows to check the accuracy of the computed results with the available one.

1.6-1 Regular boundary problem

This problem consists of solving the following Poisson's equation:

$$\frac{\partial^2 u(x,y)}{\partial x^2} + \frac{\partial^2 u(x,y)}{\partial y^2} = 2\left[x(x-a) + y(y-b)\right] \qquad (1.44)$$

Subject to $u(x,y) = 0$ on the boundary conditions of the contour (c).

It is easy to check that the following analytical solution form fulfils the PDE (1.44) as well as its boundary conditions :

$$u(x,y) = xy(x-a)(y-b)$$

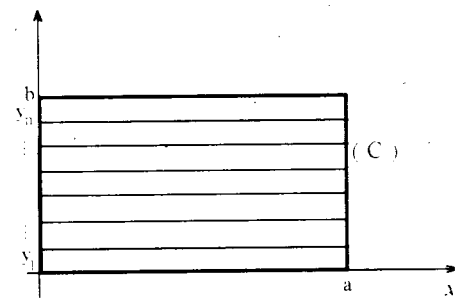

Fig. 1.7 Discretization of the domain of solution (C)

According to the preceding procedure, an established system for this PDE equation is saved as in eq. (1.24):

$$(I + \frac{\lambda}{12})\overline{U}'' + \frac{1}{h^2}\lambda\overline{U} - \overline{F} = 0 \qquad (1.45)$$

where: $T^{-1}\overline{U} = U \quad ; \quad T^{-1}\overline{F} = F$

In which U and F have already been defined. The functions $F_k(x)$ of F may be approximated by :

$$F_k(x) = 2kh(kh - b) + 2x(x - a) \tag{1.46}$$

The system (1.45) is in turn written in the following simplified form as:

$$\overline{u_k}''(x) + \alpha_k^2 \overline{u_k}(x) - \psi_k(x) = 0 \qquad k = 1,2,\cdots,n \tag{1.47}$$

Where $\alpha_k, \varphi_k(x)$ have been defined in eqs. (1.24) and (1.26). The general solution of the system (1.47) may be easily found as :

$$\overline{u_k}(x) = A_k\ sh\ \alpha_k x + B_k\ ch\ \alpha_k x + \overline{\overline{u_k}}(x) \qquad k = 1,2,\cdots,n \tag{1.48}$$

Where the particular solution $\overline{\overline{u_k}}(x)$ has a polynomial form of the second degree :

$$\overline{\overline{u_k}}(x) = v_k x^2 + w_k x + z_k \tag{1.49}$$

Since $\varphi_k(x)$ may be written as:

$$\varphi_k(x) = r_k + s_k(x^2 - ax) \tag{1.50}$$

Where r_k and s_k are known constants. However the coefficients A_k, B_k, v_k, w_k and z_k are easily found after substituting eq.(1.48), (1.49) and (1.50) into eq.(1.47) and applying the boundary conditions.

The numerically obtained data resulting from the MoL and those supplied analytically are plotted versus y-axis for different x-positions and divers contour sizes as shown in Figures 1.8, 1.9, and 1.10.

The results obtained in Figs. 1.8, 1.9 and 1.10 are in very good agreement with the analytically supplied data, where the maximum error occurred is around 10^{-5} %. Moreover the convergence behaviour represented by the maximum error versus the discretization interval is plotted in Fig. 1.11. This curve shows the optimum discretization step that yields the optimum error for the considered problem.

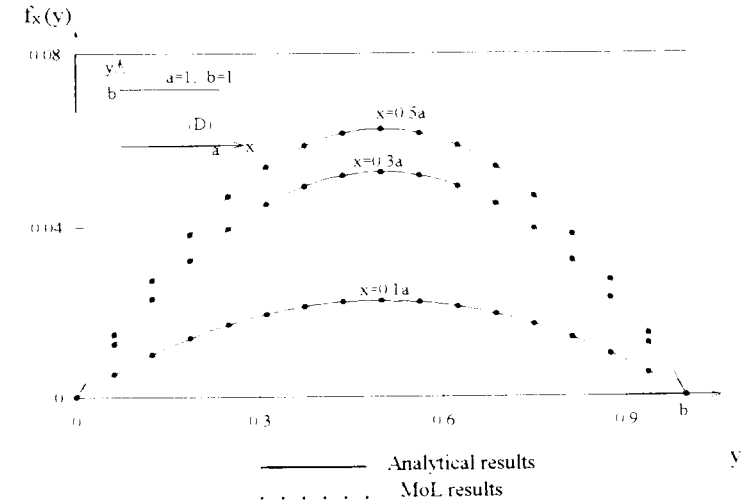

Fig 1.8 : Plot of the solution function versus y with x as parameter.

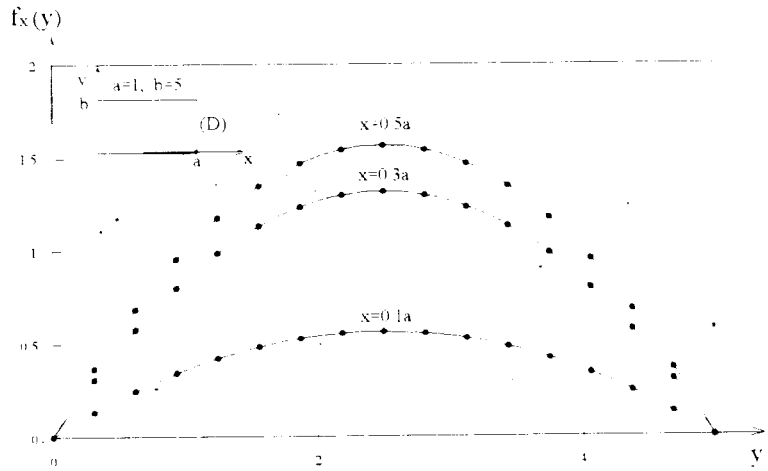

—Analytical solution, • • • Mol. results

Fig. 1.9 : Plot of the solution function versus y with x as parameter.

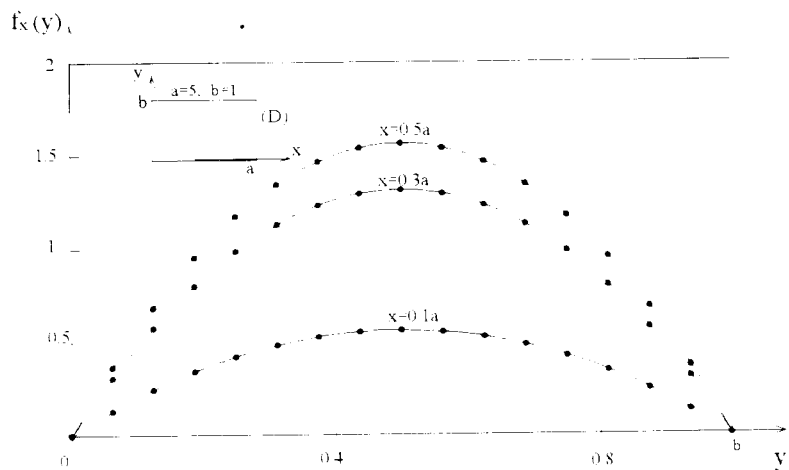

—Analytical solution, • • • Mol. results

Fig. 1.10 : Plot of the solution function versus y with x as parameter.

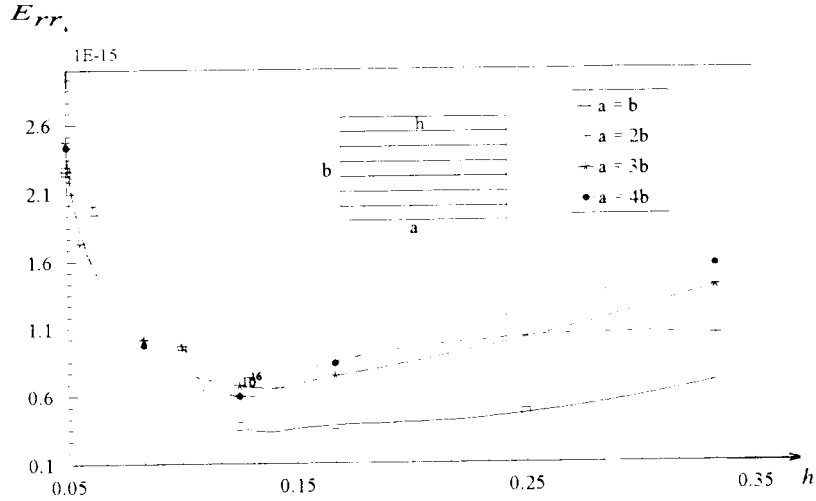

Fig. 1.11 : Maximum error between analytical data and computed one (Mol) versus discretization step h

1.6-2 Curved boundary problem

The supplementary addressed problem consists of solving the following PDE

$$\frac{\partial^2 u(x,y)}{\partial x^2} + \frac{\partial^2 u(x,y)}{\partial y^2} = -1 \tag{1.51}$$

Subject to $u(x,y) = 0$ on the boundary of the solution region delimited by :

$$\begin{cases} x^2 + y^2 = 1 \\ y > 0 \end{cases}$$

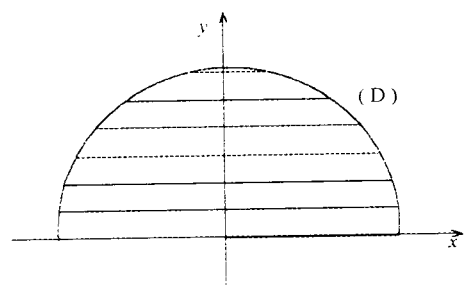

Fig. 1.12 Curved Boundary in semi-circular shape

The analytical solution of this PDE is given in mathematical literature [3] under the form:

$$u(x,y) = \frac{1}{4\pi}\left[\frac{-xy(x^2+y^2+1)(x^2+y^2-1)}{(x^2+y^2)^2}\log\frac{(1+x)^2+y^2}{(1-x)^2+y^2}\right]$$
$$-\frac{1}{4\pi}\left[\frac{(x^2-y^2-2)(x^2+y^2)^2+x^2-y^2}{(x^2+y^2)^2}\operatorname{arctg}\frac{2y}{1-x^2-y^2}+2y-\frac{2y}{x^2+y^2}\right]-\frac{y^2}{2}$$

Applying the numerical technique procedure to this PDE, the obtained data as well as the analytical one are plotted for some positions along x-axis versus the discretized space variable y as shown in Figures (1.12, 1.13, 1.14). A significant error arises for some

positions even for an optimal discretization interval and above which, leads to an additional round-off error depending on the computational capabilities. To improve the accuracy of the present method for this kind of problem, the polar co-ordinates are suggested which are more suited for this boundary shape.

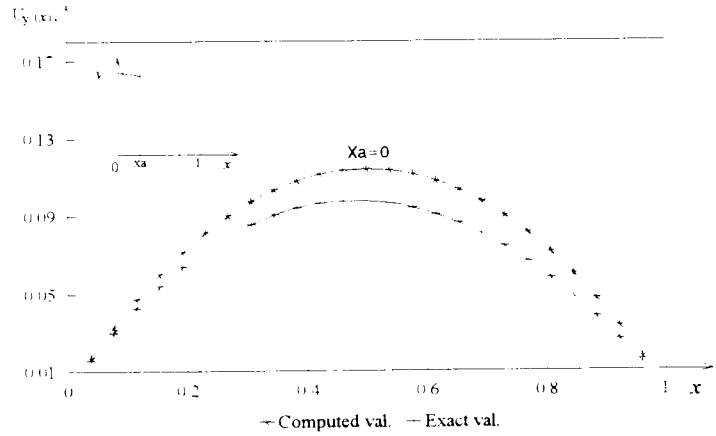

Fig. 1.13

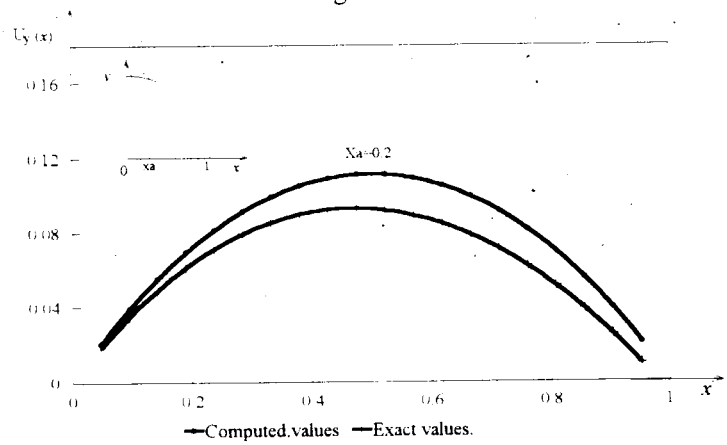

Fig. 1.14

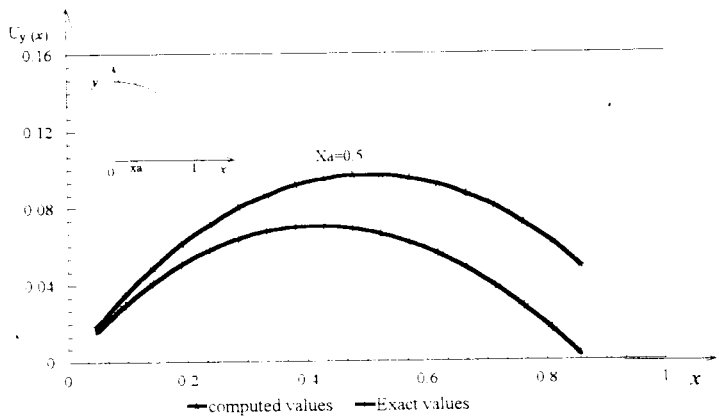

Fig. 1.15

In order to solve the considered PDE in polar co-ordinates, it is necessary in the first step, to transform this laplace equation (1.51) from the Cartesian co-ordinates to polar co-ordinates as follows :

$$\frac{\partial^2}{\partial r^2}u(r,\theta)+\frac{1}{r}\frac{\partial}{\partial r}u(r,\theta)+\frac{1}{r^2}\frac{\partial^2}{\partial \theta^2}u(r,\theta)=-1 \qquad (1.52)$$

Subject to boundary condition $u(r)=0$ on the boundary corresponding domain of solution

$$\begin{cases} r=1 \\ 0\le\theta\le\pi \end{cases}$$

Where $r=\sqrt{x^2+y^2}$, $\theta=\tan^{-1}\frac{y}{x}$ and $x=r\cos\theta$ and $y=r\sin\theta$

In the second step, in order to keep valid the presented numerical procedure, the θ-variable must be quantified at positions $\theta_i=i\theta_s$ $(i=1,2,\ldots,N)$, and θ_s is the interval angle determined from the boundary conditions as shown in Fig. (1.12).

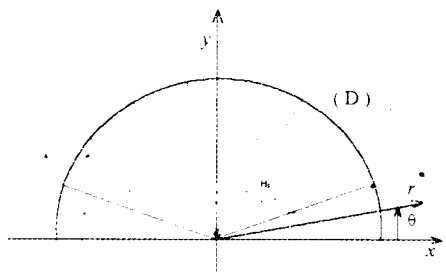

Fig. 1.16: Curved Boundary in semi-cirular shape and discretization pattern in polar co-ordinates

Discretizing now the laplace equation in polar co-ordinate by replacing the second partial derivative with respect to θ by finite difference approximation. A system of N coupled-ODE is then obtained, which can be decoupled by an appropriate transformation. Thus ,this system of ODE in the transformed domain in vector notation becomes

$$\frac{d^2}{dr^2}\bar{u}(r)+\frac{1}{r}\frac{d}{dr}\bar{u}(r)-\frac{\lambda}{r^2\theta_s^2}\bar{u}(r)=\bar{F}(r) \qquad (1.53)$$

Where $\bar{u}=T^t u$, $\bar{F}=T^t\tilde{f}$, $\tilde{f}=(-1,-1,\ldots,-1)^t$. Because λ is a diagonal matrix as previously defined in the current chapter, one can write a set of N independent ODE as:

$$\frac{d^2}{dr^2}\bar{u}_i(r)+\frac{1}{r}\frac{d}{dr}\bar{u}_i(r)-\frac{\lambda_i}{r^2\theta_s^2}\bar{u}_i(r)=\bar{F}_i(r) \quad ; \qquad i=1,2,\ldots,N \qquad (1.54)$$

Each equation of this set of ODEs can be solved analytically. The i-th solution is given by:

$$\overline{u_i}(r) = A_i r^{C_i} + B_i r^{-C_i} + \frac{\overline{F_i}}{4 - C_i^2} \tag{1.55}$$

with $$C_i^2 = \frac{\lambda_i}{\theta_s^2}$$

The coefficient A_i and B_i are determined using the boundary limit for each line. In this case, they are given by :

$$A_i = 0$$

$$B_i = -\frac{\overline{F}}{4 - C_i^2}$$

The last step is to back transform the solution given by eq. (1.55) to the original domain. The computed results are very close to the exact analytically computed ones where the maximum error is no more than 10^{-3} %.

1.7 Conclusion

This chapter established the mathematical basis of the Method of Lines (MoL) of interest, which is a semi-analytical approach for solving boundary value problems. For convenience and to show the method consistency and efficiency, this technique (MoL) has been tested for some Dirichlet boundary value problems, for which exact analytical solution are supplied. Good agreement is observed between computed results and precise solution.

The distinguished properties of this technique over some of the other numerical methods, are its easy mathematical formulation, computational efficiency, small memory space and computing time requirements. Those properties allow to adapt this method to small computer machines, since low computing capabilities are demanded, of course at the extent of the problem complexity and the required results accuracy.

The outstanding features of these inherent properties however, stimulate one to use this MoL as a mathematical tool for the analysis of microwave waveguiding structures through the present investigation.

References :

[1] A. Liskovets. "The method of lines. Review." *Differential'nye Uravneniya*. Vol.1. no.12 pp 662-1678. 1965.

[2] E. Rothe. " Z Weidimensionale parabolishe Randwertaufgaben. " math. Ann.. 102. 650-670. 1930.

[3] M.G. Slobodyanskii. " A method of approximate integration of partial equations and applications to problems of elasticity theory. " *PMM*. no.1. 75-81. 1939.

[4] V.N. Faddeeva. " The Method of Lines applied to certain boundary value problems ." *Tr. matem. in-ta im. V.A. Steklova*. 28. 73-103. 1949.

Additional References :

[5] E.O. Omarov. " Approximate solution by the Method of Lines of the Dirichlet problem for a partial differential equation of elliptic type. " *I.A.N USSR. Ser. fiz.-matem. i mekh. nauk*. no.1. 21-25. 1963;

" Question in differential equations and mechanics related to mining. " *Tr. Sekt. matem. i mekh. A.N. KazSSR, 2, 45-78*. 1963.

[6] E.O. Omarov. " Application of the Method of Lines to the solution of boundary value problem for certain partial differential equations. " Author's abstract of candidate's dissertation. *kazan state university, kazan*. 1963.

[7] E.O. Omarov. " Solution of the equation of bending of a rectangular plate with four fixed edges. " *Proceedings and mechanics [in Russian], TGU, Tomsk*. pp. 42-44. 1962.

[8] E.O. Omarov. An application of the Method of Lines to the solution of boundary value problem for one partial differential equation of elliptic type in trapezoidal domain. " proceedings of *the second Siberian conference on mathematics and mechanics* [in Russian]. TGU. Tomsk. pp. 44-46. 1962.

" Approximate solution by the Method of Lines of one first-order partial differential equation of elliptic type in trapezoidal domain. " proceedings of *aspirants in sciences conferences* [in Russian]. 1962 . (summaries of papers). kazan. pp.153-158. 1962.

[9] E.O. Omarov. " Approximate solution of a partial differential equation of the form $d^4u/dx^4 + a\,d^4u/dx^2y^2 + b\,d^4u/dy^4 = f(x,y)$ in a trapezoidal domain by the Method of Lines. " *I.A.N UzSSR, Ser. fiz.-matem. nauk*. no.4. 33-38. 1963.

[10] E.O. Omarov. " Approximate solution by the Method of Lines of partial differential equations of elliptic type .I. " *ZhVMiMF*. 4. no.3. pp. 585-592. 1964.

[11] M.G. Slobodyanskii. " Three dimensional problems in the theory of elasticity for prismatic bodies. *" Uch. Zap. MGU, Mekhanika*. no.39. 103-144. 1949.

[12] V.I. Lebedev. " Equations and convergence of the differential-difference method of lines. " no.10. pp. 47-57. 1955.

[13] William F. Ames. " Numerical methods for partial differential equations ". Academic Press . 1977

[14] Chou yü-lin. " Boundary value problem for non linear parabolic equations." *DAN SSSr 117*. no.2. 195-198. 1957; Matem. Sb. 47(89). 4. pp. 431-484. 1959.

[15] Chou yü-lin. " Boundary value problems for non linear parabolic equations." Authors abstract *candidate's dissertation. Moscow state university*. Moscow. 1957.

[16] B.M. Budak. " On homogeneous differential-difference schemes with second-order accuracy for parabolic and hyperbolic equations with discontinuous coefficients." *DAN SSSR* 142. no.5. 986-989. 1962; Vestnik Mosk. un-tu. Vol.1. no.2. 7-13. 1962.

Analysis of Microwave Structures Based on Isotropic and Anisotropic Substrates

2.1 INTRODUCTION

In recent microwave engineering, the characterization of planar waveguiding structures is of fundamental importance for an accurate design of integrated microwave techniques and optics. The Electromagnetic (EM) field theory, which has reached a state of maturity, has been intensively applied, using various numerical techniques, for the analysis of a wide class of waveguide structures. To achieve this objective, microwave literature provides several analytical procedures, which can be divided into three approaches : Quasi-static analysis [1-6,21], Full-wave frequency-domain analysis [7-20, 25, 30-34] and the Time domain analysis [22, 37]. For structures supporting TEM wave operating at lower microwave frequencies, where their structural dimensions are much lower than the used wavelength, the Quasi-static approach is adequate because of its high computation efficiency. However, for higher microwave frequencies and millimeter-wave frequencies, where the used wavelength and structural dimensions are closer, the effect of dispersion cannot be neglected and the Full-wave analysis should take place. Whereas, the Time domain analysis provides an alternative to the Full-wave frequency-domain approach and is recommended for studing the behaviour of pulsed signal and delay time occurring in structures such as high speed digital circuits.

The planar transmission line structures used in the design of Microwave Integrated Circuits (MICs) and Monolithic MICs (MMICs) are generally based on single or multidielectric layers of either isotropic or anisotropic substrates on which strip

metallizations are deposited in a single or several dielectric interfaces, as shown in Fig. 2.1. The substrates are insulator materials of low dielectric losses at frequencies of operations, used to support mechanically the strip metallization and also to maintain correct separation between them.

The dielectric substrate materials present either the isotropic dielectric property or the anisotropic one. In fact, most dielectric materials exhibit a negligible or a considerable anisotropy. The development of accurate methods and optimization techniques for the design of integrated microwave circuits require a precise knowledge of the substrate material dielectric constant. The reason for this is that variations in the value of the substrate material relative dielectric constant, as well as its possible variation for different material batches, introducing errors in the design of integrated circuits and decrease integrated circuit repeatability.

The use of anisotropic dielectric substrate materials in MICs and optical integrated circuits, has been attractive in the last few years [42-50], due first to their technological advantages and providing further flexibility in circuit design. Among many important uniaxial anisotropic substrates such as Sapphire, epsilam10, PTFE, are of great interest for the development of a variety of microwave and optical devices including electro-optical modulators [39], and equalisation of even and odd-mode phase velocities for symmetrical coupled microstrip lines [42, 48]. These substrate materials used in practice, that exhibit anisotropy behaviour [42, 44, 48], is either inherent to the material or may be acquired during the manufacturing process. Uniaxial crystalline substrates (such as, e.g. sapphire and quartz) belong to the former while fiber or ceramic impregnated plastics (such as, e.g., Epsilam10) belong to the latter class.

The analysis of microwave structures based on anisotropic substrates may have two objectives. The first objective is to bring improvement by using accurate analysis, where it has been clarified that when anisotropy is ignored in the development of design methods for single strip based on sapphire substrates [42-45, 48,49], coupled strip epsilam10 [48, 49] and finline structures [46], an error is introduced which becomes significant for small lines widths and small line separations. It follows the development of highly accurate models for integrated circuit structures should account for substrates anisotropy. The second objective is to take advantage of its property, where in certain applications of coupled lines structures, anisotropy may prove beneficial in equalising even--odd-mode phase velocities and reducing geometry tolerance sensitivity [42, 48].

In this chapter, the Method of Lines (MoL) is applied for the analysis of a general microwave planar waveguiding structures. These structures, used e.g. as transmission line in MICs and MMICs, are based on single or multidielectric layers of either isotropic

or anisotropic substrates on which are deposited metallic strips arranged over one or several dielectric interfaces.

A convenient mathematical formulation is adopted for the analysis of these structures, where the hybrid-mode solution or the full-wave approach is put to use. To derive the characteristics of the structure to be analysed, procedure to derive the dispersion, The semi-analytical MoL is employed to solve eigenvalue problems, using both the uniform and non uniform discretization . The numerical results are tested against other theoretical and experimental data available in the literature. In addition, the convergence behaviour, the anisotropy effect as well as the numerical results obtained for some useful structures are discussed.

2.2 Problem Formulation

Generally the electromagnetic fields propagating within planar waveguide, structures used in microwave and optical integrated circuits can be calculated from two independent potential functions or two field components. The mathematical formulation adopted can be adapted to treat structures based on either isotropic or anisotropic substrates. The direct electromagnetic fields (EM) formulation or the suitable Hertzian potential function must fulfil , in each separate layer, the Helmotz equations [51] :

$$\begin{aligned} &\frac{\partial^2\Phi^e}{\partial x^2}+\frac{\partial^2\Phi^e}{\partial y^2}+\frac{\partial^2\Phi^e}{\partial z^2}+k_e^2\Phi^e=0 \\ &\frac{\partial^2\Phi^h}{\partial x^2}+\frac{\partial^2\Phi^h}{\partial y^2}+\frac{\partial^2\Phi^h}{\partial z^2}+k_h^2\Phi^h=0 \\ &k_e^2=\varepsilon_e k_o^{},k_h^2=\varepsilon_h k_o^{},k_o^{}=\omega\sqrt{\varepsilon_o\mu_o} \end{aligned} \qquad (2.1)$$

Where Φ^e and Φ^h are called the electric and magnetic related functions , which have to substitute the EM. fields or the Hertzian potential functions according to the chosen formulation. In addition , Φ^e and Φ^h must fulfil the following boundary conditions:

Electrical wall : $$\Phi^e=0 \quad (D) \;;\; \frac{\partial\Phi^h}{\partial n}=0 \quad (N) \qquad (2.2\text{-a})$$

Magnetic wall : $$\frac{\partial\Phi^e}{\partial n}=0 \quad (N) \qquad (2.2\text{-b})$$

Here n means the direction of the normal on the corresponding wall and D and N stand respectively for Dirichlet-condition and Neumann-condition.

The other electromagnetic fields for both the isotropic and anisotropic dielectric cases may be derived by means of relations connecting the related function solutions to that of the electric or magnetic fields. This manipulation is performed occasionally, when required, latter on in this chapter.

2.3 Discretization Scheme

For the analysis of a wide type of waveguiding structures with constant cross-section, the discretization scheme is only done according to one direction. In the case of Fig. 2.1 the discretization is done in the direction parallel to the interface of the layer, that is, x-direction, where singularities occur near the strip. However, the individual layers are homogeneous in y-direction, and the EM. related functions are not singular but rather smooth, this is why the y-direction is left in its analytical form.

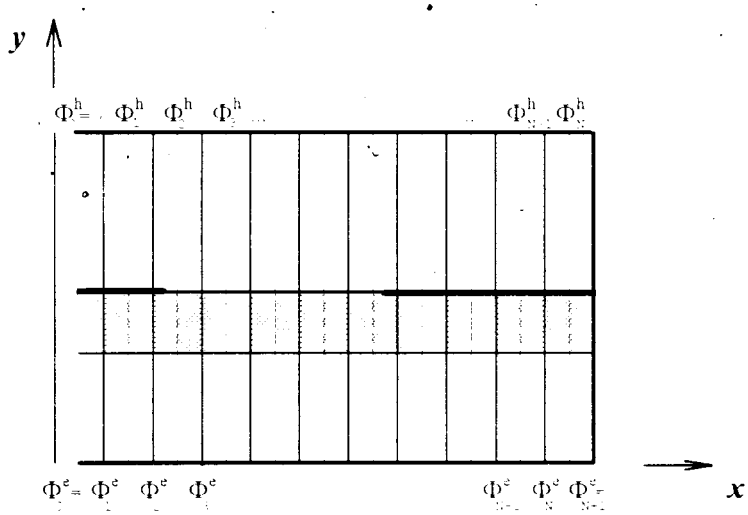

Fig. 2.1
Cross-section of planar waveguide with discretization lines
—— lines for Φ^e
- - - - lines for Φ^h

The discretization of the related functions Φ^e and Φ^h over the domain of solution, which is formed by the waveguide cross-section limits, signifies that the functions Φ^e and Φ^h are considered on straight lines. These discretization lines may be laid uniformly distant over the cross-section and are perpendicular to the interfaces. The metallic enclosure of the waveguide constitutes mathematically the boundary condition in which the Helmotz equations must be solved. For certain symmetric structures only half a cross-section has to be considered as shown in Fig. 2.1. In this case, it is necessary to insert a magnetic-wall in the middle of the structure. In order to fulfil the lateral

boundary Dirichlet conditions for the electrical related function Φ^e, it is required to put a line in the lateral boundary, which is located on the right side of the structure in Fig. 2.1, and set the electric related function component at this line to zero. Needless, to carry this component in the subsequent calculations as was done in the first chapter. While the Neumann-condition, corresponding to the left boundary in the case of Fig. 2.1, is satisfied by positioning the boundary between two lines and equating the potentials e.g. of Φ^e . These discretization lines are only valid for one potential, which is Φ^e for the case of Fig. 2.1 where it is represented by continuous lines, fulfilling its corresponding lateral boundary conditions. The boundary conditions cannot be satisfied for both Φ^e and Φ^h for the same line system of Φ^e, because of the duality of their boundary conditions, as inspected from eq. (2.2), that have to be fulfilled at each lateral limits of the cross-section. To accomplish this requirement , it is necessary to choose another shifted line system as shown in Fig. 2.1, where the magnetic related function is represented by doted line system. Moreover, the shifting of the two line systems has other advantages as indicated in [51] :

– it allows an optimal edge positioning
– it reduces the discretization error
– it results in an easy formulation

These advantages are clarified and justified at propitious positions along this analysis.

2.4 Discretization Procedure Description

In order to solve the hybrid field problem numerically, the considered cross-section depicted in Fig. 2.1 is discretized by N lines for both the E.M related function Φ^e and Φ^h with respect to x-direction. This means that the functions are calculated on lines that are perpendicular to y-direction. The related functions Φ^e and Φ^h on these two line system are denoted by Φ_i^e and Φ_i^h on the i-th line and interpreted as elements of the vectors Φ^e and Φ^h respectively. These related functions can Now be replaced by a set $(\Phi_1, \Phi_2, \ldots, \Phi_N)$ at the lines $x_i = x_0 + i\,h$ where $i = 1, 2, \ldots, N$.

For the discretization of the wave equations (2.1) and (2.2), the derivatives of Φ^e and Φ^h with respect to x are needed. Using the central difference approximation for the first derivative with respect to x, one may obtain for the i-th line

$$\frac{\partial \Phi^e}{\partial \mathrm{x}}\Big|_{x=ih} = \frac{\Phi^e_{i+1} - \Phi^e_i}{h} + O(h^2) \qquad (2.3\text{-a})$$

and

$$\frac{\partial \Phi^h}{\partial x}\Big|_{x=i\,h} = \frac{\Phi^h_{i-1} - \Phi^h_i}{h} + O(h^2) \qquad (2.3\text{-b})$$

Where h is the discretization step. For the boundary conditions of Fig. 2.1, sweeping all the components of the discretization lines, eq. (2.3-a) may be arranged in the matrix form as

$$h\frac{\partial \Phi^e}{\partial x} \rightarrow \begin{bmatrix} -1 & 1 & & \\ & \ddots & \ddots & \\ & & \ddots & 1 \\ & & & -1 \end{bmatrix} \begin{bmatrix} \Phi^e_1 \\ \Phi^e_2 \\ \vdots \\ \Phi^e_{N1} \end{bmatrix} = D\,\Phi^e \qquad (2.4)$$

The difference matrix D, is so called since it accomplishes the difference between two successive elements of the vector Φ^e, depends on the lateral boundary conditions for Φ^e (see appendix 1).

Because Φ^e and Φ^n have dual boundary conditions, that the finite difference approximation for the first derivative of Φ^h represented for the i-th component in eq. (2.3-b), may be formulated in matrix form as

$$h\frac{\partial \Phi^h}{\partial x} \rightarrow -D^t\Phi^h \qquad (2.5)$$

It is clear that, for central difference approximation, the lines of the derivatives of Φ^h are located on Φ^e lines and vice versa. This situation occurs, however, in most electromagnetic field matching equations as may be perceived latter. For instance, the derivative with respect to x of the magnetic field is needed with the electric field at the same discretization line since terms can only be added or subtracted at the same position. Fortunately, because of the two shifted line system, the derivative of one field components are formed using the difference quotient from adjacent components, and are therefore located at the position of its dual field, and reducing also the discretization error. Furthermore, we note that the operator D is used for the representation of both related functions Φ^e and Φ^h. This is another reason for using two shifted line systems. Since the central approximation is used , the derivatives of Φ^e and Φ^h are respectively on Φ^h and Φ^e lines. The second derivative is picked up by using again the central approximation of the first derivative. In this way, it is clear that the discretization lines of the related function and those of its second derivative are aligned (e.g. the $\frac{d^2\Phi^h}{dx}$-lines are aligned with those of Φ^e lines). Besides, the second derivative of Φ^e is given by

$$\frac{\partial^2 \Phi^e}{\partial x^2} = \frac{\partial}{\partial x}\left(\frac{\partial \Phi^e}{\partial x}\right) = \frac{\left.\frac{\partial \Phi^e}{\partial x}\right|_i - \left.\frac{\partial \Phi^e}{\partial x}\right|_{i-1}}{h} + O(h^2) \qquad (2.6)$$

$$= \frac{\Phi^e_{i-1} - 2\Phi^e_i + \Phi^e_{i-1}}{h^2} + O(h^2)$$

which can be written in matrix form as

$$h^2 \frac{\partial^2 \Phi^e}{\partial x^2} = h\frac{\partial \Phi^e}{\partial x}\left(h\frac{\partial \Phi^e}{\partial x}\right) = -D^t D\Phi^e = -P^e\Phi^e \qquad (2.7\text{-a})$$

The second derivative of Φ^h is performed in a similar way as that of Φ^e, and can be formulated as

$$h^2 \frac{\partial^2 \Phi^h}{\partial x^2} = h\frac{\partial \Phi^h}{\partial x}\left(h\frac{\partial \Phi^h}{\partial x}\right) = -DD^t\Phi^h = -P^h\Phi^h \qquad (2.7\text{-b})$$

It can be seen from these equations that, the second difference operator results from the product of the first differential operator for the first derivatives. This differential operator P^v (v : e or h) can be generally represented by

$$P^v = \begin{bmatrix} p_l^v & -1 & & & \\ -1 & 2 & \ddots & & \\ & \ddots & \ddots & \ddots & \\ & & \ddots & 2 & -1 \\ & & & -1 & p_r^v \end{bmatrix} \qquad (2.8)$$

The matrix P^v includes the left and right ($p^v_{l,r}$,) lateral boundary conditions. For instance, to determine the value of P_l^v, the left boundary condition is considered as shown in Fig. 2.2. At this boundary (Fig. 2.2-a), the Dirichlet condition requires $\Phi_0^v = 0$. The insertion of this relation into eq. (2.6) with i=1, yields $h^2\frac{\partial^2 \Phi^v}{\partial x^2} = \Phi^v_{i-1} - 2\Phi^v_i$, which gives $p_l^v = 2$. For the Neumman condition (Fig. 2.2-b) however, $\Phi_0^v = \Phi_1^v$ $(h\frac{\partial \Phi}{\partial n} = \Phi_i^v - \Phi^v_{i-1} = 0)$ is required. This last condition can be satisfied for $p_l^v = 1$.

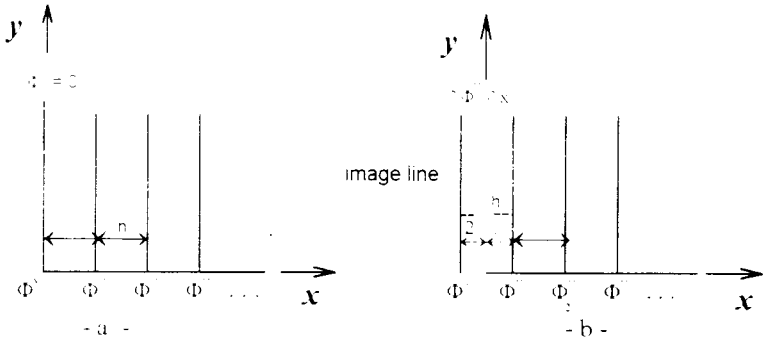

Fig. 2.2

Boundary conditions
a- Dirichlet boundary $\Phi^v = 0$
b- Neumman boundary $\dfrac{d\Phi^v}{dn} = 0$

It should be mentioned, that this is not the unique way to satisfy the boundary conditions e.g., the Neumann-boundary can be laid at $i = 0$ too, but this requires $\Phi^v_{-1} = \Phi^v_1$, which leads to a non symmetrical matrix P^v.

For constant cross section it can be assumed that the wave propagating along the z-direction is $e^{-jk_z z}$ type variation, and when substituting eq. (2.7) into eq. (2.1) and abbreviating Φ^e and Φ^h by Φ^k, a system of N coupled differentral equations is obtained

$$\frac{d^2}{dy^2}\Phi^v_i(y) + \frac{1}{h^2}(\Phi^v_{i+1}(y) - 2\Phi^v_i(y) + \Phi^v_{i-1}(y)) + (k_v^2 - k_z^2)\Phi^v_i(y) = 0 \qquad (2.9)$$

$$i = 1, 2, \ldots, N$$

which may be expressed in matrix notation as

$$\frac{d^2}{dy^2}\Psi^v + \left[(k_v^2 - k_z^2) I - h^2 P^k \right] \Psi^v = 0 \qquad (2.10)$$

Where $$\Psi^v = \left[\Phi^v_1(y), \Phi^v_2(y), \ldots, \Phi^v_N(y) \right]^t$$

Where I is the identity matrix. The matrix P^k shows that eq(2.10) is a coupled ODE system. However, because P^k is a tridiagonal matrix, then an orthogonal transformation matrix T can be used to decouple this system. Hence it is necessary that

$$(T^v)^t \, P^v \, T^v = \lambda^v \qquad (2.11\text{-a})$$

where λ^v, T^v are respectively the eigenvalue and its associated eigenvectors matrices belonging to P^k. A transformed related function is introduced such that

$$T^{t}\ \Psi^{v} = \overline{\Psi^{v}} \qquad (2.11\text{-b})$$

and by premultiplying eq. (2.10) by T^{t} and inserting eqs. (2.11-a) and (2.11-b) yields

$$\left[\left(\frac{d^2}{dy^2} + k_x^2 - k_z^2\right) I - h^2 \lambda_v \right] \overline{\Psi^{v}} = 0 \qquad (2.12)$$

A valuable property of this " transformed " domain, is that all matrices are of diagonal form that may behave as vectors. This permits matrix equation algebra, to be performed element-by-element rather than by grand manipulation, hence a set of N uncoupled ODE can be obtained in the form as

$$\frac{d^2}{dy^2} \overline{\Psi}_i^{v}(y) - k_{y_i}^2 \overline{\Psi}_i^{v}(y) = 0 \quad , \quad i = 1, 2, \ldots, N. \qquad (2.13)$$

where $\qquad k_{y_i}^2 = k^2 (\overline{\lambda}_i^{v} - \varepsilon_{r_x} + \varepsilon_{re})$

and $\qquad \overline{\lambda}_i^{v} = \dfrac{\lambda_i}{(k_0 h)^2} \quad ; \quad \varepsilon_{re} = \dfrac{k_z^2}{k_0^2}$

It is clear that eq. (2.13) can be solved analytically for each homogeneous region of the structure along y-direction. Then, the general solution for the i-th component of this system is given by :

$$\overline{\Psi}_i^{v}(y) = A_i^{v} \cosh(k_{y_i} y) + B_i^{v} \sinh(k_{y_i} y) \qquad (2.14)$$

Where the coefficients A_i^{k} and B_i^{k} are indirectly obtained upon application of boundary conditions. However, the components and their derivatives are the mostly needed on the layer interfaces. For this purpose, a relationship between the transformed related functions and their derivatives are given, for an arbitrary layer with thickness d (see Fig. 2.4) as :

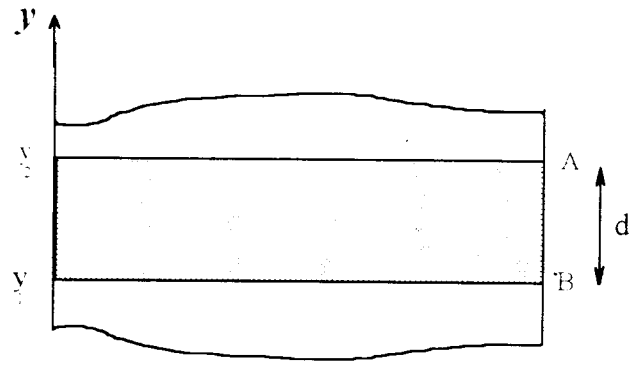

Fig. 2.3

Two interfaces A and B of a dielectric layer with arbitrary thickness d

$$\begin{bmatrix} \frac{d}{dy}\overline{\Psi}^{v}_{A} \\ \frac{d}{dy}\overline{\Psi}^{v}_{B} \end{bmatrix} = k^{2}_{vv} \begin{bmatrix} \gamma^{v} & \alpha^{v} \\ \alpha^{v} & \gamma^{v} \end{bmatrix} \begin{bmatrix} -\overline{\Psi}^{v}_{A} \\ \overline{\Psi}^{v}_{B} \end{bmatrix} \qquad (2.15\text{-a})$$

where

$$\gamma^{v} = diag\left(\frac{k_{yi}}{k_{o}} tanh(k_{yi} d) \right)^{-1} \qquad (2.15\text{-b})$$

$$\alpha^{v} = diag\left(\frac{k_{yi}}{k_{o}} sinh(k_{yi} d) \right)^{-1} \qquad (2.15\text{-c})$$

$$k_{yv} = diag\left(\frac{k_{yi}}{k_{o}} \right) \qquad (2.15\text{-c})$$

2.5 The Field Components Solutions

Since the wave equations are solved separately in each layer, their solutions must be continuous across the structure. This requires that the continuity condition on each layer should be realized. Unfortunately, the EM field Theory gives-up the continuity conditions for only the electromagnetic field. For this purpose, it is needed to carry out the electromagnetic field rather than the related field functions. To simplify the mathematical analysis of the proposed physical problem, the electromagnetic wave equation in each layer of the structure can be described either by two Hertzian potentials Φ^{e} and Φ^{h} or directly from field components.

2.5 -1 Waves Description using field components

The Helmotz wave equation is solved in each region for two field components, and the remaining space field components are derived from the former solution. In the situation of isotropic dielectric substrates, the wave equation may be solved for the electric field e_z and the magnetic field h_z. Using Maxwell's equations, the components e_x, h_x and e_y, h_y are calculated in terms of e_z and h_z according to

$$\left(\frac{\partial^2}{\partial z^2}+k^2\right)\begin{bmatrix} e_x \\ h_x \end{bmatrix} = \begin{bmatrix} \frac{\partial^2}{\partial x\,\partial z} & -jk\eta\frac{\partial}{\partial y} \\ j\frac{k}{\eta}\frac{\partial}{\partial y} & \frac{\partial^2}{\partial x\,\partial z} \end{bmatrix}\begin{bmatrix} e_z \\ h_z \end{bmatrix} \qquad (2.16)$$

$$\left(\frac{\partial^2}{\partial z^2}+k^2\right)\begin{bmatrix} e_y \\ h_y \end{bmatrix} = \begin{bmatrix} \frac{\partial^2}{\partial y\,\partial z} & jk\eta\frac{\partial}{\partial x} \\ -j\frac{k}{\eta}\frac{\partial}{\partial x} & \frac{\partial^2}{\partial y\,\partial z} \end{bmatrix}\begin{bmatrix} e_z \\ h_z \end{bmatrix} \qquad (2.17)$$

where, $\eta = \sqrt{\frac{\mu_o}{\varepsilon}} = \frac{\eta_o}{\sqrt{\varepsilon_r}}$; $\eta_o = \sqrt{\frac{\mu_o}{\varepsilon_o}}$

Assuming the wave propagating in the z-direction according to $e^{-jk_z z}$ and discretizing the field component e_z and h_z in the same way as for Φ^e and Φ^h. The field vectors E_z and H_z are therefore formed like the vectors Ψ^e and Ψ^h. In addition, since e_z and h_z are discretized, then, the fields e_x, e_y, h_x and h_y are consequently discretized. In vector form, equations (2.16) and (2.17) become

$$k_o\varepsilon_d\begin{bmatrix} E_x \\ \eta_o H_x \end{bmatrix} = j\begin{bmatrix} -\sqrt{\varepsilon_{ro}}\,h^{-1}D & -I\frac{\partial}{\partial y} \\ \varepsilon_r I\frac{\partial}{\partial y} & \sqrt{\varepsilon_{ro}}\,h^{-1}D^t \end{bmatrix}\begin{bmatrix} E_z \\ \eta_o H_z \end{bmatrix} \qquad (2.18)$$

$$k_o\varepsilon_d\begin{bmatrix} E_y \\ \eta_o H_y \end{bmatrix} = -j\begin{bmatrix} \sqrt{\varepsilon_{ro}}\,I\frac{\partial}{\partial y} & h^{-1}D^t \\ \varepsilon_r h^{-1}D & \sqrt{\varepsilon_{ro}}\,I\frac{\partial}{\partial y} \end{bmatrix}\begin{bmatrix} E_z \\ \eta_o H_z \end{bmatrix} \qquad (2.19)$$

with $\varepsilon_d = \varepsilon_r - \varepsilon_{ro}$

In the transformed domain, these equations become

$$k_o \varepsilon_d \begin{bmatrix} \overline{E}_x \\ \eta_o \overline{H}_x \end{bmatrix} = j \begin{bmatrix} -\sqrt{\varepsilon_{rc}}\,\overline{\delta} & -I \dfrac{1}{k_o} \dfrac{\partial}{\partial y} \\ \dfrac{\varepsilon_r}{k_o} I \dfrac{\partial}{\partial y} & \sqrt{\varepsilon_{rc}}\,\overline{\delta} \end{bmatrix} \begin{bmatrix} \overline{E}_z \\ \eta_o \overline{H}_z \end{bmatrix} \qquad (2.20)$$

$$k_o \varepsilon_d \begin{bmatrix} \overline{E}_y \\ \eta_o \overline{H}_y \end{bmatrix} = -j \begin{bmatrix} I \dfrac{\sqrt{\varepsilon_{rc}}}{k_o} \dfrac{\partial}{\partial y} & \overline{\delta} \\ \varepsilon_r \overline{\delta} & I \dfrac{\sqrt{\varepsilon_{rc}}}{k_o} \dfrac{\partial}{\partial y} \end{bmatrix} \begin{bmatrix} \overline{E}_z \\ \eta_o \overline{H}_z \end{bmatrix} \qquad (2.21)$$

with $\overline{\delta} = (k_o h)^{-1} \delta \quad ; \quad \delta = T_h^t D T_e$

and the field transformation are performed by

$$E_z = T_e \overline{E}_z \;,\; H_z = T_h \overline{H}_z \;,\; E_x = T_h \overline{E}_x \;,\; H_x = T_e \overline{H}_x \;,\; E_y = T_e \overline{E}_y \;,\; H_y = T_h \overline{H}_y$$

where δ is a diagonal or a quasi-diagonal matrix (according to boundary conditions) The different possible cases of δ as well as the expressions of the transformation matrices T^e and T^h are given in appendix 1.

When the system of equations (2.20) is applied at the interfaces A and B, as shown by Fig. 2.4, and associated to eqs. (2.15) then , a very useful system of equations can be established, after some algebraic manipulations, relating making the tangential magnetic fields H_x, H_z and the tangential electric field E_x, E_z, as follows :

$$\eta_o \begin{bmatrix} -j\overline{H}_{zA} \\ \overline{H}_{xA} \\ -j\overline{H}_{zB} \\ \overline{H}_{xB} \end{bmatrix} = \begin{bmatrix} -\varepsilon_d \gamma_h & \gamma_h \tilde{\delta} & -\varepsilon_d \alpha_h & \alpha_h \tilde{\delta} \\ \tilde{\delta}^t \gamma_h & \gamma_E & \tilde{\delta}^t \alpha_h & \alpha_E \\ -\varepsilon_d \alpha_e & \alpha_h \tilde{\delta} & -\varepsilon_d \gamma_h & \gamma_h \tilde{\delta} \\ \tilde{\delta}^t \alpha_h & \alpha_E & \tilde{\delta}^t \gamma_h & \gamma_E \end{bmatrix} \begin{bmatrix} \overline{E}_{xA} \\ -j\overline{E}_{zA} \\ -\overline{E}_{xB} \\ j\overline{E}_{zB} \end{bmatrix} \qquad (2.22)$$

with

$$\tilde{\delta} = \sqrt{\varepsilon_{rc}}\,\overline{\delta} \quad ; \quad \begin{Bmatrix} \alpha_E \\ \gamma_E \end{Bmatrix} = (\overline{\lambda}_e - \varepsilon_r I) \begin{Bmatrix} \alpha_e \\ \gamma_e \end{Bmatrix}$$

Introducing the abbreviations :

$$H_{A,B} = \eta_o \begin{bmatrix} -jH_{zA,B} \\ H_{xA,B} \end{bmatrix} \quad , \quad E_{A,B} = \begin{bmatrix} E_{xA,B} \\ -jE_{zA,B} \end{bmatrix}$$

and

$$\overline{y_1} = \begin{bmatrix} -\varepsilon_d \gamma_h & \gamma_h \tilde{\delta} \\ \tilde{\delta}' \gamma_h & \gamma_E \end{bmatrix} \quad , \quad \overline{y_2} = \begin{bmatrix} -\varepsilon_d \alpha_h & \alpha_h \tilde{\delta} \\ \tilde{\delta}' \alpha_h & \alpha_E \end{bmatrix}$$

Then, eq. (2.22) can be reduced to

$$\begin{bmatrix} \overline{H_A} \\ \overline{H_B} \end{bmatrix} = \begin{bmatrix} \overline{y_1} & \overline{y_2} \\ \overline{y_2} & \overline{y_1} \end{bmatrix} \begin{bmatrix} \overline{E_A} \\ -\overline{E_B} \end{bmatrix} \tag{2.23}$$

The field components along y-direction, that are necessary for the computation of the characteristic impedance, should be derived in terms of the tangential electric field components. Using eqs. (2.21), (2.22) and in conjunction with eq. (2.15), the electromagnetic fields E_y, H_y at the interfaces A and B, as shown in Fig. 2.4, can be written as

$$\varepsilon_d \begin{bmatrix} \overline{E}_{yA} \\ \overline{E}_{yB} \end{bmatrix} = -\sqrt{\varepsilon_{re}} k_{ye}^2 \begin{bmatrix} \gamma_e & \alpha_e \\ \alpha_e & \gamma_e \end{bmatrix} \begin{bmatrix} -j\overline{E}_{zA} \\ j\overline{E}_{zB} \end{bmatrix} + \tilde{\delta}' \eta_o \begin{bmatrix} -j\overline{H}_{zA} \\ j\overline{H}_{zB} \end{bmatrix} \tag{2.24}$$

$$\eta_0 \varepsilon_d \begin{bmatrix} \overline{H}_{yA} \\ \overline{H}_{yB} \end{bmatrix} = -\varepsilon_r \tilde{\delta} \begin{bmatrix} j\overline{E}_{zA} \\ j\overline{E}_{zB} \end{bmatrix} + \sqrt{\varepsilon_{re}} \eta_o k_{yh}^2 \begin{bmatrix} \gamma_h & \alpha_h \\ \alpha_h & \gamma_h \end{bmatrix} \begin{bmatrix} j\overline{H}_{zA} \\ -j\overline{H}_{zB} \end{bmatrix} \tag{2.25}$$

The H_z field components can be substituted according to eq. (2.15) as,

$$\eta_0 \begin{bmatrix} -j\overline{H}_{zA} \\ -j\overline{H}_{zB} \end{bmatrix} = \begin{bmatrix} \gamma_h & \alpha_h \\ \alpha_h & \gamma_h \end{bmatrix} \left\{ -\varepsilon_d \begin{bmatrix} \overline{E}_{xA} \\ -\overline{E}_{xB} \end{bmatrix} + \sqrt{\varepsilon_{re}} \tilde{\delta} \begin{bmatrix} -j\overline{E}_{zA} \\ j\overline{E}_{zB} \end{bmatrix} \right\} \tag{2.26}$$

Substituting eq. (2.26) into eq. (2.24) yields

$$\varepsilon_d \begin{bmatrix} \overline{E}_{yA} \\ \overline{E}_{yB} \end{bmatrix} = \sqrt{\varepsilon_{re}} \left(-k_{ye}^2 + \overline{\lambda}_e \right) \begin{bmatrix} \gamma_e & \alpha_e \\ \alpha_e & \gamma_e \end{bmatrix} \begin{bmatrix} -j\overline{E}_{zA} \\ j\overline{E}_{zB} \end{bmatrix} - \varepsilon_d \tilde{\delta}' \begin{bmatrix} \gamma_h & \alpha_h \\ \alpha_h & \gamma_h \end{bmatrix} \begin{bmatrix} \overline{E}_{xA} \\ -\overline{E}_{xB} \end{bmatrix} \tag{2.27}$$

and with the help of $k_{ye}^2 + \overline{\lambda}_e = \varepsilon_d I_e$, the relationship between E_y and the tangential field components E_x and E_z can be established as

$$\begin{bmatrix} \overline{E}_{xA} \\ \overline{E}_{xB} \end{bmatrix} = \sqrt{\varepsilon_{re}} \begin{bmatrix} \gamma_e & \alpha_e \\ \alpha_e & \gamma_e \end{bmatrix} \begin{bmatrix} -j\overline{E}_{zA} \\ j\overline{E}_{zB} \end{bmatrix} - \overline{\delta} \begin{bmatrix} \gamma_h & \alpha_h \\ \alpha_h & \gamma_h \end{bmatrix} \begin{bmatrix} \overline{E}_{xA} \\ -\overline{E}_{xB} \end{bmatrix} \qquad (2.28)$$

By substituting eq. (2.26) into eq. (2.25), we obtain for the magnetic field H_x component :

$$\eta_0 \varepsilon_d \begin{bmatrix} \overline{H}_{xA} \\ \overline{H}_{xB} \end{bmatrix} = -\varepsilon_r \overline{\delta} \begin{bmatrix} j\overline{E}_{zA} \\ j\overline{E}_{zB} \end{bmatrix} + \sqrt{\varepsilon_{re}} k_{yh}^2 \begin{bmatrix} \gamma_h & -\alpha_h \\ \alpha_h & -\gamma_h \end{bmatrix}^2 \left\{ \varepsilon_d \begin{bmatrix} \overline{E}_{xA} \\ \overline{E}_{xB} \end{bmatrix} + \sqrt{\varepsilon_{re}} \overline{\delta} \begin{bmatrix} j\overline{E}_{zA} \\ j\overline{E}_{zB} \end{bmatrix} \right\} \qquad (2.29)$$

and under the consideration of $I_h = k_{yh}^2 \begin{bmatrix} \gamma_h & -\alpha_h \\ \alpha_h & -\gamma_h \end{bmatrix}^2$, the relation for H_x is obtained as

$$\eta_0 \begin{bmatrix} \overline{H}_{xA} \\ \overline{H}_{xB} \end{bmatrix} = \sqrt{\varepsilon_{re}} \begin{bmatrix} \overline{E}_{xA} \\ \overline{E}_{xB} \end{bmatrix} - \overline{\delta} \begin{bmatrix} j\overline{E}_{zA} \\ j\overline{E}_{zB} \end{bmatrix} \qquad (2.30)$$

The relationship of the magnetic field H_x may be also derived using eq. (2.22), which gives :

$$\eta_0 \begin{bmatrix} \overline{H}_{xA} \\ \overline{H}_{xB} \end{bmatrix} = \sqrt{\varepsilon_{re}} \overline{\delta}' \begin{bmatrix} \gamma_h & \alpha_h \\ \alpha_h & \gamma_h \end{bmatrix} \begin{bmatrix} \overline{E}_{xA} \\ -\overline{E}_{xB} \end{bmatrix} + \begin{bmatrix} \gamma_E & \alpha_E \\ \alpha_E & \gamma_E \end{bmatrix} \begin{bmatrix} -j\overline{E}_{zA} \\ j\overline{E}_{zB} \end{bmatrix} \qquad (2.31)$$

In this manner, if the electric field E_x and E_z are obtained, then all the other electromagnetic field can be derived. It can be noted that this treatment is only valid for the analysis of planar structures based on isotropic homogeneous dielectric layers.

2.5-2 The two Hertzian Potentials Description

To simplify the mathematical analysis, it is convenient to choose Hertzian potential concept to describe the electromagnetic field to solve the associated wave equations in terms of two potentials. These auxiliary potential functions may or may not represent clearly definable physical entities, and so prefer to adopt the view point that these potentials are just useful mathematical functions from which the electromagnetic fields may be derived. Three types of Hertzian potentials of interest are chosen through the present work. The first one is required for the analysis of isotropic homogenous dielectric, the second is selected for a particular anisotropy, namely the uniaxial, of the dielectric region. The other Hertzian potentials is preserved for the analysis of non

homogeneous dielectric layer, and its description is postponed in the last chapter, where it is invoked.

2.5-2.a Isotropic Homogeneous dielectric

In order to treat the homogeneous isotropic substrates, it is advisable, after Collin [26], to choose two Hertzian potentials A and B, which possess only one component in the propagation direction, the z-direction in the present case, so that the boundary conditions can be easily enforced (Fig. 2.1) . In each layer the fields can be written in terms of these potentials:

$$e = \frac{1}{j\omega\varepsilon}\nabla\times\nabla\times A - \nabla\times B$$
$$h = \nabla\times A + \frac{1}{j\omega\mu}\nabla\times\nabla\times B \qquad (2.32)$$

$$A = \Psi^e(x,y)e^{-jk_z z}\hat{a}_z$$
$$B = \Psi^h(x,y)e^{-jk_z z}\hat{a}_z \qquad (2.33)$$

and the associated Helmotz equations for these potential functions Ψ^e and Ψ^h are already given by eq. (2.1).

The solution of the wave equation is derived directly from the described procedure of section 2.4.1. It is obvious that in each layer, the electromagnetic field may be expressed in terms of the obtained solution, as given by eq (2.14). The electromagnetic field can be carried out using eq. (2.32) as :

$$\begin{bmatrix} e_x \\ h_x \end{bmatrix} = \begin{bmatrix} -j\frac{\eta}{k}\frac{\partial^2}{\partial x\,\partial z} & -\frac{\partial}{\partial y} \\ \frac{\partial}{\partial y} & -\frac{j}{k\eta}\frac{\partial^2}{\partial x\,\partial z} \end{bmatrix} \begin{bmatrix} \Psi^e \\ \Psi^h \end{bmatrix} \qquad (2.34\text{-a})$$

$$\begin{bmatrix} e_y \\ h_y \end{bmatrix} = \begin{bmatrix} -j\frac{\eta}{k}\frac{\partial^2}{\partial y\,\partial z} & \frac{\partial}{\partial x} \\ -\frac{\partial}{\partial x} & -\frac{j}{k\eta}\frac{\partial^2}{\partial y\,\partial z} \end{bmatrix} \begin{bmatrix} \Psi^e \\ \Psi^h \end{bmatrix} \qquad (2.34\text{-b})$$

$$\begin{bmatrix} e_z \\ h_z \end{bmatrix} = \begin{bmatrix} -J\frac{\eta}{k}\left(\frac{\partial^2}{\partial z^2} - k^2\right) & 0 \\ 0 & -\frac{J}{k\eta}\left(\frac{\partial^2}{\partial z^2} - k^2\right) \end{bmatrix} \begin{bmatrix} \Psi^e \\ \Psi^h \end{bmatrix} \qquad (2.34\text{-c})$$

Assuming an $e^{-jk_z z}$ wave type variation along the z-direction, and discretizing these equations in the same way as done for the Hertzian potential functions Ψ^e and Ψ^h, in that case eq. (2.34) becomes :

$$\begin{bmatrix} E_x \\ \eta_o H_x \end{bmatrix} = \begin{bmatrix} -\frac{\sqrt{\varepsilon_{re}}}{\varepsilon_r} h^{-1} D & -J\frac{\partial}{\partial y} \\ J\frac{\partial}{\partial y} & \sqrt{\varepsilon_{re}} h^{-1} D' \end{bmatrix} \begin{bmatrix} \eta_o \Psi^e \\ \Psi^h \end{bmatrix} \qquad (2.35\text{-a})$$

$$\begin{bmatrix} E_y \\ \eta_o H_y \end{bmatrix} = -\begin{bmatrix} \frac{\sqrt{\varepsilon_{re}}}{\varepsilon_r} J\frac{\partial}{\partial y} & h^{-1} D' \\ h^{-1} D & \sqrt{\varepsilon_{re}} J\frac{\partial}{\partial y} \end{bmatrix} \begin{bmatrix} \eta_o \Psi^e \\ \Psi^h \end{bmatrix} \qquad (2.35\text{-b})$$

$$\begin{bmatrix} E_z \\ \eta_o H_z \end{bmatrix} = -J\begin{bmatrix} \frac{k_o}{\varepsilon_r} \varepsilon_d I & 0 \\ 0 & k_k \varepsilon_d I \end{bmatrix} \begin{bmatrix} \eta_o \Psi^e \\ \Psi^h \end{bmatrix} \qquad (2.35\text{-c})$$

In the transformed domain, the set of equations eq. (2.35) becomes :

$$\begin{bmatrix} \overline{E}_x \\ \eta_o \overline{H}_x \end{bmatrix} = \begin{bmatrix} -\frac{\sqrt{\varepsilon_{re}}}{\varepsilon_r} h^{-1} \delta & -J\frac{\partial}{\partial y} \\ J\frac{\partial}{\partial y} & \sqrt{\varepsilon_{re}} h^{-1} \delta' \end{bmatrix} \begin{bmatrix} \eta_o \overline{\Psi}^e \\ \overline{\Psi}^h \end{bmatrix} \qquad (2.36\text{-a})$$

$$\begin{bmatrix} \overline{E}_y \\ \eta_o \overline{H}_y \end{bmatrix} = -\begin{bmatrix} \frac{\sqrt{\varepsilon_{re}}}{\varepsilon_r} J\frac{\partial}{\partial y} & h^{-1} \delta' \\ h^{-1} \delta & \sqrt{\varepsilon_{re}} J\frac{\partial}{\partial y} \end{bmatrix} \begin{bmatrix} \eta_o \overline{\Psi}^e \\ \overline{\Psi}^h \end{bmatrix} \qquad (2.36\text{-b})$$

$$\begin{bmatrix} \overline{E}_z \\ \eta_o \overline{H}_z \end{bmatrix} = -J\begin{bmatrix} \frac{k_o}{\varepsilon_r} \varepsilon_d I & 0 \\ 0 & k_k \varepsilon_d I \end{bmatrix} \begin{bmatrix} \eta_o \overline{\Psi}^e \\ \overline{\Psi}^h \end{bmatrix} \qquad (2.36\text{-c})$$

Because the matching equations can not be easily established for the Hertzian potential functions, in that case the electromagnetic fields represented by eq. (2.36) may be expressed in terms of $\overline{E}_z$ and $\overline{H}_z$ as those of eqs. (2.20) and (2.21). After handling these equations eq. (2.36), the relationship eq. (2.23) between the tangential electric and magnetic fields remains valid.

2.5-2.b Uniaxial Anisotropic Dielectric

starting from Maxwell's equation for dielectrics characterised by $\mu = \mu_o$ and a diagonal tensor permittivity

$$\hat{\varepsilon} = \varepsilon_0 \begin{bmatrix} \varepsilon_x & & \\ & \varepsilon_y & \\ & & \varepsilon_z \end{bmatrix}$$

The medium with two optical axis ($\varepsilon_x \neq \varepsilon_y \neq \varepsilon_z$) is known as bi-axial anisotropic dielectric. When two of principal dielectric constants are equal; such as e.g. $\varepsilon_x = \varepsilon_z$, then only a single optical axis exists, and the medium is said to be uniaxial. In this latter case, the field can be determined from two Hertzian potentials along the optical axis. Then the electric and magnetic fields can be derived for the two modes of propagation, from a magnetic and electric Hertzian potentials having only a direction of the optical axis [26].

The ordinary wave may be found from the magnetic Hertzian potential as follows

$$\begin{aligned} \vec{\pi}_h &= \Pi_h \hat{a}_y \\ \vec{e} &= -j\omega\mu_o \nabla \times \vec{\pi}_h \\ \vec{h} &= \nabla \times \nabla \times \pi_h \end{aligned} \qquad (2.37\text{-a})$$

and Π_h is a solution of

$$\nabla^2 \Pi_h + k^2 \Pi_h = 0 \qquad (2.37\text{-b})$$

where $k^2 = \omega^2 \varepsilon_o \mu_o \varepsilon_x$

and ε_x is the other axis dielectric constant which is perpendicular to the optical axis.

The extraordinary wave is found from the electric Hertzian potential as follows

$$\vec{\pi}_e = \Pi_e \hat{a}_y$$
$$\vec{e} = -k_o^2 \vec{\pi}_e + \varepsilon_x \nabla\nabla \cdot \vec{\pi}_e \qquad (2.38\text{-a})$$
$$\vec{h} = j\omega\varepsilon_o \nabla \times \pi_e$$

and Π_e is a solution of

$$\nabla^2 \Pi_e + k^2 \Pi_e + \frac{\varepsilon_y - \varepsilon_x}{\varepsilon_x} \frac{\partial^2}{\partial \theta^2} \Pi_e = 0 \qquad (2.38\text{-b})$$

The former PDE eq. (2.38-a) gives a solution for e with no component along the optical axis, while the latter PDE eq. (2.38-b) gives a solution for h with no component along that optical axis.

For the considered waveguide system, e^{-jkz} type variation is assumed along the z-direction. The dispersion characteristics are generally supported by the hybrid-mode solution. The hybrid-mode field is a combination of both electromagnetic fields generated from the two electric and magnetic Hertzian potentials propagating modes. Moreover, at the extent of extensive practical use of substrates having optical axis along y-direction, the electromagnetic-fields may be described by the electric and magnetic Hertzian potentials selected in that direction. Assuming an $e^{j\omega t}$ time-harmonic variation, the electromagnetic fields in each homogeneous region are given by

$$\vec{\pi}^{e,h} = \Pi^{e,h}(x,y)\, e^{-jkz} \hat{a}_y \qquad (2.39\text{-a})$$

$$\vec{e}(x,y,z) = \nabla(\nabla \cdot \vec{\pi}^e) + k_x^2 \vec{\pi}^e - j\omega\mu_o \nabla \times \vec{\pi}^h \qquad (2.39\text{-b})$$

$$\vec{h}(x,y,z) = j\omega\varepsilon_o\varepsilon_x \nabla \times \vec{\pi}^e + \nabla(\nabla \cdot \vec{\pi}^h) + k_x^2 \vec{\pi}^h \qquad (2.39\text{-c})$$

with $\qquad k_x = \sqrt{\varepsilon_x}\, k_o \qquad ; \qquad k_o = \omega\sqrt{\mu_o\varepsilon_o}$

where $\Pi^{e,h}$ are solutions to the following scalar wave equations

$$\frac{\partial^2}{\partial x^2}\Pi^e(x,y) + \frac{\varepsilon_y}{\varepsilon_x}\frac{\partial^2}{\partial y^2}\Pi^e(x,y) + (k_y^2 - k_z^2)\Pi^e(x,y) = 0 \qquad (2.40\text{-a})$$

and

$$\frac{\partial^2}{\partial x^2}\Pi^h(x,y) + \frac{\partial^2}{\partial y^2}\Pi^h(x,y) + (k_x^2 - k_z^2)\Pi^h(x,y) = 0 \qquad (2.40\text{-b})$$

for each region, and associated to boundary conditions which are summarized for different cases by :

magnetic wall : $\Pi^h = 0$; $\frac{\partial \Pi^e}{\partial n} = \frac{\partial \Pi^e}{\partial x} = 0$ (2.41-a)

electric wall : $\Pi^e = 0$; $\frac{\partial \Pi^h}{\partial n} = \frac{\partial \Pi^h}{\partial x} = 0$ (2.41-b)

Top and bottom shielding walls: $\Pi^h = 0$; $\frac{\partial \Pi^e}{\partial y} = 0$ (2.41-c)

are valid according to physical boundaries related to the analyzed structures. It is worth to note the boundary condition for Π^e are the same as for e_z in previous section and those for Π^h are the same as for h_z. Note also that the isotropic homogeneous layer is merely obtained when $\varepsilon_x = \varepsilon_z = \varepsilon_r$.

Discretizing the electric and magnetic Hertzian potentials Π^e, Π^h in a similar manner as was done for Ψ^e and Ψ^h and applying the foregoing procedure, the systems of ODE's are obtained and are given in the transformed domain as :

$$\left(n^2 \frac{d^2}{dy^2} - k_0^2 \left(\frac{\lambda_e}{(k_0 h)^2} - \varepsilon_x + \varepsilon_{re} \right) \right) \overline{\Pi}^e = 0 \qquad (2.42\text{-a})$$

$$\left(\frac{d^2}{dy^2} - k_0^2 \left(\frac{\lambda_h}{(k_0 h)^2} - \varepsilon_z + \varepsilon_{re} \right) \right) \overline{\Pi}^h = 0 \qquad (2.42\text{-b})$$

where $T^e \overline{\Pi}^e = \Pi^e$; $T^h \overline{\Pi}^h = \Pi^h$ and $n^2 = \varepsilon_x / \varepsilon_z$

Since λ_e, λ_h are diagonal matrices, the systems of ODEs eqs. (2.42-a) and 2.42-b) are then reduced to an uncoupled set of ODEs which can be solved independen In this way the last systems can be solved individually for each component as

$$\frac{d^2}{dy^2} \overline{\Pi}^e - k_{y_i}^2 \overline{\Pi}^e = 0$$

$$\frac{d^2}{dy^2} \overline{\Pi}^h - k_{y_i}^2 \overline{\Pi}^h = 0 \quad ; \quad i = 1, 2, \ldots, N \qquad (2.43)$$

where

$$k_{y_{ei}}^2 = \frac{k_o^2}{n^2}(\bar{\lambda}_{ei} - \varepsilon_x + \varepsilon_{re}) \quad , \quad k_{y_{hi}}^2 = k_o^2(\bar{\lambda}_{hi} - \varepsilon_z + \varepsilon_{re})$$

and the solution for the i-th component is

$$\bar{\Pi}_i^{e,h} = A_i^{e,h}\cosh(k_{y_i^{e,h}} y) + B_i^{e,h}\sinh(k_{y_i^{e,h}} y) \qquad (2.44)$$

Where the coefficients $A_i^{e,h}$, $B_i^{e,h}$ are obtained by using both the top and bottom boundary conditions.

Solution for the Field components

The electromagnetic field components are determined from the electric and magnetic Hertzian potentials. By using equations (2.39) and (2.40) we get

$$\begin{bmatrix} e_x \\ h_x \end{bmatrix} = \begin{bmatrix} \frac{\partial^2}{\partial x\,\partial y} & j\omega\mu_o\frac{\partial}{\partial z} \\ -j\omega\varepsilon_o\varepsilon_z\frac{\partial}{\partial z} & \frac{\partial^2}{\partial x\,\partial y} \end{bmatrix} \begin{bmatrix} \Pi^e \\ \Pi^h \end{bmatrix} \qquad (2.45\text{-a})$$

$$\begin{bmatrix} e_y \\ h_y \end{bmatrix} = (k_z^2 - \frac{\partial^2}{\partial x^2}) \begin{bmatrix} \frac{1}{n^2}I & 0 \\ 0 & I \end{bmatrix} \begin{bmatrix} \Pi^e \\ \Pi^h \end{bmatrix} \qquad (2.45\text{-b})$$

$$\begin{bmatrix} e_z \\ h_z \end{bmatrix} = \begin{bmatrix} \frac{\partial^2}{\partial z\,\partial y} & -j\omega\mu_o\frac{\partial}{\partial x} \\ j\omega\varepsilon_o\varepsilon_z\frac{\partial}{\partial x} & \frac{\partial^2}{\partial z\,\partial y} \end{bmatrix} \begin{bmatrix} \Pi^e \\ \Pi^h \end{bmatrix} \qquad (2.45\text{-c})$$

The operator $\frac{\partial}{\partial z}$ is replaced by $-jk_z$ since an $e^{-jk_z z}$ type variation is assumed, and discretizing these field components by using the same procedure as the one developed for the isotropic case, these last equations become

$$\begin{bmatrix} E_x \\ \eta_o H_x \end{bmatrix} = k_o \begin{bmatrix} k_0^{-1}h^{-1}D\frac{\partial}{\partial y} & \sqrt{\varepsilon_{re}}Ik_o \\ -\sqrt{\varepsilon_{re}}k_o\varepsilon_z I & -k^{-1}h^{-1}D^t\frac{\partial}{\partial y} \end{bmatrix} \begin{bmatrix} \Pi^e \\ \eta_o\Pi^h \end{bmatrix} \qquad (2.46\text{-a})$$

$$\begin{bmatrix} E_x \\ \eta_o H_x \end{bmatrix} = k_o \begin{bmatrix} \frac{k_o}{n^2}(\varepsilon_{re} I + \frac{h^2}{k_o^2} DD^t) & 0 \\ 0 & k_o(\varepsilon_{re} I + \frac{h^2}{k_o^2} D^t D) \end{bmatrix} \begin{bmatrix} \Pi^e \\ \eta_o \Pi^h \end{bmatrix} \qquad (2.46\text{-b})$$

$$\begin{bmatrix} E_z \\ \eta_o H_z \end{bmatrix} = jk_o \begin{bmatrix} -\sqrt{\varepsilon_{re}} I k_o^{-1} \frac{\partial}{\partial y} & h^{-1} D^t \\ \varepsilon_r h^{-1} D & -\sqrt{\varepsilon_{re}} I \frac{\partial}{\partial y} \end{bmatrix} \begin{bmatrix} \Pi^e \\ \eta_o \Pi^h \end{bmatrix} \qquad (2.46\text{-c})$$

In the transformed domain, these equations are written as

$$\begin{bmatrix} \overline{E}_x \\ \eta_o \overline{H}_x \end{bmatrix} = k_o^2 \begin{bmatrix} \overline{\delta} k_o^{-1} \frac{\partial}{\partial y} & \sqrt{\varepsilon_{re}} I \\ -\sqrt{\varepsilon_{re}} \varepsilon_r I & -\overline{\delta}^t k_o^{-1} \frac{\partial}{\partial y} \end{bmatrix} \begin{bmatrix} \overline{\Pi}^e \\ \eta_o \overline{\Pi}^h \end{bmatrix} \qquad (2.47\text{-a})$$

$$\begin{bmatrix} \overline{E}_y \\ \eta_o \overline{H}_y \end{bmatrix} = k_o^2 \begin{bmatrix} \frac{1}{n^2}(\varepsilon_{re} I + \overline{\lambda}_e) & 0 \\ 0 & (\varepsilon_{re} I + \overline{\lambda}_h) \end{bmatrix} \begin{bmatrix} \overline{\Pi}^e \\ \eta_o \overline{\Pi}^h \end{bmatrix} \qquad (2.47\text{-b})$$

$$\begin{bmatrix} \overline{E}_z \\ \eta_o \overline{H}_z \end{bmatrix} = jk_o^2 \begin{bmatrix} -\sqrt{\varepsilon_{re}} I k_o^{-1} \frac{\partial}{\partial y} & \overline{\delta}^t \\ \varepsilon_r \overline{\delta} & -\sqrt{\varepsilon_{re}} I k_o^{-1} \frac{\partial}{\partial y} \end{bmatrix} \begin{bmatrix} \overline{\Pi}^e \\ \eta_o \overline{\Pi}^h \end{bmatrix} \qquad (2.47\text{-c})$$

Another possible and useful combination of these equations, namely the electric field and the magnetic field that are necessary for the matching at the interfaces. Those electromagnetic fields must be used for both interfaces A and B as shown in Fig. 2.4. Using eqs. (2.47) and substituting $\frac{\partial}{\partial y}\Pi^{e,h}$ by means of eq. (2.15), eqs. (2.47-a,-b,-c) become :

$$\begin{bmatrix} \overline{E}_{xA} \\ \overline{E}_{xB} \end{bmatrix} = k_o^2 \overline{\delta} k_{y_e}^{-2} \begin{bmatrix} -\gamma_e & \alpha_e \\ -\alpha_e & \gamma_e \end{bmatrix} \begin{bmatrix} \overline{\Pi}_{eA} \\ \overline{\Pi}_{eB} \end{bmatrix} + \sqrt{\varepsilon_{re}} k_o^2 \begin{bmatrix} \eta_o \overline{\Pi}_{hA} \\ \eta_o \overline{\Pi}_{hB} \end{bmatrix} \qquad (2.48\text{-a})$$

$$\eta_o \begin{bmatrix} \overline{H}_{xA} \\ \overline{H}_{xB} \end{bmatrix} = -k_o^2 \sqrt{\varepsilon_{re}} \varepsilon_r \begin{bmatrix} \overline{\Pi}_{eA} \\ \overline{\Pi}_{eB} \end{bmatrix} - k_o^2 \overline{\delta}^t k_{y_h}^{-2} \begin{bmatrix} -\gamma_h & \alpha_h \\ -\alpha_h & \gamma_h \end{bmatrix} \begin{bmatrix} \eta_o \overline{\Pi}_{hA} \\ \eta_o \overline{\Pi}_{hB} \end{bmatrix} \qquad (2.48\text{-b})$$

$$\begin{bmatrix} j\overline{E}_{zA} \\ j\overline{E}_{zB} \end{bmatrix} = k_o^2 \sqrt{\varepsilon_{re}} k_{y_e}^2 \begin{bmatrix} -\gamma_e & \alpha_e \\ -\alpha_e & \gamma_e \end{bmatrix} \begin{bmatrix} \overline{\Pi}_{eA} \\ \overline{\Pi}_{eB} \end{bmatrix} - k_o^2 \overline{\delta}' \begin{bmatrix} \eta_o \overline{\Pi}_{hA} \\ \eta_o \overline{\Pi}_{hB} \end{bmatrix} \qquad (2.48\text{-c})$$

$$\eta_o \begin{bmatrix} j\overline{H}_{zA} \\ j\overline{H}_{zB} \end{bmatrix} = -k_o^2 \varepsilon_r \overline{\delta} \begin{bmatrix} \overline{\Pi}_{eA} \\ \overline{\Pi}_{eB} \end{bmatrix} - k_o^2 \sqrt{\varepsilon_{re}} k_{y_h}^2 \begin{bmatrix} -\gamma_h & \alpha_h \\ -\alpha_h & \gamma_h \end{bmatrix} \begin{bmatrix} \eta_o \overline{\Pi}_{hA} \\ \eta_o \overline{\Pi}_{hB} \end{bmatrix} \qquad (2.48\text{-d})$$

The electromagnetic fields along y-direction that are useful for computing characteristic impedance are also given for both interfaces by means of eq. (2.47-b) as :

$$\begin{bmatrix} \overline{E}_{xA} \\ \overline{E}_{xB} \end{bmatrix} = \frac{k_o^2}{n^2} (\varepsilon_{re} I + \overline{\lambda}_e) \begin{bmatrix} \overline{\Pi}_{eA} \\ \overline{\Pi}_{eB} \end{bmatrix} \qquad (2.49\text{-a})$$

$$\eta_o \begin{bmatrix} \overline{H}_{xA} \\ \overline{H}_{xB} \end{bmatrix} = k_o^2 (\varepsilon_{re} I + \overline{\lambda}_h) \begin{bmatrix} \eta_o \overline{\Pi}_{hA} \\ \eta_o \overline{\Pi}_{hB} \end{bmatrix} \qquad (2.49\text{-b})$$

Since it is difficult to establish a matching equations for electric and magnetic Hertzian potentials Π_e and Π_h, it is either necessary to discard them. To this end, Π_e and Π_h are expressed in terms of E_x and E_z as

$$\begin{bmatrix} \overline{\Pi}_{eA} \\ \overline{\Pi}_{eB} \end{bmatrix} = k_o^{-2} \left(\overline{\lambda}_e + \varepsilon_{re} I \right)^{-1} \begin{bmatrix} -\gamma_e & \alpha_e \\ -\alpha_e & \gamma_e \end{bmatrix} \left\{ \overline{\delta}' \begin{bmatrix} \overline{E}_{xA} \\ \overline{E}_{xB} \end{bmatrix} + \sqrt{\varepsilon_{re}} \begin{bmatrix} j\overline{E}_{zA} \\ j\overline{E}_{zB} \end{bmatrix} \right\} \qquad (2.50\text{-a})$$

$$\eta_o \begin{bmatrix} \overline{\Pi}_{hA} \\ \overline{\Pi}_{hB} \end{bmatrix} = k_o^{-2} \left(\overline{\lambda}_h + \varepsilon_{re} I \right)^{-1} \left\{ \sqrt{\varepsilon_{re}} \begin{bmatrix} \overline{E}_{xA} \\ \overline{E}_{xB} \end{bmatrix} - \overline{\delta} \begin{bmatrix} j\overline{E}_{zA} \\ j\overline{E}_{zB} \end{bmatrix} \right\} \qquad (2.50\text{-b})$$

and substituting these equations into eqs. (2.48-b) and (2.48-d), a relation between the tangential components in both interfaces A and B is obtained as

$$\eta_o \begin{bmatrix} \overline{H}_{xA} \\ \overline{H}_{xB} \end{bmatrix} = \left(\overline{\delta} k_{y_e}^2 \begin{bmatrix} \gamma_h & \alpha_h \\ \alpha_h & \gamma_h \end{bmatrix} \left(\overline{\lambda}_h + \varepsilon_{re} I \right)^{-1} + \varepsilon_r \left(\overline{\lambda}_e + \varepsilon_{re} I \right)^{-1} \begin{bmatrix} \gamma_e & \alpha_e \\ \alpha_e & \gamma_e \end{bmatrix} \overline{\delta} \right) \begin{bmatrix} \overline{E}_{xA} \\ -\overline{E}_{xB} \end{bmatrix}$$
$$+ \left(\overline{\delta} k_{y_e}^2 \begin{bmatrix} \gamma_h & \alpha_h \\ \alpha_h & \gamma_h \end{bmatrix} \left(\overline{\lambda}_h + \varepsilon_{re} I \right)^{-1} - \varepsilon_{re} \varepsilon_r \left(\overline{\lambda}_e + \varepsilon_{re} I \right)^{-1} \begin{bmatrix} \gamma_e & \alpha_e \\ \alpha_e & \gamma_e \end{bmatrix} \right) \begin{bmatrix} -j\overline{E}_{zA} \\ j\overline{E}_{zB} \end{bmatrix} \qquad (2.51\text{-a})$$

$$\begin{bmatrix} -j\overline{H}_{zA} \\ -j\overline{H}_{zB} \end{bmatrix} = \left(\varepsilon_{re} k_{y_n}^2 \begin{bmatrix} \gamma_h & \alpha_h \\ \alpha_h & \gamma_h \end{bmatrix} (\overline{\lambda}_h + \varepsilon_{re} I)^{-1} - \varepsilon_{re} \overline{\delta} (\overline{\lambda}_e + \varepsilon_{re} I)^{-1} \begin{bmatrix} \gamma_e & \alpha_e \\ \alpha_e & \gamma_e \end{bmatrix} \overline{\delta}^{-1} \right) \begin{bmatrix} \overline{E}_{xA} \\ -\overline{E}_{xB} \end{bmatrix}$$
$$+ \left(\varepsilon_{re} \overline{\delta} (\overline{\lambda}_e + \varepsilon_{re} I)^{-1} \begin{bmatrix} \gamma_e & \alpha_e \\ \alpha_e & \gamma_e \end{bmatrix} + k_{y_n}^2 \begin{bmatrix} \gamma_h & \alpha_h \\ \alpha_h & \gamma_h \end{bmatrix} (\overline{\lambda}_h + \varepsilon_{re} I)^{-1} \overline{\delta} \right) \begin{bmatrix} -j\overline{E}_{zA} \\ j\overline{E}_{zB} \end{bmatrix}$$

(2.51-b)

The electromagnetic fields along y-direction are finally given by

$$\begin{bmatrix} \overline{E}_{xA} \\ \overline{E}_{xB} \end{bmatrix} = \begin{bmatrix} \gamma_e & \alpha_e \\ \alpha_e & \gamma_e \end{bmatrix} \overline{\delta}^{-1} \begin{bmatrix} \overline{E}_{xA} \\ -\overline{E}_{xB} \end{bmatrix} + \varepsilon_{re} \begin{bmatrix} \gamma_e & \alpha_e \\ \alpha_e & \gamma_e \end{bmatrix} \begin{bmatrix} -j\overline{E}_{zA} \\ j\overline{E}_{zB} \end{bmatrix} \qquad (2.52\text{-a})$$

$$\eta_o \begin{bmatrix} \overline{H}_{xA} \\ \overline{H}_{xB} \end{bmatrix} = \sqrt{\varepsilon_{re}} \begin{bmatrix} I & 0 \\ 0 & -I \end{bmatrix} \begin{bmatrix} \overline{E}_{xA} \\ -\overline{E}_{xB} \end{bmatrix} - \overline{\delta} \begin{bmatrix} I & 0 \\ 0 & -I \end{bmatrix} \begin{bmatrix} -j\overline{E}_{zA} \\ -j\overline{E}_{zB} \end{bmatrix} \qquad (2.52\text{-b})$$

The relation between the tangential magnetic field H_x and H_z and the tangential electric field E_x and E_z, is now established and has the form

$$\eta_o \begin{bmatrix} -j\overline{H}_{zA} \\ \overline{H}_{xA} \\ -j\overline{H}_{zB} \\ \overline{H}_{xB} \end{bmatrix} = \begin{bmatrix} -\tilde{\gamma}_H & \tilde{\delta}\overline{\gamma}_e + \tilde{\gamma}_h\tilde{\delta} & -\tilde{\alpha}_H & \tilde{\delta}\overline{\alpha}_e + \overline{\alpha}_h\tilde{\delta} \\ \overline{\gamma}_e\tilde{\delta}^t + \tilde{\delta}^t\tilde{\gamma}_h & \tilde{\gamma}_E & \overline{\alpha}_e\tilde{\delta}^t + \tilde{\delta}^t\overline{\alpha}_h & \tilde{\alpha}_E \\ -\tilde{\alpha}_H & \tilde{\delta}\overline{\alpha}_e - \overline{\alpha}_h\tilde{\delta} & -\tilde{\gamma}_H & \tilde{\delta}\overline{\gamma}_e - \tilde{\gamma}_h\tilde{\delta} \\ \overline{\alpha}_e\tilde{\delta}^t - \tilde{\delta}^t\overline{\alpha}_h & \tilde{\alpha}_E & \overline{\gamma}_e\tilde{\delta}^t + \tilde{\delta}^t\tilde{\gamma}_h & \tilde{\gamma}_E \end{bmatrix} \begin{bmatrix} \overline{E}_{xA} \\ -j\overline{E}_{zA} \\ -\overline{E}_{xB} \\ j\overline{E}_{zB} \end{bmatrix} \qquad (2.53)$$

with the following abbreviation :

$$\overline{\alpha}_e = \varepsilon_{re} (\overline{\lambda}_e + \varepsilon_{re} I)^{-1} \alpha_e \quad ; \quad \tilde{\alpha}_E = \overline{\delta}^t \overline{\alpha}_h \overline{\delta} - \varepsilon_{re} \overline{\alpha}_e$$
$$\overline{\gamma}_e = \varepsilon_{re} (\overline{\lambda}_e + \varepsilon_{re} I)^{-1} \gamma_e \quad ; \quad \tilde{\gamma}_E = \overline{\delta}^t \tilde{\gamma}_h \overline{\delta} - \varepsilon_{re} \overline{\gamma}$$
$$\overline{\alpha}_h = k_{y_n}^2 \alpha_h (\overline{\lambda}_h + \varepsilon_{re} I)^{-1} \quad ; \quad \tilde{\alpha}_H = \overline{\delta} \overline{\alpha}_e \overline{\delta}^t - \varepsilon_{re} \overline{\alpha}_h$$
$$\overline{\gamma}_h = k_{y_n}^2 \gamma_h (\overline{\lambda}_h + \varepsilon_{re} I)^{-1} \quad ; \quad \tilde{\gamma}_H = \overline{\delta} \overline{\gamma}_e \overline{\delta}^t - \varepsilon_{re} \tilde{\gamma}_h$$
$$\tilde{\delta} = \sqrt{\varepsilon_{re}}\, \overline{\delta}$$

Collating these equations and using the definition according to eq. (2.23), eq. (2.53) becomes :

$$\begin{bmatrix} \overline{H}_A \\ \overline{H}_B \end{bmatrix} = \begin{bmatrix} \overline{y}_1 & \overline{y}_2 \\ \overline{y}_2 & \overline{y}_1 \end{bmatrix} \begin{bmatrix} \overline{E}_A \\ -\overline{E}_B \end{bmatrix} \qquad (2.54)$$

$$\bar{y}_1 = \begin{bmatrix} -\tilde{\gamma}_H & \tilde{\delta}\bar{\gamma}_e + \tilde{\gamma}_h\tilde{\delta} \\ \bar{\gamma}_e\tilde{\delta}' + \tilde{\delta}'\tilde{\gamma}_h & \tilde{\gamma}_E \end{bmatrix} \quad ; \quad \bar{y}_2 = \begin{bmatrix} -\tilde{\alpha}_H & \tilde{\delta}\bar{\alpha}_e + \bar{\alpha}_h\tilde{\delta} \\ \bar{\alpha}_e\tilde{\delta}' + \tilde{\delta}'\bar{\alpha}_h & \tilde{\alpha}_E \end{bmatrix} \qquad (2.55)$$

The representation of eq. (2.54) is in conformity with eq. (2.23) which was developed earlier. We note also that the matrices $\bar{y}_1$ and $\bar{y}_2$ are diagonal or quasi-diagonal matrices depending on the lateral boundaries.

2.6 Field Transformations between Dielectric Interfaces

In a general microwave structure of multi-layer dielectrics, the scalar wave equations (2.33) and (2.41) are considered in each separate layer. The general form of the solution in each region has been derived and are described by eqs. (2.14) and (2.44), but it is still not completely determined, since at each discretization line, two constants of which are yet unknown. This can only be achieved by using low and high limit conditions of each layer. However , each layer does not possess top and bottom boundary conditions, but it is rather interfaced to its neighbourhood layers. This is so, except for the first and the last layers that are subject to boundary conditions, due to the shielding of the considered structure as shown in Fig. 2.5. The treatment of this situation may be alleviated when the electromagnetic field continuity conditions are supplied.

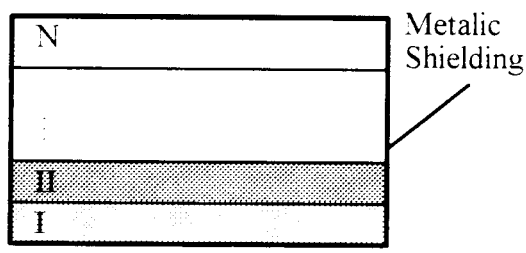

Fig. 2.4 Structure of multidielectric layers

It has been established [26,27] that in the absence of metallization conductors, the tangential electromagnetic fields are continuous along a dielectric interfaces whereas in the presence of metallization the discontinuity takes place. Using the continuity conditions of dielectric interfaces, the unknown coefficients are translated to the supplied top and bottom boundary conditions. In order to fulfil this requirement, a suitable relation that transforms the tangential field components from one plane to the other is performed, and hence, constituting a formal way for several dielectric layers case.

It is convenient to set up a relationship between the tangential electromagnetic fields of one plane A with those of the other plane B as depicted in Fig. 2.4. It is easy to convert eqs. (2.23) and (2.54) to

$$\begin{bmatrix} \overline{E_B} \\ \overline{H_B} \end{bmatrix} = \begin{bmatrix} \overline{\Gamma} & \overline{Z} \\ \overline{Y} & \overline{\Gamma} \end{bmatrix} \begin{bmatrix} \overline{E_A} \\ \overline{H_A} \end{bmatrix} \qquad (2.56\text{-a})$$

Where

$$\overline{\Gamma} = \overline{y}_2^{-1}\overline{y}_1 = \overline{y}_1\overline{y}_2^{-1} \quad ; \quad \overline{Y} = \overline{y}_2 - \overline{y}_1\overline{y}_2^{-1}\overline{y}_1 \quad ; \quad \overline{Z} = -\overline{y}_2^{-1} \qquad (2.56\text{-b})$$

The inversion of eq. (2.47) is

$$\begin{bmatrix} \overline{E_A} \\ \overline{H_A} \end{bmatrix} = \begin{bmatrix} \overline{\Gamma} & -\overline{Z} \\ -\overline{Y} & \overline{\Gamma} \end{bmatrix} \begin{bmatrix} \overline{E_B} \\ \overline{H_B} \end{bmatrix} \qquad (2.57)$$

For the case of the structure shown in Fig. 2.5, $\overline{E_0} = 0$ for a metallic shielding at the interface 0. In the first step, for the first dielectric interface, the relation of the tangential magnetic and electric field can be obtained using eq. (2.56)

$$\overline{H}_1 = \overline{Y}_t^{(1)}\,\overline{E}_1 \qquad (2.58\text{-a})$$

with

$$\overline{Y}_t^{(1)} = \overline{\Gamma}_1\overline{Z}_1^{-1} = -\overline{y}_1 \qquad (2.58\text{-b})$$

$\overline{y}_1$, $\overline{Z}_1$ are determined according to the properties of dielectric layer 1. At the interface 1, the top plane of the first dielectric layer is in turn superposed to the bottom plane of the second dielectric layer. Then, by means of this last equation (2.58), for the second layer equation (2.56) becomes :

$$\begin{bmatrix} \overline{E_2} \\ \overline{H_2} \end{bmatrix} = \begin{bmatrix} \overline{\Gamma}_2 & \overline{Z}_2 \\ \overline{Y}_2 & \overline{\Gamma}_2 \end{bmatrix} \begin{bmatrix} \overline{E_1} \\ \overline{Y}_t^{(1)}\overline{E}_1 \end{bmatrix} \qquad (2.59)$$

In the same way as eq. (2.58), the relation of the tangential component at the interface 2 is given by :

$$\overline{H}_2 = \overline{Y}_t^{(2)}\,\overline{E}_2 \qquad (2.60\text{-a})$$

with

$$\overline{Y}_t^{(2)} = \left(\overline{Y}_2 + \overline{\Gamma}_2 \overline{Y}_t^{(1)} \right) \left(\overline{\Gamma}_2 + \overline{Z}_2 \overline{Y}_t^{(1)} \right)^{-1} \qquad (2.60\text{-b})$$

generalising this relation to an arbitrary interface k by means of a recurrence relation, we obtain

$$\overline{H}_k = \overline{Y}_t^{(k)} \, \overline{E}_k \qquad (2.61\text{-a})$$

with

$$\overline{Y}_t^{(k)} = \left(\overline{Y}_k + \overline{\Gamma}_k \overline{Y}_t^{(k-1)} \right) \left(\overline{\Gamma}_k + \overline{Z}_k \overline{Y}_t^{(k-1)} \right)^{-1} \qquad (2.61\text{-b})$$

$\overline{Y}_t^{(k)}$ can be represented in the following form

$$\overline{Y}_t^{(k)} = \begin{bmatrix} \overline{y}_{11} & \overline{y}_{12} \\ \overline{y}_{21} & \overline{y}_{22} \end{bmatrix}_k \qquad (2.62)$$

When a magnetic wall occurs at the interface 0, then instead of $\overline{E}_0 = 0$ there is $\overline{H}_0 = 0$. The recurrence relation (2.61) is performed in the same way as above except for the first step, where from eq. (2.40) we can get

$$\overline{Y}_t^{(1)} = \overline{Y}_1 \overline{\Gamma}_1^{-1} \qquad (2.63)$$

We can also start from the upper boundary in the same manner as that developed above for the lower boundary case. But in this case we use eq. (2.57) instead of eq. (2.56) and transform the field components downwards.

For the first interface, we obtain either $\overline{E}_0 = 0$ or $\overline{H}_0 = 0$ according to boundary condition at the interface 0. From eq. (2.57), it follows

$$\overline{H}_1 = -\overline{Y}_t^{(1)} \, \overline{E}_1 \qquad (2.64)$$

Where, for the electric wall starting boundary conditions, we have

$$\overline{Y}_t^{(1)} = \overline{\Gamma}_1 \overline{Z}_1^{-1} \qquad (2.65)$$

and for the magnetic wall boundary condition

$$\overline{Y}_t^{(1)} = \overline{Y}_1 \overline{\Gamma}_1^{-1} \qquad (2.66)$$

At interface l , the following equation for the field components are then derived

$$\overline{H}_l = -\overline{Y}_l^{(l)} \overline{E}_l \qquad l = 2,3,\ldots \tag{2.67}$$

with the recurrence relation,

$$\overline{Y}_l^{(l)} = \left(\overline{Y}_l + \overline{\Gamma}_l \overline{Y}_l^{(l+1)} \right) \left(\overline{\Gamma}_l - \overline{Z}_l \overline{Y}_l^{(l+1)} \right)^{-1} \tag{2.68}$$

The relationship between the tangential components has been established in the case where no metallization is present at dielectric interfaces. However, if a metallization exists at the interface m, the discontinuity of the tangential magnetic field occurs at the interface and is given by

$$H_{m^+} - H_{m^-} = -J_m \tag{2.69}$$

In the transformed domain eq.(2.69) becomes

$$\overline{H}_{m^+} - \overline{H}_{m^-} = -\overline{J}_m \tag{2.70}$$

This situation is valid only when the metallization has vanishing thickness, hence, only the tangential components of the current density are taken into account, that is $\overline{J}_m = \eta_n \left(j\overline{J}_x^t, \overline{J}_z^t \right)^t$. The upper side of the metallization interface is designated by m^+ and the lower side by m^- as shown in Fig. 2.5.

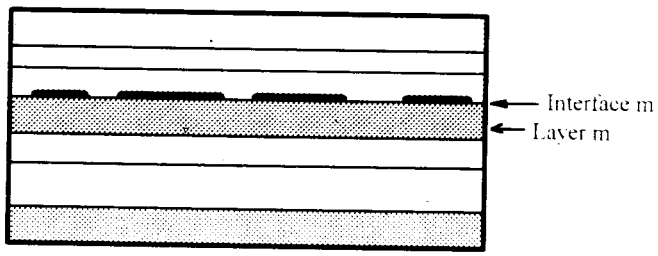

Fig 2.5 A typical structure of multi-layers and single metallization interface

When the lower boundary limit is considered as starting case, it is useful to compute the tangential magnetic field for a subsequent transformation over the substrate layer m+1, H_{4^-} in the right hand side of eq. (2.56) must be substituted with

$$\overline{H}_{m^+} = \overline{H}_{m^-} - \overline{J}_m = \overline{Y}_l^{(m)} \overline{E} - \overline{J}_m \tag{2.71}$$

For the components at the interface m+1, by using eq. (2.47) we obtain

$$\overline{H}_{m+1} = \overline{Y}_t^{(m+1)}\overline{E}_{m+1} - (\overline{Y}^{(m+1)}\overline{Z}_{m+1} - \overline{\Gamma}_{m+1})\overline{J}_m \qquad (2.72)$$

with a recurrence relations

$$\overline{Y}^{(m+1)} = \overline{Y}_{m+1} + \overline{\Gamma}_{m+1}\overline{Y}_t^{(m)} \qquad (2.73\text{-a})$$

and

$$\overline{Y}_t^{(m+1)} = \overline{Y}^{(m+1)}\left(\overline{\Gamma}_{m+1} + \overline{Z}_{m+1}\overline{Y}_t^{(m)}\right)^{-1} \qquad (2.73\text{-b})$$

In the same way it is also possible to start form the upper cover and performing transformations downwards rather than starting from lower boundary limit as previously done.

2.7 Field Matching in the Transformed Domain

Steeping further our objective to obtain a complete determination of the solution over all the structure, where, after inserting the top and bottom boundary conditions and by means of the field transformations between dielectric plane interfaces and matching the field at the metallic interface, an algebraic relation is obtained. This relation connects the tangential field components of the electric field $\overline{E} = \left(\overline{E}_x', -j\overline{E}_z'\right)^t$ with the current densities $\overline{J} = \eta_o\left(j\overline{J}_x', \overline{J}_z'\right)^t$ in the transformed domain as.

$$\overline{J}_M = f(\overline{E}_M) \quad \text{or} \quad \overline{E}_M = f(\overline{J}_M)$$

This retrieved relation has to be performed for structures of multilayer dielectrics with single or multiple metallization interfaces of perfect metallic conductors with vanishing thickness.

2.7-1 Multilayers Single Metallization Interface Structures

The concerned structure consists of an arbitrary number of substrate layers below and above the metallization interface (MI), which are respectively denoted by n_l and n_h as shown in Fig. 2.6.

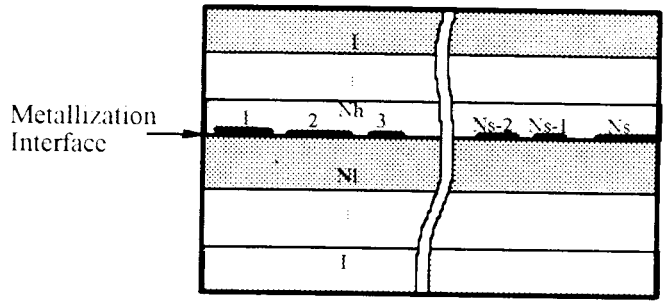

Fig. 2.6

A structure of Multilayer and single metallization interface

The transformation of the fields from above and below of the MI must be matched to each other at the remaining dielectric interfaces. Let e.g. the interface n_l (counted from the bottom) and the interface n_h (counted from the top) be identical at the metallization interface (marked M, Fig. 2.1 with $n_l = 2$, $n_h = 1$). At this interface, the matching equations are given by

$$\overline{E}_{nl} = \overline{E}_{nh} = \overline{E}_M \qquad (2.74\text{-a})$$

$$\overline{H}_{nh} - \overline{H}_{nl} = \overline{J}_M \qquad (2.74\text{-b})$$

Using eqs. (2.61) and (2.67) and with the help of eq. (2.74-b), we get the following algebraic relation for the transformed current densities in terms of the transformed electric field

$$\left(\overline{Y}_t^{(n_h)} + \overline{Y}_t^{(n_l)}\right)\overline{E}_M = \overline{J}_M \qquad (2.75)$$

This previous relation form is used when the strip metallization has small width, however, an inverse relation is preferred as long as the slot is of small width. In the transformed domain where all the matrices are diagonal, it is easy to invert eq. (2.75) to get the required relation that connects the electric field to the current densities given by

$$\left(\overline{Y}_t^{(n_h)} + \overline{Y}_t^{(n_l)}\right)^{-1}\overline{J}_M = \overline{E}_M \qquad (2.76)$$

The ultimate reason for the choice between the two settled relations (2.75) and (2.76) is to minimise the size of matrices in the original domain. Consequently, this brings significant reduction of memory space as well as computing time. This is clarified in the next section.

2.7-2 Structures of Multilayers Multi-metallization Interfaces

For a general structure which consists of a multidielectric layer dielectrics multi-metallization interfaces as shown in Fig. 2.7. The integer m designate the number of arbitrary MI and N_i, the number of dielectric layers between each successive (i and $i-1$) MI. The top layer set is designated by N_{m+1}.

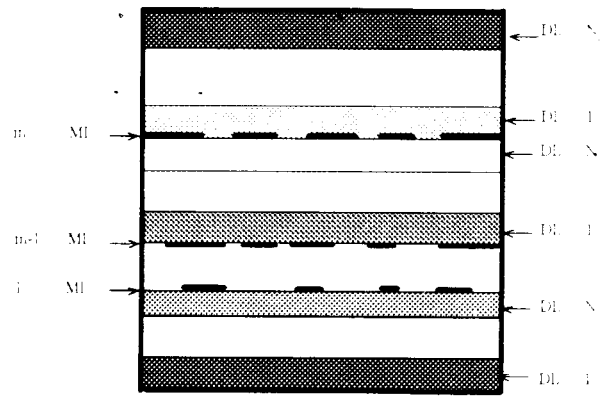

Fig. 2.7
A typical multidielectric layer multi-metallization interfaces structure

MI : Metallization Interface
DL : Dielectric layer

At metallization interfaces MI_1 and MI_m, according to the relations (2.59) and (2.68), the following equations must hold

$$\overline{H}_1^{n_1} = \overline{Y}_t^{(n_1)} \overline{E}_1 \qquad (2.77\text{-a})$$

$$\overline{H}_m^{n_{m+1}} = -\overline{Y}_t^{(n_{m+1})} \overline{E}_m \qquad (2.77\text{-b})$$

Besides the set of layers located below MI_1 and MI_m, a helpful relation must be deri[illegible] connecting the tangential field components at the MI_k and those of MI_{k-1}. For this purpose, a set of N_k successive dielectric layers located between two metallization interfaces MI_k and MI_{k-1}, as shown in Fig. 2.8.

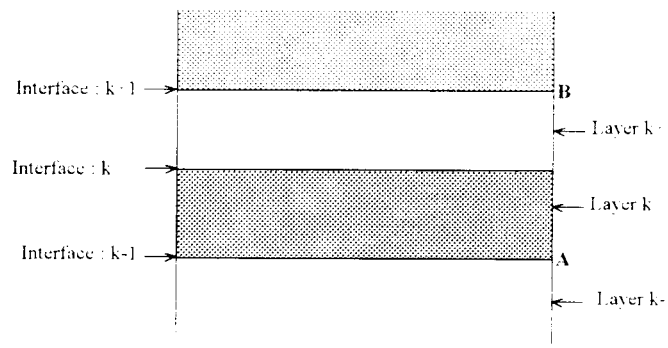

Fig 2.8 A successive dielectric interfaces with no metallization interface

According to eq.(2.54), the relationship of the tangential field components for the k-th layer are governed by

$$\begin{bmatrix} \overline{H}_{k-1} \\ \overline{H}_k \end{bmatrix} = \begin{bmatrix} \overline{y}_1^k & \overline{y}_2^k \\ \overline{y}_2^k & \overline{y}_1^k \end{bmatrix} \begin{bmatrix} \overline{E}_{k-1} \\ -\overline{E}_k \end{bmatrix} \qquad (2.78\text{-a})$$

and for the layer $k-1$, they are given by :

$$\begin{bmatrix} \overline{H}_k \\ \overline{H}_{k-1} \end{bmatrix} = \begin{bmatrix} \overline{y}_1^{k-1} & \overline{y}_2^{k-1} \\ \overline{y}_2^{k-1} & \overline{y}_1^{k-1} \end{bmatrix} \begin{bmatrix} \overline{E}_k \\ -\overline{E}_{k-1} \end{bmatrix} \qquad (2.78\text{-b})$$

Where (-) and (+) designate respectively the bottom and top sides of the appropriate layer.

Using the continuity condition of the field component at the dielectric interface k, it is easy to obtain the relationship between the field component of the bottom side of layer k or top side of layer $k-1$, and those of top side of layer $k-1$, as shown in Fig. 2.8.

The resulted equation can be described by the following general recurrence relation :

$$\begin{bmatrix} \overline{H}_k \\ \overline{H}_{k-1} \end{bmatrix} = \begin{bmatrix} \overline{y}_{11_r}^{k-1} & \overline{y}_{12_r}^{k-1} \\ \overline{y}_{21_r}^{k-1} & \overline{y}_{22_r}^{k-1} \end{bmatrix} \begin{bmatrix} \overline{E}_k \\ -\overline{E}_{k-1} \end{bmatrix} \qquad (2.79\text{-a})$$

with

$$\overline{y}_{11_r}^{k-1} = \overline{y}_1^k - \overline{y}_2^k \left(\overline{y}_1^k + \overline{y}_1^{k-1} \right)^{-1} \overline{y}_2^k \quad ; \quad \overline{y}_{12_r}^{k-1} = \overline{y}_2^k \left(\overline{y}_1^k + \overline{y}_1^{k-1} \right)^{-1} \overline{y}_2^{k-1}$$

$$\overline{y}_{21_r}^{k-1} = \overline{y}_2^{k-1} \left(\overline{y}_1^k + \overline{y}_1^{k-1} \right)^{-1} \overline{y}_2^k \quad ; \quad \overline{y}_{22_r}^{k-1} = \overline{y}_1^{k-1} - \overline{y}_2^{k-1} \left(\overline{y}_1^k + \overline{y}_2^{k-1} \right)^{-1} \overline{y}_2^{k-1} \qquad (2.79\text{-b})$$

$$k = 0, \ldots, N_i + 1$$

Where N_i is the number of dielectric layers between two MIs as illustrated in Fig. 2.9 .

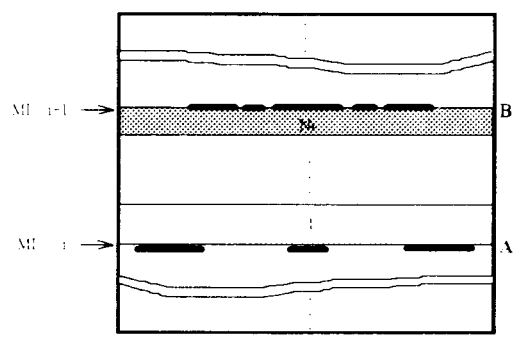

Fig 2.9

Illustration of Ni dielectric layers between two metallization Interfaces i and i+1

In order to get a relation for the tangential field components between interfaces A and B, it is necessary to use *Ni-1* times the recurrence relation to reach the final relationship. For the interfaces i and $i-1$ as indicated in Fig. 2.9, the following equation form is obtained as :

$$\begin{bmatrix} \overline{H}_A^i \\ \overline{H}_B^i \end{bmatrix} = \begin{bmatrix} \overline{y}_{11}^i & \overline{y}_{12}^i \\ \overline{y}_{21}^i & \overline{y}_{22}^i \end{bmatrix} \begin{bmatrix} \overline{E}_A^i \\ -\overline{E}_B^i \end{bmatrix} \qquad (2.80)$$

and $y_{p,q}^i$ ($p, q = 1, 2$) are derived from the recurrence relation (2.79).

In the next step, we consider three arbitrary successive MIs, *i-1*, *i*, $i-1$. According to eq. (2.80), the following relations for MI i and $i-1$ must hold :

$$\begin{bmatrix} \overline{H}_l^i \\ \overline{H}_h^i \end{bmatrix} = \begin{bmatrix} \overline{y}_{11}^i & \overline{y}_{12}^i \\ \overline{y}_{21}^i & \overline{y}_{22}^i \end{bmatrix} \begin{bmatrix} \overline{E}_l^i \\ -\overline{E}_h^i \end{bmatrix} \qquad (2.81\text{-a})$$

$$\begin{bmatrix} \overline{H}_l^{i-1} \\ \overline{H}_h^{i-1} \end{bmatrix} = \begin{bmatrix} \overline{y}_{11}^{i-1} & \overline{y}_{12}^{i-1} \\ \overline{y}_{21}^{i-1} & \overline{y}_{22}^{i-1} \end{bmatrix} \begin{bmatrix} \overline{E}_l^{i-1} \\ -\overline{E}_h^{i-1} \end{bmatrix} \qquad (2.81\text{-b})$$

Where the subscript *l*, *h* designate respectively the lower and higher sides of the regions. Matching the field component at the interface i , we get

$$\overline{H}_h^i - \overline{H}_l^{i-1} = \overline{J}_i \qquad (2.82\text{-a})$$

$$\overline{E}_h^i = \overline{E}_l^{i-1} = \overline{E}_i \qquad (2.82\text{-b})$$

This yields the following recurrence relation for the i-th arbitrary MI :

$$\overline{L}_i \overline{E}_{i-1} + \overline{K}_i \overline{E}_i + \overline{R}_i \overline{E}_{i-1} = \overline{J}_i \quad ; \quad i = 2, 3, \ldots, m-1 \qquad (2.83\text{-a})$$

Where $\overline{L}_i = \overline{y}_{21}^i \quad ; \quad \overline{K}_i = -\overline{y}_{22}^i - \overline{y}_{11}^{i-1} \quad ; \quad \overline{R}_i = \overline{y}_{12}^{i-1}$

(2.83-b)

This equation is not valid for the first and the last MI, but it may be extended after matching the fields at these interfaces using eqs. (2.77-a) and (2.77-b). Thus, eq. (2.83) becomes

$$\overline{L}_i \overline{E}_{i-1} + \overline{K}_i \overline{E}_i + \overline{R}_i \overline{E}_{i-1} = \overline{J}_i \quad ; \quad i = 1, 2, \ldots, m \qquad (2.84\text{-a})$$

and

$$\overline{L}_i = \begin{cases} \overline{y}_{21}^{\,i} & \text{for} \quad i = 2,3,\ldots,m \\ 0 & i = 1 \end{cases} \qquad (2.84\text{-b})$$

$$\overline{K}_i = \begin{cases} \overline{y}_{22}^{\,i} - \overline{y}_{11}^{\,i-1} & \text{for} \quad i = 2,3,\ldots,m-1 \\ \overline{y}_{22}^{\,m} - \overline{y}_{t}^{\,(m)} & i = m \\ \overline{y}_{t}^{\,(1)} - \overline{y}_{t}^{\,(1)} & i = 1 \end{cases} \qquad (2.84\text{-c})$$

$$\overline{R}_i = \begin{cases} \overline{y}_{12}^{\,1} & \text{for} \quad i = 1 \\ \overline{y}_{12}^{\,i-1} & i = 2,3,\ldots,m-1 \\ 0 & i = m \end{cases} \qquad (2.84\text{-d})$$

Where $\overline{y}_t^{(m)}$ and $\overline{y}_t^{(1)}$ are respectively defined in eq. (2.77-a) and eq. (2.77-b) for the case of the metallic shielding where $\overline{E}_0 = \overline{E}_{m-1} = 0$. This relation may be represented in matrix form as

$$\begin{bmatrix} \overline{K}_1 & \overline{R}_1 & & & \\ \overline{L}_2 & \overline{K}_2 & \overline{R}_2 & & \\ & \ddots & \ddots & \ddots & \\ & & \overline{L}_{m-1} & \overline{K}_{m-1} & \overline{R}_{m-1} \\ & & & \overline{L}_m & \overline{K}_m \end{bmatrix} \begin{bmatrix} \overline{E}_1 \\ \overline{E}_2 \\ \vdots \\ \overline{E}_{m-1} \\ \overline{E}_m \end{bmatrix} = \begin{bmatrix} \overline{J}_1 \\ \overline{J}_2 \\ \vdots \\ \overline{J}_{m-1} \\ \overline{J}_m \end{bmatrix} \qquad (2.85\text{-a})$$

or in a shorten form as

$$\overline{\overline{Y}}\,\overline{\overline{E}} = \overline{\overline{J}} \qquad (2.85\text{-b})$$

For reasons indicated in section (2.6.1), it is advised to have the electric field in terms the current densities. Therefore an inversion of this tridiagonal block matrices may be accelerated, by applying a suitable algorithm [ ] " Gauss elimination for tridiagonal matrices" since the elements of block matrices are diagonals, such that :

$$\overline{\overline{Z}}\,\overline{\overline{J}} = \overline{\overline{E}} \qquad (2.86)$$

Where $\overline{\overline{Z}} = \overline{\overline{Y}}^{-1}$

It is worth also to note that other developments are not excluded in order to obtain an optimal system of equations. That is in situations as indicated so far, where a mixed vector containing electric fields and current densities are expressed in terms of the

remaining electric fields $\overline{\overline{E}}$ and current densities $\overline{\overline{J}}$ components. It is not simple to generalise the optimal system for all possible structure cases. For simplicity we adopt either system of eq. (2.85) or that of eq. (2.86) , which leads namely to a simple optimal system.

2.8 Field Matching in Spatial Domain

The established systems in the transformed domain eq. (2.75) or (2.76) and eq. (2.85) or (2.86) mutually relate the current densities and the electric field components. These systems should be solved since both of them are yet unknown. The considered system may be dissociated by introducing further conditions that have to be fulfilled on the metallization interface. However, these conditions are valid only in the original domain. As known in EM. theory, the tangential electric field components on the metallization (metal strip) and the current densities in the dielectric (slots) must be zero.

$$E_{x_j} = E_{z_j} = 0 \qquad j: \text{ strip number}$$
$$J_{x_k} = J_{z_k} = 0 \qquad k: \text{ region on the slot number}$$

2. 8-1 Single Metallization Interface

For the case of a single metallization interface M containing p metallic strips as shown in Fig. 2.10, the electric field components E and the current densities J can be represented by

$$J_{x_M} = \begin{bmatrix} J_{xm_1} \\ 0 \\ \vdots \\ J_{xm_p} \\ 0 \end{bmatrix} \; ; \; J_{z_M} = \begin{bmatrix} J_{zm_1} \\ 0 \\ \vdots \\ J_{zm_p} \\ 0 \end{bmatrix} \; ; \; E_{z_M} = \begin{bmatrix} 0 \\ E_{zs_1} \\ \vdots \\ 0 \\ E_{zs_p} \end{bmatrix} \; ; \; E_{x_M} = \begin{bmatrix} 0 \\ E_{xs_1} \\ \vdots \\ 0 \\ E_{xs_p} \end{bmatrix} \qquad (2.87)$$

The subscript m in J_x and J_z stands for metallization and the subscript s in E_x and E_z stands for slots between strip conductors.

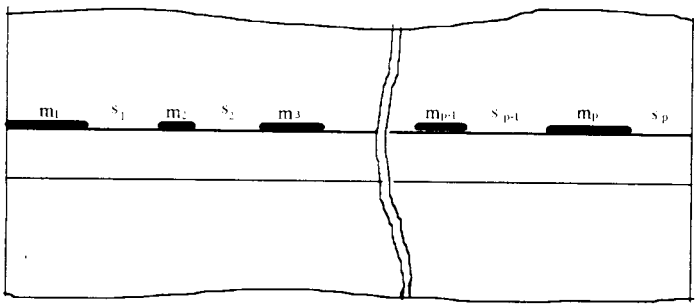

Fig. 2.11 A typical partial cross-section view of a structure with a Metallization interface of p-strip conductors

Note that the number of metallic strips p is assumed to be equal to that of the slots, but practically the two numbers can be different. Note also that the metallic strip is supposed to constitute the starting region, while the slot represent the ending region. The transformation of eqs. (2.75) or (2.76) to the original domain is accomplished by inverse transformation, into which the components are substituted with eq. (2.87). Assuming that the width of the slot is smaller than the width of the metallization conductors, and therefore it is preferable to use eq. (2.75), which may be written as

$$\begin{bmatrix} \overline{y}_{11} & \overline{y}_{12} \\ \overline{y}_{21} & \overline{y}_{22} \end{bmatrix} \begin{bmatrix} \overline{E}_{xM} \\ -j\overline{E}_{zM} \end{bmatrix} = \begin{bmatrix} j\overline{J}_{xM} \\ \overline{J}_{zM} \end{bmatrix} \tag{2.88}$$

The original domain of this equation is obtained by back transforming, the quantities $\overline{E}_x$ and $\overline{J}_x$ by T_h, and the quantities $\overline{E}_z$ and $\overline{J}_z$ with T_e. Since T_e and T_h are orthogonal matrices, the inverse transformation of eq. (2.88) in the spatial domain is performed as follows

$$\begin{bmatrix} T_h & 0 \\ 0 & T_e \end{bmatrix} \begin{bmatrix} \overline{y}_{11} & \overline{y}_{12} \\ \overline{y}_{21} & \overline{y}_{22} \end{bmatrix} \begin{bmatrix} T_h^t & 0 \\ 0 & T_e^t \end{bmatrix} \begin{bmatrix} E_{xM} \\ -jE_{zM} \end{bmatrix} = \begin{bmatrix} jJ_{xM} \\ J_{zM} \end{bmatrix} \tag{2.89}$$

This can be written as

$$\begin{bmatrix} y_{11} & y_{12} \\ y_{21} & y_{22} \end{bmatrix} \begin{bmatrix} E_{xM} \\ -jE_{zM} \end{bmatrix} = \begin{bmatrix} jJ_{xM} \\ J_{zM} \end{bmatrix} \tag{2.90}$$

where $y_{ij} = T\overline{Y}_{ij}T^t$. Herein T is an appropriate transformation which may be either T_e or T_h. Inserting the conditions according to eq. (2.87) into eq. (2.90), the following system is then obtained

$$\begin{bmatrix} y_{11} & y_{12} \\ y_{21} & y_{22} \end{bmatrix} \begin{bmatrix} 0 \\ E_{xs_1} \\ \vdots \\ 0 \\ E_{xs_p} \\ 0 \\ E_{zs_1} \\ \vdots \\ 0 \\ E_{zs_p} \end{bmatrix} = \begin{bmatrix} J_{xm_1} \\ 0 \\ \vdots \\ J_{xm_p} \\ 0 \\ J_{zm_1} \\ 0 \\ \vdots \\ J_{zm_p} \\ 0 \end{bmatrix} \tag{2.91}$$

It is important to note that the vectors E_{xM} and E_{zM} of this system contains null sub vectors. The columns of the block matrices y_{ij} that are used in the multiplication of the zero elements of the vectors E_x and E_z, have no contribution for the next calculations. Consequently, needless to perform computation of these elements. Then, to simplify the calculations only the necessary parts of the transformation matrices, corresponding to no zero elements of the vector (e.g. $(E_x, E_z)^t$ in eq. (2.91)), are retained. Therefore the corresponding columns block matrix of y_{ij} have no contribution for the next calculations, consequently, needless to compute these block matrices at all. For instance, the necessary part of the transformation matrices corresponding to the reduced vectors is illustrated in Fig. 2.12.

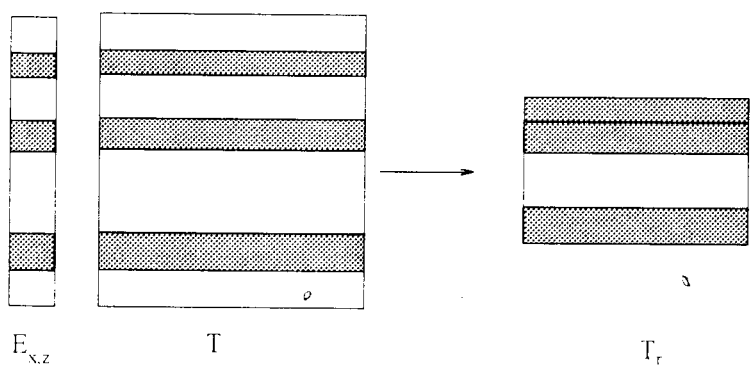

Fig. 2.12 Illustration of reduction part of the transformation matrix T

This allows us to reduce this system by reducing the size of y_{ij} matrices. Hence the system (2.91) can be reduced to :

$$\begin{bmatrix} y_{11}^{r} & y_{12}^{r} \\ y_{21}^{r} & y_{22}^{r} \end{bmatrix} \begin{bmatrix} Ex_{s1} \\ \vdots \\ Ex_{sp} \\ -jEz_{s1} \\ \vdots \\ -jEz_{sp} \end{bmatrix} = \begin{bmatrix} jJx_{m1} \\ 0 \\ \vdots \\ jJx_{mp} \\ 0 \\ Jz_{m1} \\ 0 \\ \vdots \\ Jz_{mp} \\ 0 \end{bmatrix} \tag{2.92}$$

In addition, it can be observed from the right hand side of this system (2.92) that the vector current densities possess also sub vectors of zeros. Hence this system, in turn, may be further divided into two systems. Indeed, the reduced matrices y_{ij}^{r} are partitioned, into parts marked with *rn* according to the part of the non zero sub-vectors current on the metallic strips at the right hand side of eq. (2.92), while the other part is represented by *rz* and corresponds to parts of zero sub-vectors. Thus, the system (2.92) becomes

$$\begin{bmatrix} y_{11}^{rz} & y_{12}^{rz} \\ y_{21}^{rz} & y_{22}^{rz} \end{bmatrix} \begin{bmatrix} E_{xs1} \\ \vdots \\ E_{xs\,p} \\ -jE_{zs1} \\ \vdots \\ -jE_{zs\,p} \end{bmatrix} = \begin{bmatrix} 0 \\ \vdots \\ 0 \end{bmatrix} \tag{2.93}$$

and

$$\begin{bmatrix} y_{11}^{rn} & y_{12}^{rn} \\ y_{21}^{rn} & y_{22}^{rn} \end{bmatrix} \begin{bmatrix} E_{xs1} \\ \vdots \\ E_{xs\,p} \\ -jE_{zs1} \\ \vdots \\ -jE_{zs\,p} \end{bmatrix} = \begin{bmatrix} jJ_{xm1} \\ \vdots \\ jJ_{xmp} \\ J_{zm1} \\ \vdots \\ J_{zmp} \end{bmatrix} \tag{2.94}$$

Equation (2.93) is an indirect eigenvalue problem which has nontrivial solutions only for the following determinental equation

$$\det\left|Y_{red}(\varepsilon_{re}, \omega)\right| = 0 \tag{2.95}$$

The matrix elements y_{ij}^{rz} { i, j = 1,2 } of eq. (2.93) constitute the reduced matrix Y_{red} in eq. (2.95), and contain the eigenvalue $\varepsilon_{re} = \frac{k_z^2}{k_0^2}$. This eigenvalue ε_{re} is progressively modified until the determinental equation (2.95) is fulfilled. The tangential electric field vector at the metallization interface $\left[E_{xs1}^t, \cdots, E_{xsp}^t, -jE_{zs1}^t, \cdots, -jE_{zsp}^t\right]^t$ is determined afterward as an eigenvector for the resulted eigenvalue ε_{re}. Once the eigenvalue ε_{re} and the electric field eigenvector are calculated, all the other electric field components are evaluated at the metallization interface , after which at the other interfaces, using equations that are described in previous sections (e.g. eq. (2.23)) but, they have to be back transformed to the original domain. Besides, the vector $\left[jJ_{xs1}^t, \cdots, jJ_{xsp}^t, J_{zs1}^t, \cdots, J_{zsp}^t\right]^t$ can be determined from eq. (2.94). Moreover all the electromagnetic field components can be estimated on each discretization line at any y-position within the cross-section of the structure. However, if the slot width is smaller than the strip width, then, instead of considering eq.(2.76) or eq.(2.88) the reciprocal equation (2.75) should take place. Likewise, a back transformation to the original domain must be performed first, and then the obtained system must be reduced in a similar way as that in eqs. (2.93) and (2.94). For this alternative, the current densities $\left[jJ_{xs1}^t, \cdots, jJ_{xsp}^t, J_{zs1}^t, \cdots, J_{zsp}^t\right]^t$ play the role of the tangential electric field $\left[E_{xs1}^t, \cdots, E_{xsp}^t, -jE_{zs1}^t, \cdots, -jE_{zsp}^t\right]^t$ in eqs. (2.93) and (2.94). From the two new systems, one which represent the eigenvalue system of which one obtains both the eigenvalue $\varepsilon_{re} = \frac{k_z^2}{k_0^2}$ and the current density as an eigenvector, in the other hand, the second system allows the calculation of the tangential electric field vector $\left[E_{xs1}^t, \cdots, E_{xsp}^t, -jE_{zs1}^t, \cdots, -jE_{zsp}^t\right]^t$ in a complementary way as that of eq. (2.94).

2.8-2 Multi-metallizations interfaces

For a general multi-metallization interfaces, the general condition for the tangential electric field E components and the current densities J are given by

$$\begin{aligned} E_{x_i}^t &= E_{z_i}^t = 0 \\ J_{x_k}^t &= J_{z_k}^t = 0 \end{aligned} \qquad (2.96)$$

where i, j and k stand for :

i : vectors on the metallization interface i

j : components of the vector on the metallic strip

k : components of the vectors on the slot

We designate by E_{xM_i}, E_{zM_i} the tangential electric fields and J_{xM_i}, J_{zM_i} the current densities in the spatial domain at the metallization interface i. At each interface, these vectors look like the vectors represented for the single metallization interface in eq. (2.87) where the metallic strips occur. We suppose that at each interface the width of the metallic strips is greater than the width of the slots, in a such case eq. (2.85) is recommended. The inverse transformation of eq. (2.85) to the original domain is done as follows

$$\begin{bmatrix} \hat{T} & & & \\ & \hat{T} & & \\ & & \ddots & \\ & & & \hat{T} \end{bmatrix} \begin{bmatrix} \overline{K}_1 & \overline{R}_1 & & & \\ \overline{L}_2 & \overline{K}_2 & \overline{R}_2 & & \\ & \ddots & \ddots & \ddots & \\ & & \overline{L}_{m-1} & \overline{K}_{m-1} & \overline{R}_{m-1} \\ & & & \overline{L}_m & \overline{K}_m \end{bmatrix} \begin{bmatrix} \hat{T} & & & \\ & \hat{T} & & \\ & & \ddots & \\ & & & \hat{T} \end{bmatrix}^t \begin{bmatrix} \overline{E}_{M_1} \\ \overline{E}_{M_2} \\ \vdots \\ \overline{E}_{M_{m-1}} \\ \overline{E}_{M_m} \end{bmatrix} = \begin{bmatrix} \overline{J}_{M_1} \\ \overline{J}_{M_2} \\ \vdots \\ \overline{J}_{M_{m-1}} \\ \overline{J}_{M_m} \end{bmatrix} \tag{2.97}$$

Where

$$\hat{T} = \begin{bmatrix} T_h & \\ & T_e \end{bmatrix}, \quad E_{M_i} = \begin{bmatrix} E_{xM_i} \\ -jE_{zM_i} \end{bmatrix}, \quad J_{M_i} = \begin{bmatrix} jJ_{xM_i} \\ J_{zM_i} \end{bmatrix}$$

equation (2.97) can be represented in the form

$$\begin{bmatrix} K_1 & R_1 & & & \\ L_2 & K_2 & R_2 & & \\ & \ddots & \ddots & \ddots & \\ & & L_{m-1} & K_{m-1} & R_{m-1} \\ & & & L_m & K_m \end{bmatrix}^t \begin{bmatrix} E_{M_1} \\ E_{M_2} \\ \vdots \\ E_{M_{m-1}} \\ E_{M_m} \end{bmatrix} = \begin{bmatrix} J_{M_1} \\ J_{M_2} \\ \vdots \\ J_{M_{m-1}} \\ J_{M_m} \end{bmatrix} \tag{2.98}$$

Where $X_i = \hat{T}\overline{X_i}\hat{T}^t$ and X_i may be either L, K or R.

Using the same reduction procedure, as the one used for single metallization interface, we can split this system into two systems. If we designate by E_{MS_i} the tangential electric field on the slots and J_{MM_i} the current densities on the strips over the i-th metallization interface. Then, eq. (2.98) is divided into two systems

$$\begin{bmatrix} K_1^{TE} & R_1^{TE} & & & \\ L_2^{TE} & K_2^{TE} & R_2^{TE} & & \\ & \ddots & \ddots & \ddots & \\ & & L_{m-1}^{TE} & K_{m-1}^{TE} & R_{m-1}^{TE} \\ & & & L_m^{TE} & K_m^{TE} \end{bmatrix} \begin{bmatrix} E_{MS_1} \\ E_{MS_2} \\ \vdots \\ E_{MS_{m-1}} \\ E_{MS_m} \end{bmatrix} = \begin{bmatrix} 0 \\ 0 \\ \vdots \\ 0 \\ 0 \end{bmatrix} \tag{2.99}$$

and

$$\begin{bmatrix} K_1^{rn} & R_1^{rn} & & & \\ L_2^{r} & K_2^{rn} & R_2^{rn} & & \\ & \ddots & \ddots & \ddots & \\ & & L_{m-1}^{rn} & K_{m-1}^{rn} & R_{m-1}^{rn} \\ & & & L_m^{rn} & K_m^{rn} \end{bmatrix} \begin{bmatrix} E_{Ms_1} \\ E_{Ms_2} \\ \vdots \\ E_{Ms_{m-1}} \\ E_{Ms_m} \end{bmatrix} = \begin{bmatrix} J_{M\bar{m}1} \\ J_{M\bar{m}2} \\ \vdots \\ J_{M\bar{m}m-1} \\ J_{M\bar{m}m} \end{bmatrix} \tag{2.100}$$

The superscript rz, and rn in the matrices L, K, R have been already defined for the single MI. The size of the two systems (2.99) and (2.100) depends on both m, number of MI, s, number of slots at each MI and the number of discretization lines that crosses each slot. The eigenvalue system has to be solved, from which the eigenvalue $\varepsilon_{re} = \frac{k_z^2}{k_0^2}$ is firstly obtained and then the tangential electric field $[E_{Ms_1}, E_{Ms_2}, \cdots, E_{Ms_{m-1}}, E_{Ms_m}]$ is obtained as eigenvector. In the second step the current densities are computed using eq. (2.100) at all the metallization interfaces as well as the electromagnetic field in the other regions or interfaces using the relations that connect the obtained tangential electric field in a similar way to that used in the single MI.

2.9 Positions of Discretization Lines at Edges

The study of electromagnetic problems involving sharp edges, such as the case of a perfect conductor strip with vanishing thickness, where some of the electromagnetic field can have unbounded behaviour in the vicinity of these edges. The field singularities must satisfy the energy function

$$W = \frac{1}{4}\int_V \left(\varepsilon |E|^2 + \mu |H|^2 \right) dV \tag{2.101}$$

to remain bounded within an infinitesimal volume V surrounding the edge.

In order to reduce the mathematical labour for solving these electromagnetic problems, a knowledge of the field singularities is very helpful. These singularities when taken into account and implemented in modern mathematical methods leads to a considerable improvements. Including particularly the accuracy enhancement of the numerical solution, avoiding the relative convergence for some other mathematical techniques (i.e. convergence to a non physical solution) and also increasing the computation efficiency. The MoL has not the problem of relative convergence since, the convergence is guaranteed as the discretization step decreases. Indeed, for large discretization steps, the solution at the discretization lines in the vicinity of the edge miscounts the singularities

and therefore errors can arise. A valuable study to minimise these errors have been demonstrated by U.Shulz [28]. For this purpose, as it is proposed in [28], we simply consider a microstrip line with perfect conductor strip of vanishing thickness as shown in Fig. 2.13.

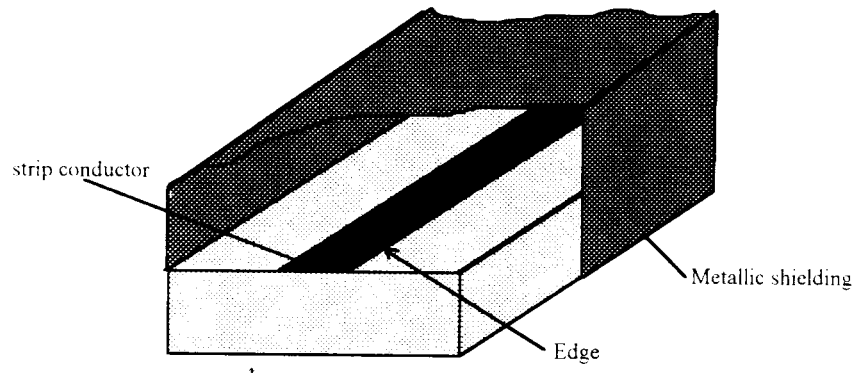

Fig 2.13 Microstrip line structure

An effective strip width or an optimal position between the discretization lines and the metallic strip-edges, as shown in Fig. 2.14 ,represented by the edge parameter p or q is evaluated. The tangential field components parallel to the strip conductor exhibit a regular behaviour [29]. It has been shown [28, 29] that the field e_z, h_z near the edge conductor, in polar co-ordinate ($\rho \to 0$), can be described by

$$e_z \cong \rho^{\frac{1}{2}} \sin\frac{\phi}{2} \tag{2.102}$$

and

$$h_z \cong \rho^{\frac{1}{2}} \cos\frac{\phi}{2} \tag{2.103}$$

Applying the discretization procedure for the Helmotz equations, and using eq. (2.9) for the i-th line yields

$$\frac{d^2}{dy^2}\Phi_i^{(e,h)}(y) + \frac{1}{h^2}(\Phi_{i-1}^{(e,h)}(y) - 2\Phi_i^{(e,h)}(y) + \Phi_{i-1}^{(e,h)}(y)) + (k_k^2 - k_z^2)\Phi_i^{(e,h)}(y) = 0 \tag{2.104}$$

with $\Phi^e = E_z$ and $\Phi^h = H_z$ and, E_z and H_z represent the vector of the discretized electric and magnetic field components respectively.

Besides the boundary conditions at the top and the bottom of the shielding and the lateral boundaries, the electromagnetic field has to satisfy additional boundary conditions at

discrete points ($i < k_1$) as shown in Fig. 2.14 on the strip at $y = d$ with $E_{zi} = 0$ or $\frac{\partial H_z}{\partial y} = 0$ respectively for the Helmotz equations (2.104)

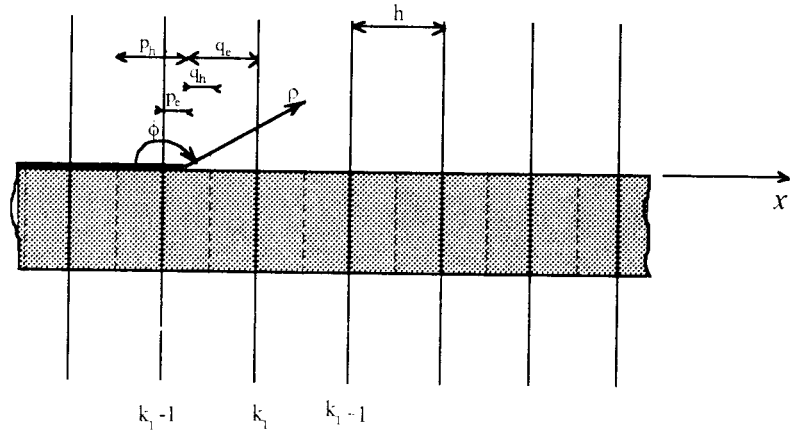

Fig 2.14 Considered region with perfect conducting edge
and illustration of edge parameters p and q

With the help of Fig. 2.14, it is easy to show that ρ and ϕ are given by

$$y = \rho \sin\phi \quad ; \quad x = -\rho\cos\phi \quad ; \quad \rho = \left((x - (k_1 - 1 + q_h)h)^2 + y^2\right)^{\frac{1}{2}}$$

moreover, we can also show that when $i < k_1$

$$\lim_{\rho \to 0} \frac{\partial^2 \Phi^h}{\partial y^2} = \frac{1}{4} r^{-\frac{3}{2}} \tag{2.105}$$

and at the interface $y = 0$ and for $i = k_1 - 1$ we have

$$\Phi^h_{k_1-1} = (p_h h)^{\frac{1}{2}} \quad ; \quad \Phi^h_{k_1} = 0 \quad ; \quad \Phi^h_{k_1-2} = (1 + p_h h)^{\frac{1}{2}} \quad ; \quad h^2 \frac{\partial^2 \Phi^h}{\partial y^2} = \frac{1}{4} h^{\frac{1}{2}} p_h^{-\frac{3}{2}} \tag{2.106}$$

Substitution of the relation (2.105) into Helmotz equation (2.104) leads to

$$\frac{1}{4} p_h^{-\frac{3}{2}} + (1 + p_h)^{\frac{1}{2}} - (2 + h^2(k^2 - \beta^2)) p_h^{\frac{1}{2}} = 0 \tag{2.107}$$

Following the same procedure for Φ^e , after computing the corresponding Helmotz equation elements for Φ^e at $y=0$ and for the k_1 line, the following equation is resulted

$$\frac{1}{4}q_e^{-\frac{3}{2}}+(1+q_e)^{\frac{1}{2}}-(2+h^2(k^2-\beta^2))q_e^{\frac{1}{2}}=0 \qquad (2.108)$$

The conditional equation (2.107) for q or eq. (2.108) for p can be formulated in the same form as that derived in [28]

$$\frac{1}{4}\xi^{-\frac{3}{2}}+(1+\xi)^{\frac{1}{2}}-(2+h^2(k^2-\beta^2))\xi^{\frac{1}{2}}=0 \qquad (2.109)$$

Where $$\xi=\begin{cases} q_e \rightarrow \Phi^e \\ p_h \rightarrow \Phi^h \end{cases}$$

In addition, Fig. 2.14 shows that p_e and q_h must satisfy the discretization condition of the two lines system as

$$q_e+p_h=\frac{3}{2} \qquad (2.110)$$

The equation (2.109) depends on the normalized frequency k^2 and the discretization step h. It has been found [28] that for $2\pi/h(k^2-\beta^2)^{\frac{1}{2}}\geq 30$, the influence of frequency is vanishing and the optimal approximation $\xi=0.75$, fitting both eqs. (2.109) and (2.110), is satisfied.

In order to discard these factors k,h, it has been noted [30,51] that, from eqs. (2.102) and (2.103) , we can obtain $\Phi^e_{k_1-1}=0$ and $\Phi^h_{k_1-1}=0$. Once these last relations are substituted into Helmotz equation, at the line $i=k_1-1$ for Φ^h and at the line $i=k_1-1$ for Φ^e at the interface $y=0$, leads however, to the following conditional equation for p_e or q_h respectively

$$\frac{1}{4}(1-\zeta)^{-\frac{3}{2}}+2(2-\zeta)^{\frac{1}{2}}-4(1-\zeta)^{\frac{1}{2}}=0 \qquad (2.111)$$

Where $$\zeta=\begin{cases} p_e \rightarrow \Phi^e \\ q_h \rightarrow \Phi^h \end{cases}$$

and the auxiliary condition that must be accomplished

$$p_e+q_h=\frac{1}{2} \qquad (2.112)$$

The obtained optimal solution $\zeta = 0.265$ fulfilling at the same time eqs. (2.111) and (2.111) is obtained. For practical purpose $p_e = q_h = \frac{1}{4}$ is chosen. The optimal edge condition $\zeta = 0.25$ is also valid for the quasi-static analysis since eq. (2.111) is frequency independent. It must be emphasised, that this two line shifting system were found to be an expedient requirement for fast convergence, where the edge condition is easily satisfied for both Φ^e and Φ^h simultaneously. Hence, this is a further advantage of this two line system. However, it should be noted that this edge parameter was determined for an infinitely long strip conductor, but it is not generally valid for a finite conductor, and therefore, according to each structure shape of finite length, the edge parameter must be determined.

2.10 Non uniform Discretization

The draw back of the method of lines for the analysis of planar microwave structures is due to the fact that, in the case of extreme differences in the width of the strip conductors or the line gaps between strips, the total number of discretization must be considerably increased in order to take account of these small regions. This increases either the memory space and the computing time. A further disadvantage of this method comes from the difficulty to realise the optimal edge condition for multistrip conductors and to satisfy in addition the lateral boundaries of the considered structure. A tractable solution of these problems is the non uniform discretization. This concept has been introduced in the method of lines [31] without changing its useful transformation properties. In this section only the specific difference changes are emphasised. The cross-section of the structure is divided by a number of lines but with variable discretization interval. The interval sizes e_i and h_i of the two lines system as shown in Fig. 2.15, decreases near the strip conductor edges where the field singularity (field concentration) occurs.

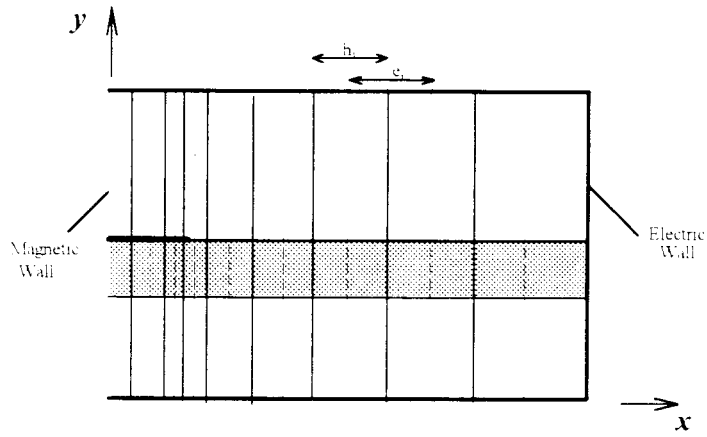

Fig 2.15 Illustration of the non-uniform discretization for a suspended microstrip-line structure
—— for Φ^e lines
– – for Φ^h lines

In order to obtain symmetric second-order operators, the related potential functions Ψ^e and Ψ^h are normalised according to

$$\Psi_i^e = \sqrt{\frac{e_i}{h}}\Psi_i^{ne} \qquad \text{(a)}$$
$$\Psi_i^h = \sqrt{\frac{h_i}{h}}\Psi_i^{nh} \qquad \text{(b)} \qquad (2.113)$$

Where h represents the interval size obtained for the equidistant discretization case.
In matrix notation eq. (2.113) becomes

$$\Psi_i^e = r_e \Psi_i^{ne}$$
$$\Psi_i^h = r_h \Psi_i^{nh} \qquad (2.114)$$

With $$r_h = diag\left(\sqrt{\frac{h_i}{h}}\right) \quad , \quad r_e = diag\left(\sqrt{\frac{e_i}{h}}\right)$$

Note that the vectors and the matrices with sub- and super-scripts e and h are of order N_e and N_h respectively.
The finite difference quotient for the first derivative of Ψ^e with respect to x is evaluated on the discretization lines for Ψ^h. Therefore, for the i-th line of Ψ^h, the first derivative of Ψ^e is approximated by

$$\left.\frac{\partial \Psi^e}{\partial x}\right|_i \longrightarrow \frac{\Psi_{i-1}^e - \Psi_i^e}{h_i} \qquad (2.115)$$

In matrix notation, this equation becomes after normalization,

$$r_h^{-1}\left(h\frac{\partial\Psi_e}{\partial x}\right)\longrightarrow r_h D\Psi_e$$
$$= r_h D r_e^{-1}\Psi_{ne} = \tilde{D}\Psi_{ne} \tag{2.116}$$

Where the difference operator D is previously defined in the equidistant discretization scheme in eq. (2.4). In analogous way, the first derivative of Ψ_h with respect to x is approximated by

$$r_e^{-1}\left(h\frac{\partial\Psi_h}{\partial x}\right)\longrightarrow -r_e D^t\Psi_h$$
$$= -r_e D^t r_h^{-1}\Psi_{nh} = -\tilde{D}^t\Psi_{nh} \tag{2.117}$$

The second order differential operator is just a combination of the first-order differential operator. The second derivative of Ψ_e and Ψ_h are approximated by

$$r_e^{-1}\left(h\frac{\partial}{\partial x}\left(h\frac{\partial\Psi_e}{\partial x}\right)\right)\longrightarrow -\tilde{D}^t\tilde{D}\Psi_{ne}$$
$$= -\tilde{P}_{ND}\Psi_{ne} = -\tilde{P}_e\Psi_{ne}$$
$$r_h^{-1}\left(h\frac{\partial}{\partial x}\left(h\frac{\partial\Psi_h}{\partial x}\right)\right)\longrightarrow -\tilde{D}\tilde{D}^t\Psi_{nh} \tag{2.118}$$
$$= -\tilde{P}_{DN}\Psi_{nh} = -\tilde{P}_h\Psi_{nh}$$

Because the second order operators $\tilde{P}_{ND}$ and $\tilde{P}_{DN}$ are real symmetric tridiagonal matrices, which means that the related potential function components are related to each other, they can be diagonalized by orthogonal transformation, with distinct eigenvalues

$$T_{e,h}^t\tilde{P}_{e,h}T_{e,h} = \tilde{\lambda}_{e,h} \tag{2.119}$$

The diagonal matrix $\tilde{\lambda}_{e,h}$ formed by the eigenvalues, and the transformation matrix $T_{e,h}$ formed by the eigenvectors are determined numerically by means of the " Implicit QL-method " [36], a stable and fast technique, which has been proved to be specially suited for this kind of matrices.

In the transformed domain, the two system of ODE's corresponding to eq. (2.12) is given by

$$\left(\left(\frac{d^2}{dy^2}+k_x^2-k_z^2\right)I-h^{-2}\lambda_k\right)\overline{\Psi}^{ne,h} = 0 \tag{2.120}$$

Where $\overline{\Psi}_{ne,h} = T^t_{e,h}\Psi_{ne,h}$

The on-going part of the analysis remains similar to that developed for the equidistant discretization but it is only necessary to replace the vector components, such as the electromagnetic field, current densities and so on, with the normalised vectors by the appropriate normalisation. For instance instead of $\Psi_{e,h}$, $J_{x,z}$, $E_{x,z}$, $H_{x,z}$ they are replaced by $\Psi_{ne,h}$, $J_{nx,z}$, $E_{nx,z}$, $H_{nx,z}$. Thus, the remaining part of analysis is yet disregarded.

2.10-1 Discretization Intervals

It has been mentioned in the previous section that singularities occur in the vicinity of the conductor edges and introduce a considerable error. This error can be effectively reduced by either fulfilling the edge condition parameters and decreasing the discretization intervals when the considered points are closer to regions where the functions have rapid variations. Whereas, the discretization line intervals can be chosen larger as long as they are far-off from the singular regions where the functions are smooth.

Generally the shapes of these functions, i.e. the potential function and the current densities, are unknown. In this case, the functions can not be approximated and a first run of program for equidistant discretization with $r_e = r_h = 1$ shall provide this approximation. However if the function under consideration is approximately known, then an approximation may be developed to obtain optimum discretization. In the present problem indeed, an approximate function for the surface charge density $\sigma(x)$ and consequently the current density on the conductor is given by the Maxwell distribution [6], which holds only for an isolated strip conductor.

When the potential lines are sinusoidaly spaced [1] on the strip at

$$x_i = \sin\left(\frac{2i - M_n}{2M_n}\pi\right) \tag{2.121}$$

Where M_n is the total number of lines for the n-th strip and $-1 \le x \le 1$, the same amount of charges or current is located between any two successive lines [6]

$$\frac{1}{\pi}\int_{x_{i-1}}^{x_i} \frac{dx}{\sqrt{1-x^2}} = \frac{1}{M_n} \tag{2.122}$$

Because of the singular behaviour of the charge current density at the conductor edges, then fine discretization step intervals or more lines are located in the vicinity of the strip. Therefore, the line position are determined by adopting eq. (2.121). Hence one obtain for the n-th strip located at $x_{na} \le x \le x_{nb}$

$$x_i = \frac{x_{na} + x_{nb}}{2} + \frac{x_{na} - x_{nb}}{2} \sin\left(\frac{2i - M_n}{2M_n}\pi\right) \quad , \quad i = 0, 1, \ldots, M_n \tag{2.123}$$

This equation is also valid for the gaps or regions between edges of two neighbourhood strips. This allows to keep the same small interval size, which is located near each edge for all regions, so that [6] in the vicinity of each edge the interval sizes are small and nearly symmetric. With the smallest interval size $h_i = \Delta = x_{M\min} - x_{M\min-1}$ where M_{min} is the number of lines for the smallest strip width or region, and can be derived from eq. (2.122) so that, at $x_{na} \le x \le x_{nb}$ we have the integer

$$M_n = INT\left(\frac{2\pi}{\pi - 2\sin^{-1}(1 - 2\Delta\ (x_{nb} - x_{na})}\right) \tag{2.124}$$

The calculations of the interval sizes $h_i = x_{i-1} - x_i$ can be done from eq. (2.123). The exterior regions situated between the first strip and the lateral walls, can be treated analogously if the interval sizes are calculated for twice the regions. This is so, because near the wall there are not singularities but rather smooth functions, the interval sizes h_i have then maximum values. This non uniform discretization present another significant advantage over the uniform one. This comes from the fact that, when the electric walls are only secondary quantities, they can be shifted sufficiently far away from the strip conductors without increasing discretization lines [6], since interval sizes are largely spaced within this region, from the wall to the first strip conductor. Thus, the numerical computation are performed without a large effort compared to the uniform discretization. Indeed, the interval size h of equidistant discretization is fixed by the minimum number of lines M_{min} chosen for the smallest region, and hence the number of lines is increased and an important numerical effort is provided to analyse the same considered structure, especially if widths of strips or gaps are smaller to the structure width.

It has been seen for the equidistant discretization case, that the rate of convergence is optimum for an adequate edge parameters. This result is also exploited for the non uniform discretization. This can be achieved if the first line on either sides of each edg must be always located at $0.25h_i$ for the related electric potential and at $0.75h_i$ for the related magnetic potential function. The positions of the lines in the space or strip

regions are determined by means of eqs. (2.123) and (2.124). In order to include the edge condition, the interval sizes have to be shortened by a certain reduction factor. If the gap is the smallest region at the metallization interface of the structure, then the interval sizes on the strip conductor must be shortened by $(w-2\Delta/3)/w$ (w:strip width), while they are not corrected in space regions. In the other case where the strip conductor represents the smallest region, then it is necessary to shorten the intervals sizes that are within the gap or space regions by the factor $(w-6\Delta)/w$ (w:slot width) and the positions as well as the interval sizes of the strip regions are determined by means of eq. (2.123). With the help of this simple procedure, the edge condition is satisfied at each strip edge, i.e. the error is nearly the same for all strips, as the results shown in [6].

It has been shown in [6] that the mean value $e_i = (h_i + h_{i-1})/2$, as shown in Fig. 2.16 , does not lead to the best possible finite difference approximation (e.g. eq.(2.115)). Moreover a more accurate approximation for the second derivative is obtained, if the discretization error for each of the first derivatives and the error for the total expression (e.g. eq. (2.115)) are of equal order, as it is given for equidistant discretization (eq. (2.3)). This requires that the change of the subinterval sizes t_k has to be similar to the change of the h_i.

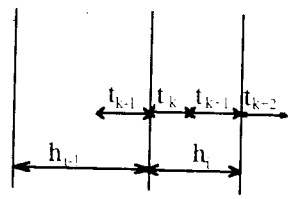

Fig 2.16 Illustration of the non central difference discretization line positions between the function and their derivatives

The subintervals t_k are derived from the following relation [6]

$$\frac{h_i}{h_{i-1}} = \frac{t_k + t_{k-1}}{t_{k-2} + t_{k-1}} = p_k\left(p_{k-1}\frac{p_{k-1}+1}{p_{k-1}+1}\right) \cong p_k^2 \qquad (2.125)$$

Where $p_k = \frac{t_k}{t_{k-1}}$ and $k = 2i$. For common values of p_k , i.e. for $0.5 \le p_k^2 \le 2$, this approximation is accurate to 1%. From eq. (2.14) all quotients with odd subscripts are given by the mean value

$$p_{k-1} = (p_k + p_{k-2})/2 \qquad k = 0,2,\ldots,2M \qquad (2.126)$$

Whereas all the sub-interval sizes are, for the subsequent step, calculated by means of

$$t_k = \frac{h_i}{1+p_{k-1}} \quad , \quad t_{k-1} = h_i - t_k \tag{2.127}$$

with $k = 0,2,\ldots,2M$ and $k = 2i$. The interval sizes e_i are now determined by

$$e_i = t_{k-1} + t_k \tag{2.128}$$

Using this choice of interval sizes the corresponding quotients h_i / h_{i-1}, e_i / e_{i-1} and t_k / t_{k-1} approximately form smooth curves [6].

2.11 Characteristic Impedance Calculations

In microwave engineering, matching circuits are of fundamental importance, such as amplifiers, oscillators, mixers etc. characteristic impedance is a property of great interest for microwave circuit designers. For the hybrid-mode analysis, several definitions of characteristic impedance are possible depending on the nature of the structure e.g. for microstrip line, it is defined as

$$Z_p = \frac{P}{I^2} \tag{2.129}$$

and for microslot line, as

$$Z_p = \frac{U^2}{P} \tag{2.130}$$

Where I is the total current flowing through the strip in the direction of wave propagation and U is the voltage of the slot (gap). The total current I is calculated according to

$$I = \int_{(s)} \bar{J} d\bar{s} \tag{2.131}$$

and the voltage U is defined by

$$U = \int_{\text{over gap}} E_x dx \tag{2.132}$$

The power transfer P, propagating along the z-direction, is determined as the integral of the Poynting vector over the waveguide cross-section S, and is given by

$$P = \int_{(S)} (\bar{E} \times \bar{H}) d\bar{s} \tag{2.133}$$

Using the components of the electromagnetic field, this expression becomes

$$P = \iint_{(S)} (e_x h_y - e_y h_x) dx dy \tag{2.134}$$

The power transfer must be calculated by summing up the power computed separately for each layer of the cross-sectional structure. In the x-y plane, using the discretized field and for an arbitrary layer l bounded by its bottom y_{l-1} and top y_l interface, the integral may be approximated with respect to x-direction (discretization axis) by means of the rectangular or trapezoidal rule, which becomes for the uniform discretization as

$$P_l = h \int_{y_{l-1}}^{y_l} (E_x^l H_y - E_y^l H_x) dy \tag{2.135}$$

For the non uniform discretization the power can be approximated by

$$P_l = h \int_{y_{l-1}}^{y_l} \left\{ \left([r_h]^{-1} Ex_n^l \right)^t [r_h]^{-1} Hy_n - \left([r_e]^{-1} Ey_n^l \right) [r_e]^{-1} Hx_n \right\} dy \tag{2.136}$$

The computation of the eq. (2.136) is identical to that of eq. (2.135) where only the diagonal matrices $[r_{e,h}]$ are inserted.

Because the discretization lines of the field E_x are aligned with H_y lines, then they have the same transformation matrices and the same matter for the E_y and H_x,. This fact allows to use the transformed field components by their corresponding spatial field components. Indeed there is e.g.

$$E_y H_x = \overline{E}_x^t T^t T \overline{H}_x = \overline{E}_x^t \overline{H}_x. \tag{2.137}$$

This represents an advantage, since it avoids the matrix multiplication used to calculate the spatial field components. Substituting eq. (2.137) into eq. (2.136) yields

$$P \quad h \quad (\overline{E} \ \overline{H} \quad \overline{E} \ \overline{H} \ ) dy \tag{2.138}$$

For the computation of integral over y-axis in eq. (2.138), we introduce for each vector R and layer l, the following settings,

$$\overline{R} = \alpha \left(P_1 \overline{R}_{l-1} + P_2 \overline{R}_l \right) \tag{2.139}$$

with α as given in eq. (2.15-c) and

$$P_1 = diag\left(\frac{k_{yl}}{k_0}\sinh k_{yl}(y_l - y)\right) \tag{2.140}$$

$$P_2 = diag\left(\frac{k_{yl}}{k_0}\sinh k_{yl}(y - y_{l-1})\right) \tag{2.141}$$

Therefore, the first term of equation (2.138) can be written as

$$\int_{yl-1}^{yl} \overline{E}_x^t \overline{H}_x dy = \int_{yl-1}^{yl} \begin{bmatrix} \overline{E}_{xl-1} \\ \overline{E}_{xl} \end{bmatrix}^t \left(\alpha_h^2 \begin{bmatrix} P_1 \\ P_2 \end{bmatrix} \begin{bmatrix} P_1 \\ P_2 \end{bmatrix}^t \begin{bmatrix} \overline{H}_{yl-1} \\ \overline{H}_{yl} \end{bmatrix} \right) dy \tag{2.142}$$

This gives the following relation

$$\int_{yl-1}^{yl} \overline{E}_x^t \overline{H}_x dy = \frac{1}{2} \begin{bmatrix} \overline{E}_{xl-1} \\ \overline{E}_{xl} \end{bmatrix} \begin{bmatrix} g_{1h} & g_{2h} \\ g_{2h} & g_{1h} \end{bmatrix} \begin{bmatrix} \overline{H}_{yl-1} \\ \overline{H}_{yl} \end{bmatrix} \tag{2.143}$$

with

$$\begin{aligned} g_{1h} &= k_0^{-1}(\gamma_h - k_0 d\, k_{yh}^2 \alpha_h^2) \\ g_{2h} &= k_0^{-1}(k_0 d\, k_{yh}^2 \alpha_h \gamma_h - \alpha_h) \end{aligned} \tag{2.144}$$

Proceeding in the same way as for the first term, the result of the second term may be achieved and is given by

$$\int_{yl-1}^{yl} \overline{E}_y^t \overline{H}_x dy = \frac{1}{2} \begin{bmatrix} \overline{E}_{yl-1} \\ \overline{E}_{yl} \end{bmatrix} \begin{bmatrix} g_{1e} & g_{2e} \\ g_{2e} & g_{1e} \end{bmatrix} \begin{bmatrix} \overline{H}_{xl-1} \\ \overline{H}_{xl} \end{bmatrix} \tag{2.145}$$

with

$$\begin{aligned} g_{1e} &= k_0^{-1}(\gamma_e - k_0 d\, k_{ye}^2 \alpha_e^2) \\ g_{2e} &= k_0^{-1}(k_0 d\, k_{ye}^2 \alpha_e \gamma_e - \alpha_e) \end{aligned} \tag{2.146}$$

The field components that are necessary for the computation of the power transfer and the current densities are derived by solving the characteristic equation. This is however achieved, when the transformed tangential electric fields $\overline{E}_x, \overline{E}_z$ are obtained, and then all the other electromagnetic field components can be obtained every where in the structure according to relations established in the previous sections. These relations establish, in one hand the connection of the tangential fields from one interface to the other, in the other hand relate the non tangential fields $\overline{E}_y, \overline{H}_y$ to the tangential one. In addition, these relations are given according to substrate type which yet might be isotropic or anisotropic substrates.

For a general multiconductor structure, we can also calculate the characteristic line impedance of the i-th strip conductor Z_{Li} by the current-power definition [40] as :

$$Z_{Li} = \frac{P_i}{I_i^2} \tag{2.147}$$

Where I_i is the eigenmode current on the i-th conductor strip

$$I_i = \sum_{i=c} e_i J_{Zi}^k \tag{2.148}$$

In equation (2.146) C denotes the subscripts of the electric related function Ψ^e lines which intersect the i-th conductor strip. P_i is the partial power associated with the line

$$P_i = \int_{(S)} E_t \times H_i^* ds \tag{2.149}$$

Where E_t is the total field and H_i, the magnetic field created only by the current on the i-th line. For the non uniform discretization, this last integral (2.149) becomes

$$P_i = h \int_y \left\{ \left([r_h]^{-1} \overline{E}_x^t \right)^t \left([r_h]^{-1} \overline{H}_{yn} \right)^* - \left([r_e]^{-1} \overline{E}_y \right)^t \left([r_e]^{-1} \overline{H}_{tx} \right)^* \right\} dy \tag{2.150}$$

Similarly, we can derive the procedure for calculating the line impedance Z_{Lm} based on the voltage-power definition for slot configuration, and which can be easily ex ended to configurations with more dielectric layers and strip conductors.

2.12 Numerical Results

In this section, in order to check the performance of the above described techni que, some numerical results are presented as examples. First, Fig. 2.17 shows the dispersion characteristics of the effective dielectric constant $\varepsilon_{eff} = \frac{k_z^2}{k_0^2}$ and the ch. cteristic impedance Zc versus the normalized frequency $k_0 d$ for both the single an. coupled microstrip lines.

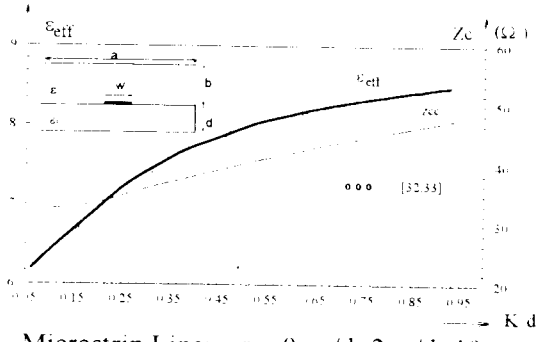

Microstrip Line: εr = 9, w/d=2, a/d=19

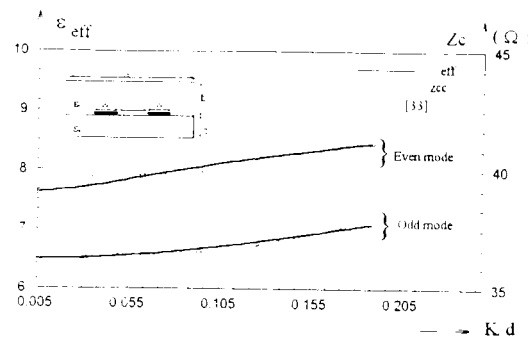

Coupled Microstrip Line: εr = 10.2, w/d=0.5, s/d=1.5, a/d=19

Fig. 2.17 Effective dielectric constant ε_{eff} and Characteristic impedance Zc for a single and Coupled Microstrip Line

These Figures demonstrate the verification of the algorithm using the uniform discretization procedure. Good agreement with other available results [32,33] may be stated.

In the Second step, the convergence behaviour, a crucial criterion for such numerical methods, is treated using the equidistant discretization approach. Fig. 2.18 shows the convergence behaviour of ε_{eff} and Zc for a single microstrip line. M is the number of Ez-lines on half the strip, h/d is the discretization distance to substrate thickness ratio, and p the edge parameter as defined in section 2.9.

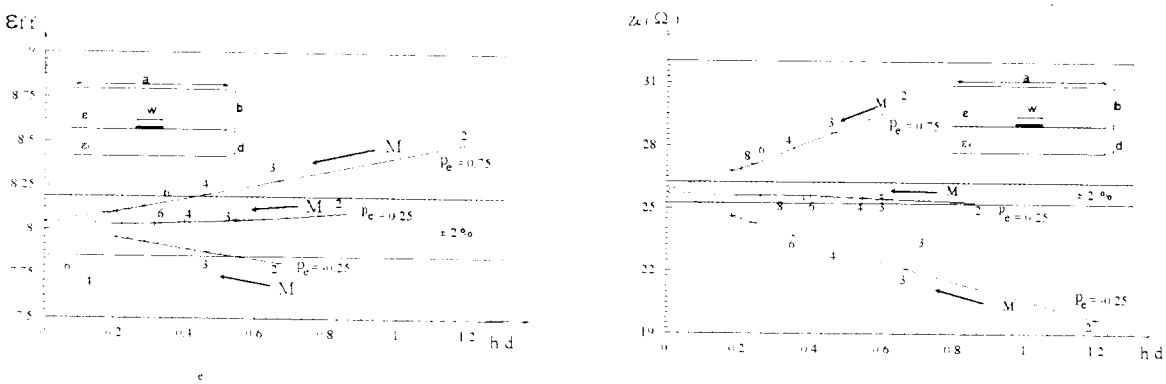

Fig. 2.18 Convergence behaviour of ε_{eff} and Zc for a single microstrip line εr = 10, w/d=3, a/d=18, d/λo=0.02.

All these curves are smooth and show the monotonicity function, and the discrete solution asymptotically approaches the continuous solutions. It is then possible to extrapolate the accurate result.

In Fig. 2.19-a the dispersion characteristic ε_{eff} and Zc as a function of normalized frequency d/λo are given for the even and odd-mode of the coplanar waveguide. It can be seen that the computed results agree, to within the accuracy that data can be read from the graphs, with the results obtained by Diestel and Warm using the same method [31] and along with those resulting from the integral equation technique [37].

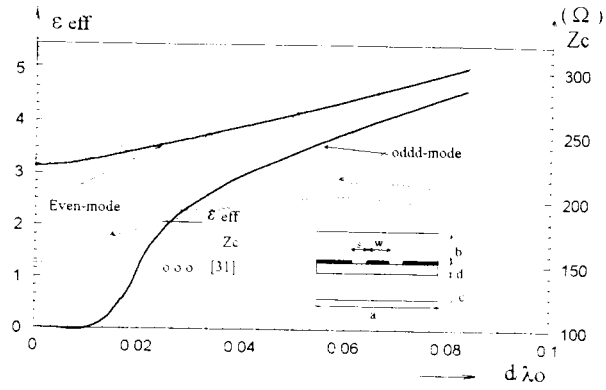

Fig. 2.19
The dispersion characteristics ε_{eff} and Zc versus d/λo for a coplanar waveguide with a/d=20. b/d=c/d=4.5. s/d=w/d=2 and εr=9.35.

Fig. 2.19-b illustrates the convergence behaviour of the propagation constant k_z/k_o as a function of the smallest interval size to the substrate thickness ratio h'/d. This curve indicates that both equidistant and non equidistant discretization procedures converge asymptotically to the exact solution as long as the discretization interval decreases. The integers in the curves represent the number of discretization on the strip.

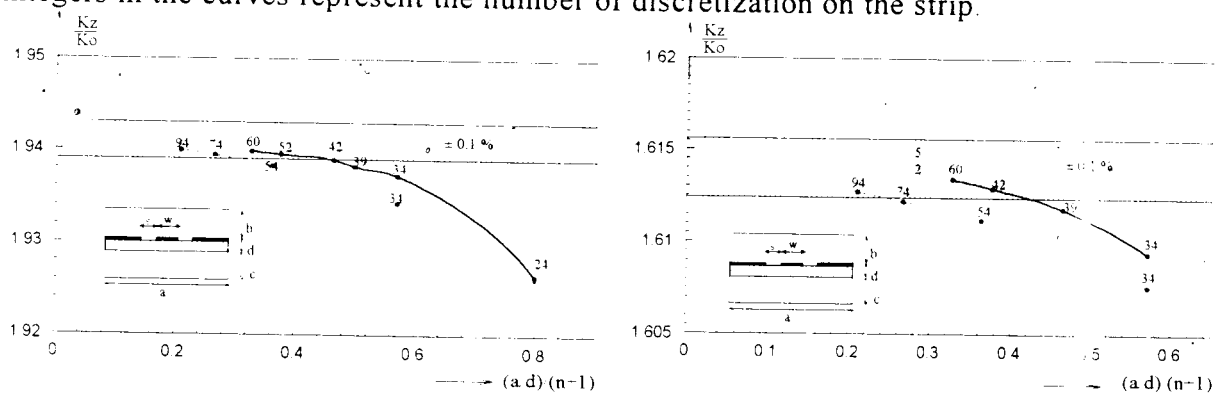

Fig. 2.19-b Convergence behaviour of the propagation constant kz/ko as a function of the normalized interval size (a/d)/(n+1) for the coplanar waveguide using the uniform and non uniform discretization. a/d=20. b/d=c/d=4.5. s/d=w/d=2. εr=9.35. d/λo=0.033
non uniform discret. uniform discret.

It can be noted that, to reach the solution corresponding to the one obtained with e.g. 52 lines using the non uniform discretization (within the doted area < 0.1%) for the even mode, which can be obtained for more than 74 lines using the equidistant discretization. Moreover the computation time depends on the total number of lines, and particularly on the number of lines through the conducting structure (optimized for strips or slots) and that determines the order of the reduced matrix derived from the characteristic equation.

Knowing these facts, it becomes evident that the non equidistant discretization procedure is advantageous with respect to the equidistant one.

In order to pursue the verification of the developed algorithm, the dispersion characteristics of the planar waveguide is computed for different values of the dielectric permittivity as shown in Fig. 2.20. The frequency dependent characteristics ε_{eff} and Zc are in good agreement with the results obtained by the integral method [37]. Note also that this structure supports a non-TEM mode which, consequently, cannot be analysed using the quasi-static approximation.

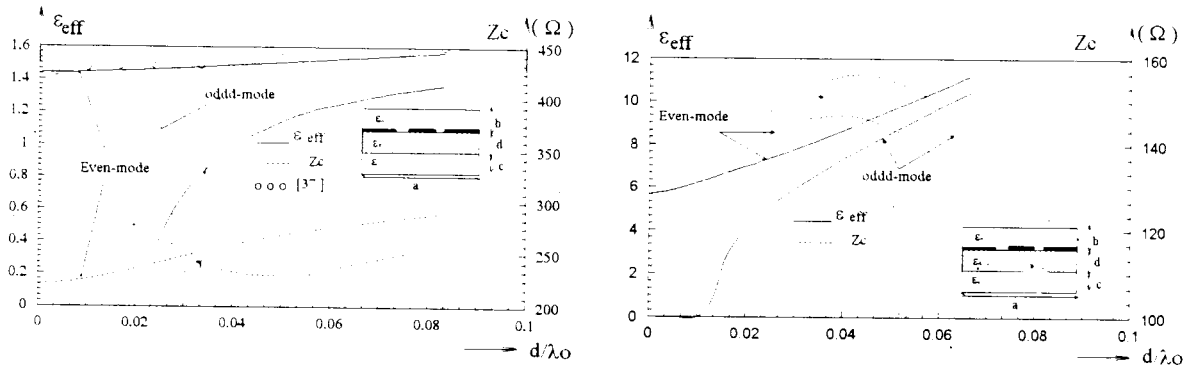

Fig. 2.20 The dispersion characteristics ε_{eff} and Zc for the planar waveguidea/d=20 , b/d=c/d=4.5; left εr = 2.55 ; right εr = 20.

The next addressed problem is the dispersion characteristic of structures based on anisotropic substrates. The microstrip line based on Sapphire substrate is firstly treated. The achieved results shown in Fig. 2.21 agree very closely (better than 1 %), to within the accuracy of reading graphical data, with those of Kretch and Collin [38].

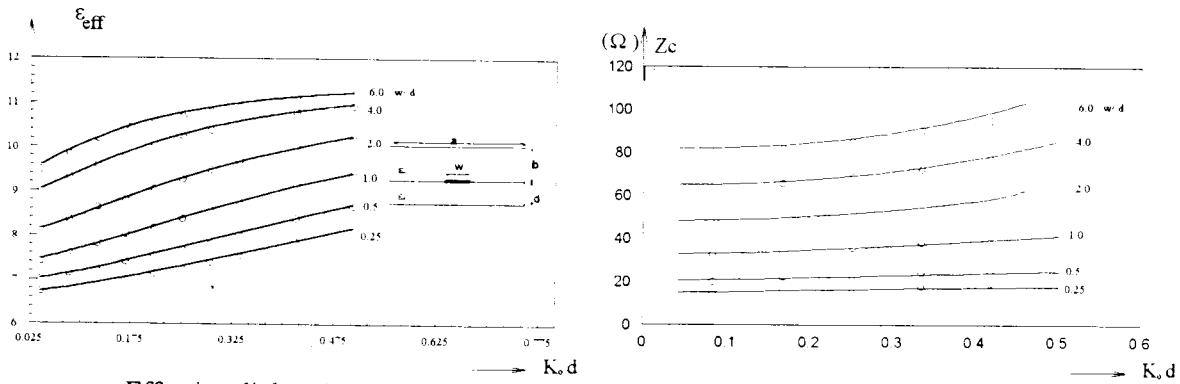

a- Effective dielectric constant

b- Characteristic impedance

Fig. 2.21 The Dispersion characteristics of a microstrip line for a Sapphire Substrate

Fig. 2.21-a shows the effective dielectric constant ε_{eff} versus the normalized frequency k_0d for a sapphire substrate with $\varepsilon_{\_}$ = 9.4 and ε_{θ}=11.6 for different values w/d. Fig. 2.21-b presents the corresponding dispersion of the characteristic impedance. It is worth to note that all the frequencies are scaled by the substrate thickness factor. This is so used in order to support thinner or thicker substrates according to the desired frequency range of operation.

An additional investigation has been carried out to estimate and determine the error introduced when the anisotropy nature of a given substrate is neglected for both ε_{eff} and Zc characteristics. Fig. 2.22 shows the dispersion characteristics ε_{eff} as a function of the normalized frequency k_0d for a microstrip line based on sapphire substrate.

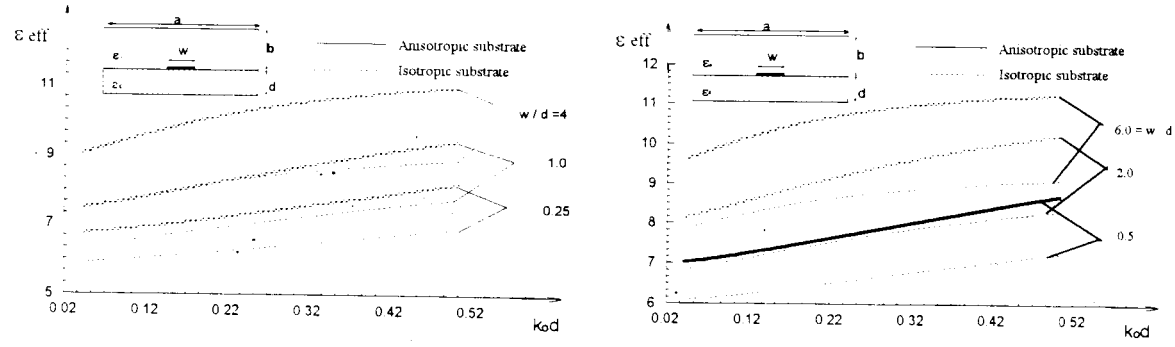

Fig. 2. 22 ε_{eff} for a microstrip line on a sapphire substrate with various strip width to substrate thickness w/d parameters.

The solid curves represent the results when anisotropy (sapphire $\varepsilon_{\_}$ = 9.4, ε_{θ}=11.6) is taken into account, while the doted curves represent the computed data when anisotropy is disregarded ($\varepsilon_{\_}$ = ε_{θ}=9.4).

Fig. 2.23 indicates the frequency dependent characteristic impedance of the microstrip line for the same parameters described above.

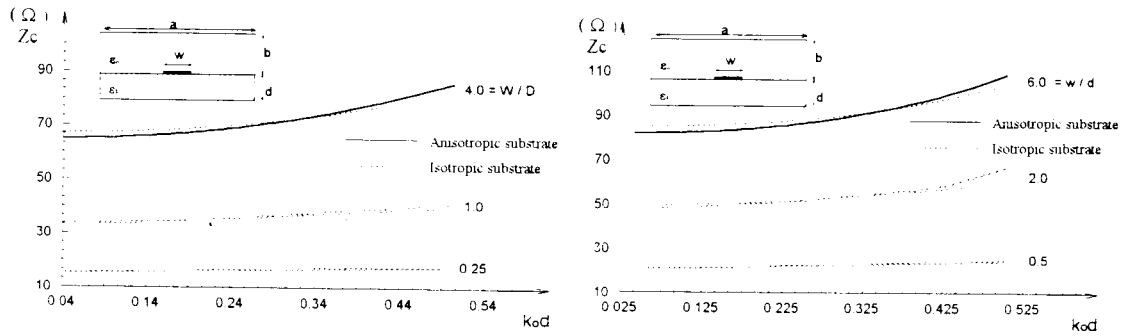

Fig. 2.23 Characteristic impedance Zc for a microstrip line on a sapphire substrate with various strip width to substrate thickness w/d parameters.

It can be noted from these two last figures that the error, between computed data when the anisotropy is considered and that when the anisotropy is disregarded , increases for narrow line widths and higher frequencies. This can be explained by the fact that the fringing field is not correctly taken into consideration when anisotropy is neglected, leading to an error in computing the wavelength and consequently the characteristic impedance.

Fig. 2.24-a shows the dispersive behaviour of $\lambda g/\lambda o$ for coupled slotline on sapphire substrate. Comparison of this results with the dispersive behaviour of the coupled slots obtained by the equivalent network method [35] and the spectral domain technique [36] indicates good agreements between the three methods. For this case in order to simulate an open structure, the geometrical dimensions are $a\ d$=20 and b/d=10. Fig. 2.24-b demonstrates the effective dielectric constant ε_{eff} for even and odd-modes for an epsilam10 substrate, when anisotropy counted for and when it is neglected. As the curves show the error when anisotropy is ignored increases as the frequency increases.

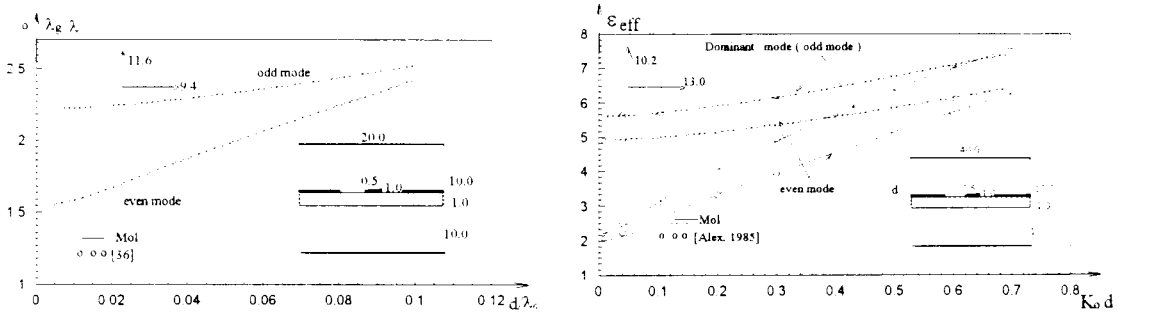

a- Structure using sapphire substrate

b- Structure using epsilam10 substrate

Fig. 2.24 Dispersion characteristics $\lambda g/\lambda o$ and ε_{eff} for a coupled slottline structure

In order to estimate this error as function of frequency, table 2.1 summarizes a comparison results for ε_{eff} using epsilam10 with ($\varepsilon_{\_}$ =13, ε_{θ}=10) as a dielectric layer.

	ε_{eff} for Even-mode			ε_{eff} for Odd-mode		
$k_o d$	Anisotropic sub. $\varepsilon_{\_}$=13, ε_{θ}=10	Isotropic sub. $\varepsilon_{\_}$=13, ε_{θ}=10	% Error	Anisotropic sub. $\varepsilon_{\_}$=13, ε_{θ}=10	Isotropic sub. $\varepsilon_{\_}$=13, ε_{θ}=10	% Error
0.01	5.6135	4.9242	12.28	2.2449	2.0095	10.48
0.7	7.6011	6.2795	17.39	7.4206	6.4324	13.31

Table 2.1 Error in neglecting substrate anisotropy (epsilam10) for a coupled slottline structure

This table 2.1 illustrates that, for the dominant mode (odd-mode) the error is 10.48 % at low frequencies when $k_o d$=0.01 and it increases to 13.31 % when $k_o d$=0.7 at higher frequencies. For the even-mode the error increases from 12.28 % when $k_o d$=0.01 to 17.39 % when $k_o d$=0.7. This example demonstrates also the significance of including substrate anisotropy in the development of highly accurate design algorithms for microwave and millimeter-wave circuits.

For a particular choice of physical dimensions of the microstrip line, the relative strip-current/slot-field distributions depend still upon the frequency and the mode number. The distribution of the electric fields *Ex*, *Ey* and *Ez* along the normalized slot (structure width/substrate width) are represented for d/λ_o=0.1 in Fig. 2.25-a and for $d\ \lambda_o$=0.3 in Fig. 2.25-b.

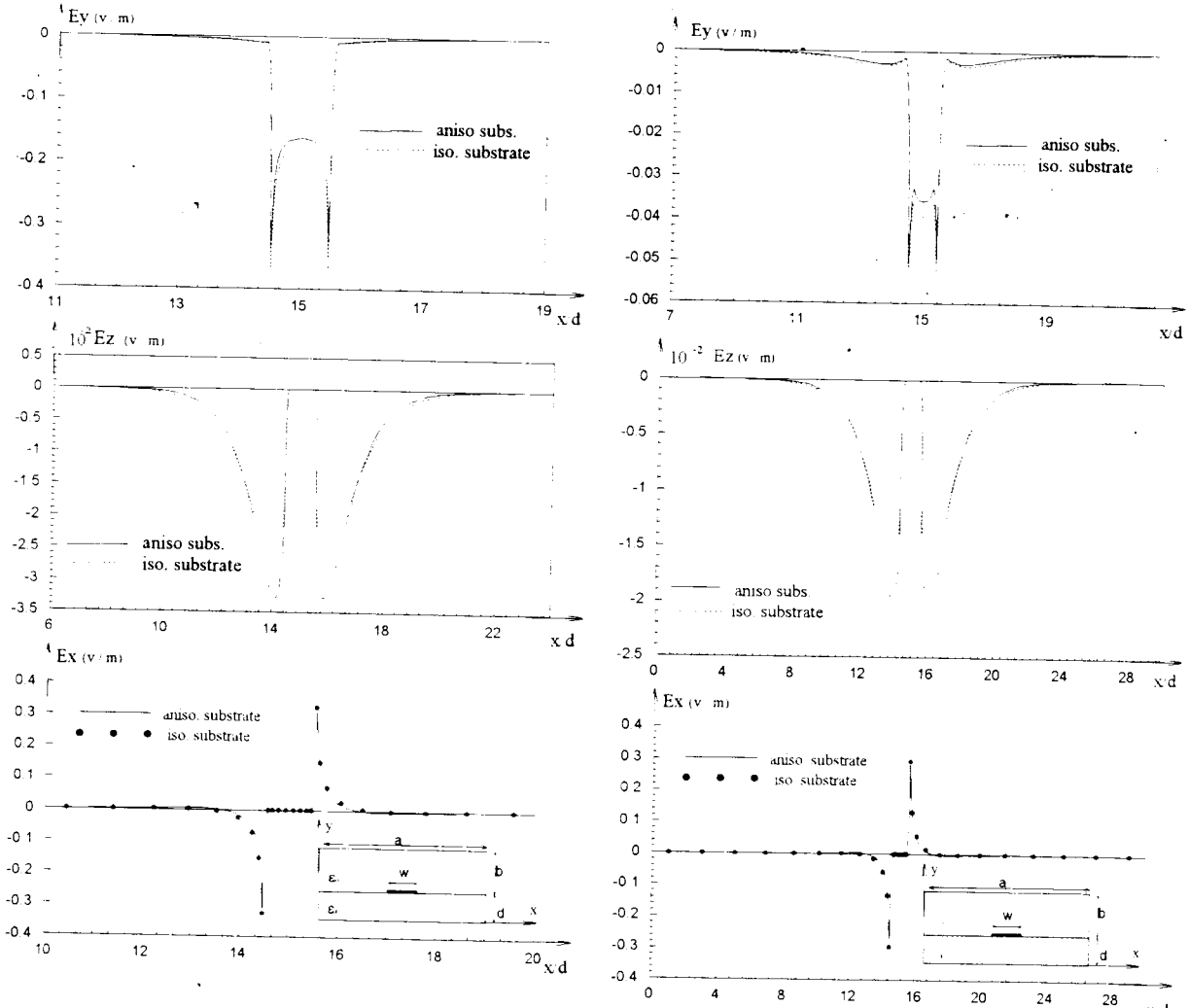

a- at the normalized frequency $k_o d$=0.1

b- at the normalized frequency $k_o d$=0.3

Fig. 2.25 Electric field Ey, Ez and Ex distribution along the normalized structure width for a microstrip line based on sapphire substrate with a/d=30, w/d=1, b/d=300

The distribution of the electric fields Jx and Jz along the normalized slot (structure width/substrate width) are represented in Fig. 2.26-a for $k_0d = 0.1$ and in Fig. 2.26-b for $k_0d = 0.3$.

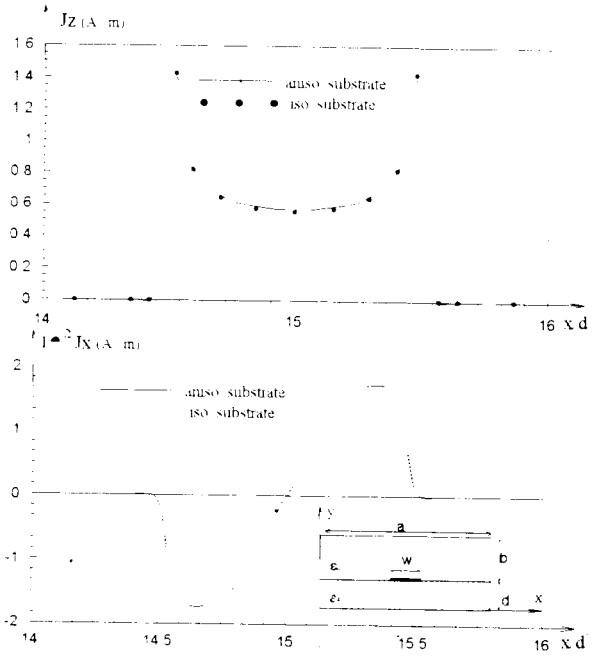

a- at the normalized frequency $d/\lambda_0=0.1$

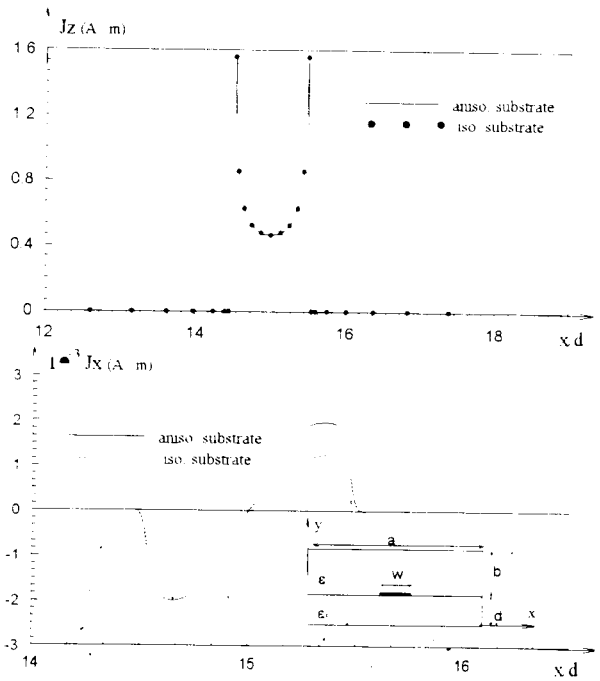

a- at the normalized frequency $d/\lambda_0=0.3$

Fig. 2.26 Current density Jz and Jx distribution along the normalized structure width for a microstrip line
based on sapphire substrate with a/d=30, w/d=1, b/d=300

All these distributions were presented for both isotropic and anisotropic substrates at the metallization interface y=d. The number of discretization lines is of 17 on each slot and 8 on the strip for $d/\lambda_0 = 0.1$, while for $d/\lambda_0 = 0.3$ a number of 20 discretization lines on each slot and 10 on the strip. It is clear from these distributions that near strip-edges the fields as well as the current distribution vary rapidly, so that a small discretization interval should be chosen there. Exterior to the strip-edge regions of high energy concentration, the functions are smooth. Hence, a coarse discretization is taken in this case.

Finally, it is instructive to plot the spatial field component for a coupled slotline structure where its physical dimensions are specified in Fig. 2.27

The distribution of the tangential electric field components over the cross-section viewed in Fig. 2.27 are represented in Fig. 2.28 for both the even and odd-mode at $d/\lambda_0 = 0.02$.

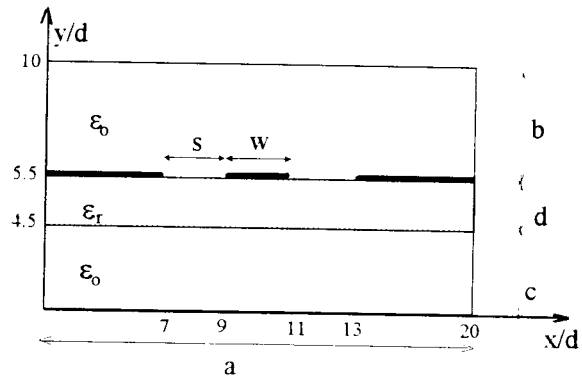

Fig. 2.28
Coplanar waveguide structure
With a/d=20. w/d=2. s/d=2.
b/d=c/d=4.5 and ε_r = 9.35.

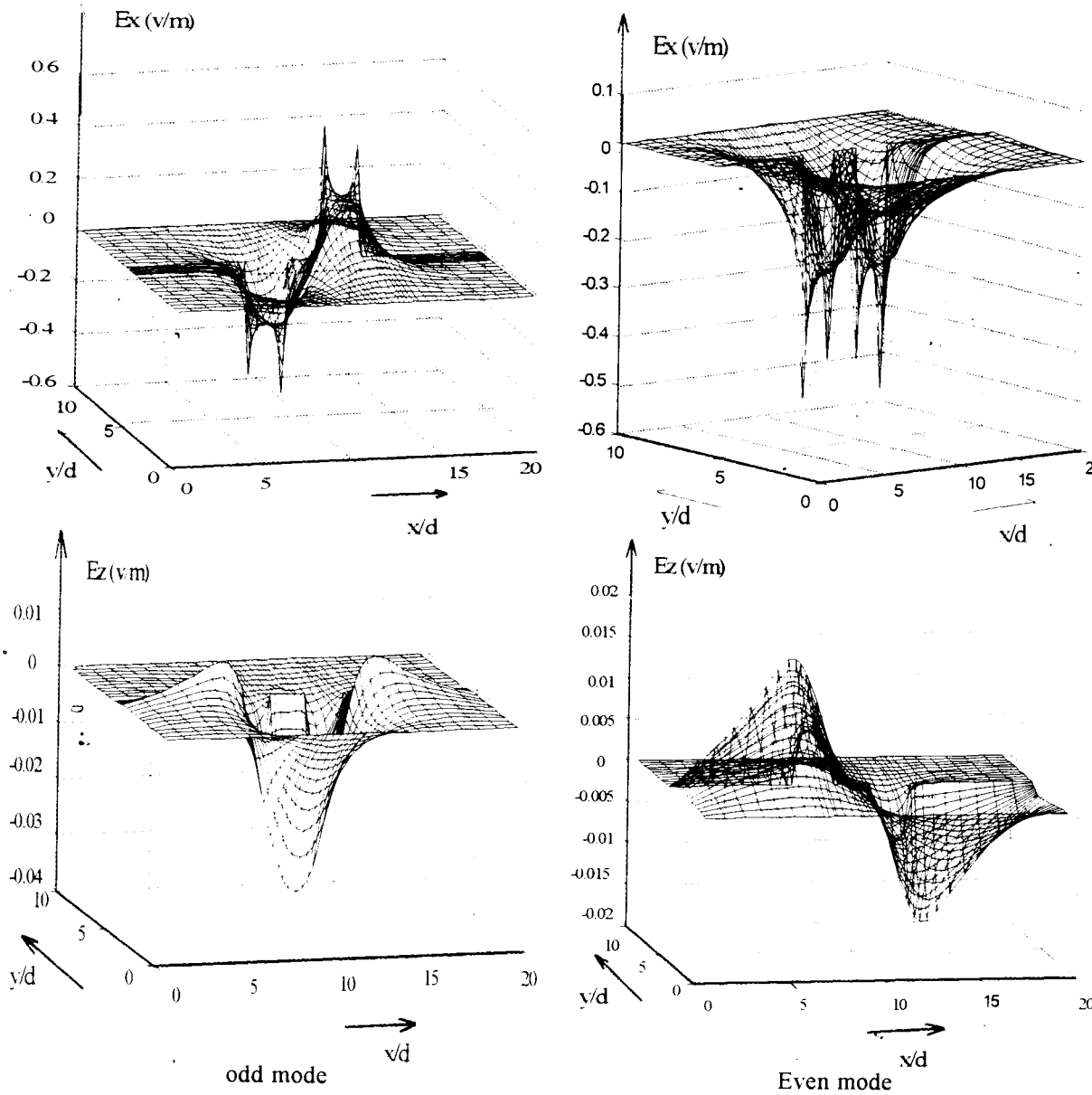

Fig. 2.28 The distribution of the electric fields Ex and Ez for the Even and Odd-mode of the Coplanar waveguide at $d/\lambda_o = 0.02$

2.13 Conclusion

A generalized full-wave analysis based on the MoL for the modelling of the dispersive properties of planar integrated circuits (MICs and MMICs) including both isotropic and anisotropic substrates is established. The derived algorithm utilizes either the uniform and the non uniform discretization approach. The exact solution can be attained by extrapolation since both approaches converge always to the exact value. However, the non uniform discretization procedure has the advantage over the uniform approach since it reduces both memory space and computing time. The numerical results obtained using this method have been presented and compared to other existing data. Good agreement was obtained in all cases, establishing thus, the accuracy and the applicability of this method for the full range of planar structures.

Moreover, the various studied planar structures have shown that when anisotropy is not accounted for in the computation of the waveguiding structure properties, an error is incurred which increases as long as the line width is decreased and/or the frequency is increased.

Knowing the above facts, it can be concluded that the MoL is an effective method to derive the dispersive properties of the distributed circuit elements on a rectangular waveguide with very good accuracy. Among its distinguished advantages, in addition to those noted in chapter 1, is the simplicity of the resulting computer algorithm allowing efficient circuit parameter computation on a personal computer.

References

[1] David W. Kammler. " Calculation of Characteristic Admittances and Coupling Coefficients for Strip Transmission Lines ". *IEEE Trans. Microwave Theory and Tech.*. MTT-16. pp. 925-937. Nov. 1968.

[2] Tajima Y.. and Kamihashi S. ." Multiconductor Couplers ". *IEEE Trans. Microwave Theory and Tech.*.. MTT-26. pp. 795-801. Oct. 1978.

[3] R. P. Owens. J. E. Aitken. " Quasi-static Characteristics of Microstrip on an Ainsotropic Sapphire Substrate ". *IEEE Trans. Microwave Theory and Tech.* . MTT-24. pp. 499-505. Aug. 1976.

[4] M. Kobayashi. " Analysis of the Microstrip and the Electrooptic light Modulator ". *IEEE Trans. Microwave Theory and Tech.*. MTT-26. N.2. pp. 119-126. Feb. 1978.

[5] S. K. Koul. and B. Bhat. "A Generalized TEM Analysis of Broadside-coupled planar Transmission lines with Isotropic or Anisotropic Substrates ". AEÜ. Band. 38. 1984. pp. 37-45.

[6] Diestel R. H.. " Analysis of Planar Multiconductor Transmission-line Systems with the Method of Lines ". Arch. Elecktron. & Ubertragungstech.. 1987. 41. pp. 169-175.

[7] R. Mittra. T. Itoh. " A new Technique for the Analysis of the Dispersion Characteristics of Microstrip Lines ". *IEEE Trans. Microwave Theory and Tech.*. MTT-19. pp. 47-56. Jan. 1971.

[8] Jansen R. H.. " Fast Accurate Hybrid-mode Computation of Non-Symmetrical Coupled Microstrip Characteristics ". Proc. 7 th European Microwave Conf.. 1977. pp. 135-139.

[9] Jansen R. H.. " High-speed Computation of the Single and Coupled Microstrip Including Dispersion. High-order modes. Loss and Finite strip Thickness ". *IEEE Trans. Microwave Theory and Tech.*. MTT-26. pp. 75-82. 1978.

[10] T. Itoh. R. Mittra. " A technique for Computing Dispersion Characteristics of Shielded Microstrip Lines ". *IEEE Trans., Microwave Theory and Tech.*. pp. 896-989. Oct. 1974.
[11] T. Itoh. " Analysis of Microstrip Resonators ". *IEEE Trans. Microwave Theory and Tech.*. MTT-22. pp. 946 - 952. Nov. 1974.
[12] T. Itoh. R. Mittra. Analysis of a Microstrip Disk Resonators ". AEÜ. Band 27. 1978. pp. 456-458.
[13] T. Itoh and R. Mittra. " Spectral-Domain approach for Calculating the Dispersion Characteristics of Microstrip Lines ". *IEEE Trans. Microwave Theory and Tech.*. pp. 496-499. July 1973.
[14] W. J. Getsinger. " Microstrip Dispersion Model ". IEEE Trans.. MTT-21. pp. 34-39. Jan. 1973
[15] A. Kamal Saad and K. Schünemann. " A Simple Method for Analyzing Finline Structures ". *IEEE Trans. Microwave Theory and Tech.*. MTT-26. pp. 1002-1007. Dec. 1978.
[16] W. Menzel and I. Wolff. " A method for Calculating the Frequency Dependent Properties of Microstrip Discontinuities ". *IEEE Trans. Microwave Theory and Tech.*. MTT-25. pp. 107-112. Feb. 1977.
[17] D. Mirshekar-Syakhal and J. B. Davies. " An accurate Unified solution to various Fin-Line Structures of Phase Constant. Characteristic Impedance. Attenuation ". *IEEE Trans. Microwave Theory and Tech.*. MTT-30. pp. 1854-1861. Nov. 1982.
[18] D. Mirshekar-Syakhal and J. B. Davies. " An accurate Analysis of Coupled Strip Finline Structure for Phase Constant. Characteristic Impedance. Dielectric and Conductor Losses ". *IEEE Trans. Microwave Theory and Tech.*. MTT-30. pp. 906 - 910. June 1982.
[19] H. Lee and V. Tripathi. " Spectral Domain Analysis of Frequency Dependent Propagation Characteristics of Planar Structures on Uniaxial Medium ". *IEEE Trans. Microwave Theory and Tech.*. MTT-30. pp. 1188-1193. Aug. 1982.
[20] R. Sorrentino and T. Itoh. " Transverse Resonance Analysis of Finline Discontinuities ". *IEEE Trans. Microwave Theory and Tech.*. MTT-32. pp. 1633-1638. Dec. 1984.
[21] V. Tripathi and R. J. Bucolo. " A Simple Network Analogue Approach for the Quasi-static Characteristics of General Lossy. Anisotropic. Layered Structures ". *IEEE Trans. Microwave Theory and Tech.*.. MTT-33. pp. 1458-1464. Dec. 1985.
[22] Y. Fukuoka. Q. D. P. Neikirk and T. Itoh. " Analysis of Multilayer Interconnection Lines for a High-speed Digital Integrated Circuits ". *IEEE Trans. Microwave Theory and Tech.*.. MTT-33. pp. 527-532. June 1985.
[23] K. Bierwirth. N. Schulz and F. Arndt. " Finite difference Analysis of Rectangular Dielectric Waveguide Structures ". *IEEE Trans. Microwave Theory and Tech.*. MTT-34. pp. 1104-1114. Nov. 1986.
[24] N. H. L. Koster and R. H. Jansen. " The Microstrip Discontinuity : A Revised Description ". *IEEE Trans. Microwave Theory and Tech.*. MTT-34. pp. 213-223. Feb. 1986.
[25] R. Pregla " Analysis of Planar Microwave Structures on Magnetized Ferrite Substrate ". AEÜ. Band 40. pp. 270-274. 1986.
[26] R. Collin. Field of Guided Waves . New York : McGraw-Hill. 1960
[27] R. E. Collin. Foundations for Microwave Engineering . McGraw-Hill. 1966.
[28] Schulz U.. " On the Edge condition with the method of Lines in Planar Waveguides ". Arch. Elekron. Uebertragungstech.. 34. pp. 176-178. 1980.
[29] J. Meixner. " The Behaviour of Electromagnetic fields at edges ". IEEE AP-20 (1972). pp. 442-446.
[30] Schulz U. and Pregla R.. " A New Technique for the analysis of the Dispersion Characteristics of Planar waveguides and its Application to Microstrip with Tuning Septums. Radio Science 16. No. 6. pp. 1173-1178. 1981.
[31] Diestel H. and S. B. Worm. " Analysis of Hybrid Field Problems by the Method of Lines with non equidistant Discretization ". *IEEE Trans. Microwave Theory and Tech.*. MTT-32(6). pp. 633-638. 1984.
[32] Kowalski G. and Pregla R.. " Dispersion Characteristics of Shielded Microstrip with Finite Thickness ". AEÜ pp. 193-196. [1971].
[33] U. Shulz and R. Pregla. " A New technique for the Analysis of the Dispersion Characteristics of Planar waveguides ". AEÜ. band. 34. Half 4. pp. 169-173. 1980.
[34] U. Rogge and R. Pregla. " The Method of Lines for the Analysis of Strip-Loaded Optical Waveguides ".
[35] T. Kitazawa and Y. Hayashi. " Coupled slots on an Anisotropic Sapphire Substrate ".*IEEE Trans. Microwave Theory and Tech.*. Vol. MTT-29. pp. 1035 - 1040. Oct. 1981.
[36] R. Jansen. " Unified user-oriented computation of shielded. covered and open planar millimeter-wave transmission Line characteristics ". IEE Proc. Microwaves. Opt. & Accoust.. 1979. 3. pp. 14-22
[37] S. N. Hoa Ling and T. Itoh. " Time domain method of lines applied to planar guided wave structures. ". *IEEE Trans. Microwave Theory and Tech.*. MTT-37. pp. 897-901. May 1989.

[38] V. K. Wirth and J. Siegl. " Time-domain circuit simulation including including coupled multiconductor transmission lines. " Frequenz. 42. pp. 305-313. oct. 1988.
[39] A. C. Keen. M. J. Wale. M. I. Sobhy and A. J. Holden. " quasi-static analysis of elctrooptic modulators by the method of lines. " J. Lightwave Technol.. vol. 8. pp. 42-50. 1990.
[40] M.Kobayashi. " Analysis of the microstrip and the electrooptic light modulators. " *IEEE Trans. Microwave Theory and Tech.*. MTT-26. pp. 119-126. Feb. 1978.
[41] R. Pregla and F. J. Scmükle. " The method of lines for the analysis of planar wave structures with finite metallization thickness. " (in German). *Kleinheubacher Berichte*. Vol. 31. 431-438. 1988.
[42] N.G. Alexopoulos. " Integrated-circuit structures on anisotropic substrates. " *IEEE Trans. Microwave Theory and Tech.*. MTT-33. pp. 847-881. 1985.
[43] R. C. Gupta. R. Garg and I. J. Bahl. Microstrip lines and slotlines. MA: Artech. House. 1979
[44] T. C. Edwards. Foundations for microstrip circuit design. New York : Wiley 1981.
[45] R.P. Owens. J. E. Aitken. and T. C. Edwards. " Quasi-static characteristics of microstrip on an anisotropic sapphire substrate. " *IEEE Trans. Microwave Theory and Tech.*. MTT-24. pp. 499-505. 1976.
[46] B. M. Sherill and N. Alexopoulos. " The method of lines applied to a finline/strip configuration on an anisotropic substrate. " *IEEE Trans. Microwave Theory and Tech.*. MTT-35. pp. 568-575. 1987.
[47] S. K. Koul and B. Bhat. " A generalized TEM analysis of broadside coupled planar transmission lines with isotropic and anisotropic substrates. " AEÜ. Band 38. Heft 1. pp. 37-45. dec. 1984.
[48] A. Nakatani and N. G. Alexopoulos. " Toward a generalized algorithm for the modelling of the dispersive properties of integrated circuit structures on anisotropic substrates. "*IEEE Trans. Microwave Theory and Tech.*. MTT-33. pp. 1436-1441. dec. 1985.
[49] B. E. Kretch and R. E. Collin. " Microstrip dispersion including anisotropic substrates. "*IEEE Trans. Microwave Theory and Tech.*. MTT-35. pp. 710-718. Aug. 1987.
[50] N. G. Alexopoulos and S. Maas. " Characteristics of microstrip directional couplers on anisotropic substrates. " *IEEE Trans. Microwave Theory and Tech.*. MTT-30. pp. 1267-1270. Aug. 1982.
[51] R. Pregla and W. Pasher. " The method of lines " in Numerical Techniques for Microwave and Millimeter wave Passif Structures. T. Itoh. Ed. New-York : Wiley. 1989. pp. 381-446.

Chapter 3

Analysis of Microwave Structures With Finite Metallization Thickness

3.1 Introduction

The actual trend of microwave engineering is toward integrating circuits operating at higher frequencies that overtake the millimeter-wave region or the spectrum above 30 GHz. The planar and quasi-planar transmission line structures used in MICs, MMICs and optical integrated circuits operating at higher frequencies are of reduced size. This is in accordance with the desired electrical characteristics that are imposed by circuit design constraint, and satisfying in addition the commercial pressure to increase the on-chip component density. This size-reduction of a cross-sectional dimension of the planar transmission line structure leads consequently to shorten the metallization strip and gap widths. It is then obvious that the metallic thickness of strips become more significant at higher frequencies, as it is in the same order of magnitude as strip and/or slot's width. However, it will not be approved [1,7] to neglect this metallization thickness at millimeter wave frequencies. This is, in fact, another area for improving the analysis of MICs and MMICs by taking into account the effect of metal thickness on the dispersion characteristics of the transmission line structures.

The vectorial method of lines, since only vectors or diagonal matrices are carried out during the numerical computations simultaneously with its other pertinent properties, is more adequate over many other techniques particularly for the analysis of microwave planar structures with finite metallization thickness.

3.2 Hybrid-mode Analysis using Uniform Discretization

A typical cross-section of planar structure of multidielectric layer multi-strip conductors is represented in Fig. 3.1 and is considered to illustrate the mathematical formulation. The analysis is only demonstrated for this planar structure but its extension to multi-metallization interfaces is straight forward, as it has been previously done for the zero metal thickness so far in chapter 2. Because of symmetry, only half of a cross-section as represented in Fig. 3.1 is considered. It consists of a set of p layers used as substrates located at the underneath of the metallization interface (MI), and a set of m layers as superstrates at the upper side of the MI. The MI is generally formed by a set of even or odd number of strip conductors.

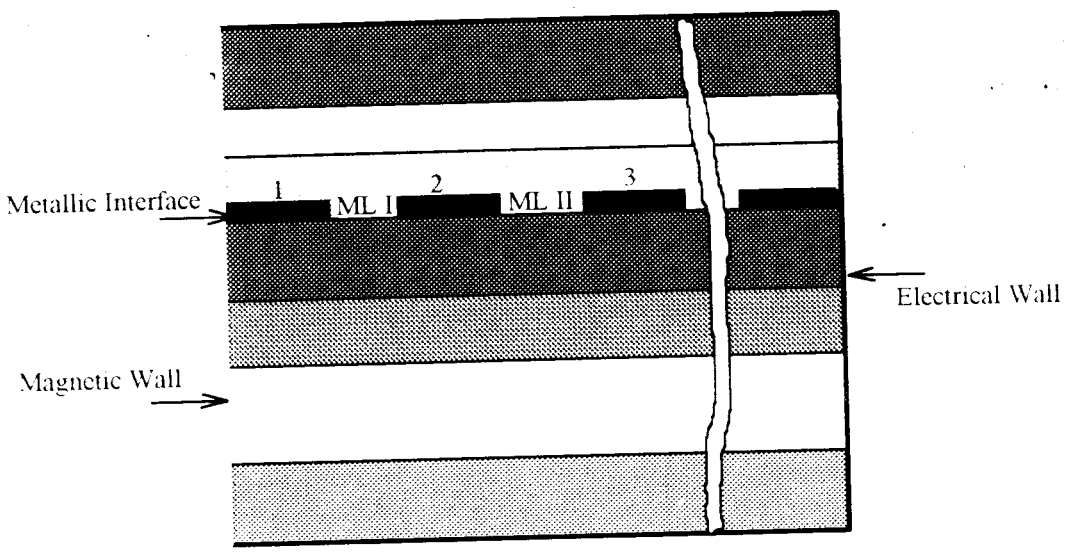

Fig. 3.1 A half cross-section of multilayers and single metallization interface of multistrip conductors

It has been shown in chapter 2 that, for a set of dielectric layers, a single equivalent layer may be obtained by using reccurence relation eq.(2. 79). However,this leads to more simplified formulation and instead of Fig.3.1 an equivalent structure may be adopted as shown in Figure3.2.

3.2 Hybrid-mode Analysis using Uniform Discretization

A typical cross-section of planar structure of multidielectric layer multi-strip conductors is represented in Fig. 3.1 and is considered to illustrate the mathematical formulation. The analysis is only demonstrated for this planar structure but its extension to multi-metallization interfaces is straight forward, as it has been previously done for the zero metal thickness so far in chapter 2. Because of symmetry, only half of a cross-section as represented in Fig. 3.1 is considered. It consists of a set of p layers used as substrates located at the underneath of the metallization interface (MI), and a set of m layers as superstrates at the upper side of the MI. The MI is generally formed by a set of even or odd number of strip conductors.

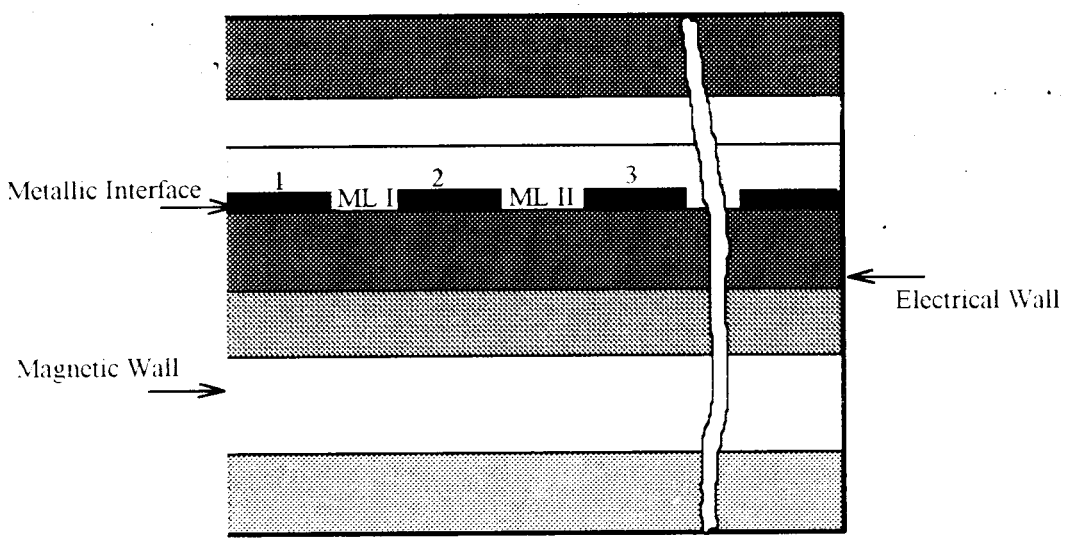

Fig. 3.1 A half cross-section of multilayers and single metallization interface of multistrip conductors

It has been shown in chapter 2 that, for a set of dielectric layers, a single equivalent layer may be obtained by using reccurence relation eq.(2. 79). However,this leads to more simplified formulation and instead of Fig.3.1 an equivalent structure may be adopted as shown in Figure3.2.

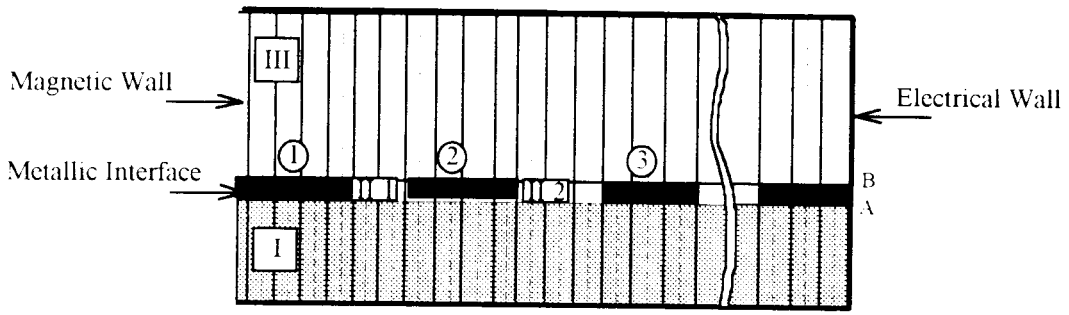

Fig. 3.2 An equivalent planar structure of multilayer and single metallization interface

The region II contains the metallization strip conductors of thickness t, and are typically arranged as shown in Fig. 3.2. The gap between the strip conductors can be filled by different dielectrics with thickness t. In order to derive the electromagnetic field within the gaps, we must consider for each region II_i a metalic or an electric wall on either side, constituted by the lateral sides of the strip conductors. To realize this condition, the discretization lines of the electric field should coincide with the metallization edges, satisfying thus, the physical boundary conditions in either side of the intermediate region. We consider that each region II_i is discretized by N^i_{II} related electric field function and $N^i_{II}+1$ related magnetic field function. Moreover the relationship connecting the tengential electric and magnetic field components at the interfaces A and B is still valid. According to eq. (2.22) for isotropic dielectric layer and eq. (2.53) for anisotropic layer, the tengential electromagnetic fields can be described for each intermediate region i by

$$\eta_0 \begin{bmatrix} -j\overline{H}_{zA} \\ \overline{H}_{xA} \\ -j\overline{H}_{zB} \\ \overline{H}_{xB} \end{bmatrix}_{II_i} = \begin{bmatrix} \overline{Y}^{II_i}_{11} & \overline{Y}^{II_i}_{12} & \overline{Y}^{II_i}_{13} & \overline{Y}^{II_i}_{13} \\ \overline{Y}^{II_i}_{21} & \overline{Y}^{II_i}_{22} & \overline{Y}^{II_i}_{23} & \overline{Y}^{II_i}_{24} \\ \overline{Y}^{II_i}_{13} & \overline{Y}^{II_i}_{13} & \overline{Y}^{II_i}_{11} & \overline{Y}^{II_i}_{12} \\ \overline{Y}^{II_i}_{23} & \overline{Y}^{II_i}_{24} & \overline{Y}^{II_i}_{21} & \overline{Y}^{II_i}_{22} \end{bmatrix} \begin{bmatrix} \overline{E}_{xA} \\ -j\overline{E}_{zA} \\ -\overline{E}_{xB} \\ j\overline{E}_{zB} \end{bmatrix}_{II_i} \qquad i = 1,2,\ldots,r \qquad (3.1)$$

Where r is the number of intermediate regions. The elements of the system (3.1) for each intermediate region are generally different from each other. This is because, there are different numbers of discretization lines, leading to different matrices λ and T. In addition, it is obvious that these quantities are also differents from those of the region I and III, e.g. λ, T, and ε_r. This system may be compressed by assembling subvectors of the same kind and at the same interface according to

$$E_{A,B\,\mathrm{II}_i} = \begin{bmatrix} E_{xA,B} \\ -jE_{zA,B} \end{bmatrix}_{\mathrm{II}_i} \quad ; \quad H_{A,B\,\mathrm{II}_i} = \eta_o \begin{bmatrix} -jH_{zA,B} \\ H_{xA,B} \end{bmatrix}_{\mathrm{II}_i} \tag{3.2}$$

Then, the system (3.1) may be reduced to

$$\begin{bmatrix} \overline{H}_A \\ \overline{H}_B \end{bmatrix}_{\mathrm{II}_i} = \begin{bmatrix} \overline{y}_1^{\mathrm{II}_i} & \overline{y}_2^{\mathrm{II}_i} \\ \overline{y}_2^{\mathrm{II}_i} & \overline{y}_1^{\mathrm{II}_i} \end{bmatrix} \begin{bmatrix} \overline{E}_A \\ -\overline{E}_B \end{bmatrix}_{\mathrm{II}_i} \tag{3.3}$$

with

$$\overline{y}_1^{\mathrm{II}_i} = \begin{bmatrix} \overline{y}_{11} & \overline{y}_{12} \\ \overline{y}_{21} & \overline{y}_{22} \end{bmatrix}_{\mathrm{II}_i} \quad ; \quad \overline{y}_2^{\mathrm{II}_i} = \begin{bmatrix} \overline{y}_{13} & \overline{y}_{14} \\ \overline{y}_{23} & \overline{y}_{24} \end{bmatrix}_{\mathrm{II}_i} \tag{3.4}$$

and $\overline{y}_{ij}$ are appropriate quantities relative to each region (II_i, i = 1,2,..., r) and they are defined in eq. (2.23) for the isotropic dielectric layer and eq. (2.55) from the anisotropic case.In addition, these matrices $\overline{y}_{ij}$ can also be determined for a set of dielectric layers, within which no metallization is assumed to exist, by means of reccurence relation (2.79) as illustrated in chapter 2.

The relation of the transformed tengential field, that connects the tengential magnetic fields to the tengential electric fields at the lower interface A of the region I can be written as:

$$\eta_0 \begin{bmatrix} -j\overline{H}_{zA} \\ \overline{H}_{xA} \end{bmatrix} = \begin{bmatrix} \overline{y}_{11}^{I} & \overline{y}_{12}^{I} \\ \overline{y}_{21}^{I} & \overline{y}_{22}^{I} \end{bmatrix} \begin{bmatrix} \overline{E}_{xA} \\ -j\overline{E}_{zA} \end{bmatrix} \tag{3.5}$$

or abreviated by

$$\overline{H}_A = \overline{y}_1^{I}\, \overline{E}_A \tag{3.6}$$

the diagonal matrices $\overline{y}_{ij}^{I}$ are determined in a similar way as described in section 2.6 for a single and multidielectric layers . In the case of single dielectric layer they are given by eq. (2.58). In the same way as that for the zero metallization thickness case, at the upper interface B (Fig. 3.2) one can develop a relationship between the tengential magnetic and that of the electric field , which is given for the upper region III by

$$\eta_0 \begin{bmatrix} j\overline{H}_{zB} \\ -\overline{H}_{xB} \end{bmatrix} = \begin{bmatrix} \overline{y}_{11}^{III} & \overline{y}_{12}^{III} \\ \overline{y}_{21}^{III} & \overline{y}_{22}^{III} \end{bmatrix} \begin{bmatrix} \overline{E}_{xB} \\ -j\overline{E}_{zB} \end{bmatrix} \tag{3.7}$$

or may be compressed to

$$\overline{H}_B = -\overline{y}_1^{III}\,\overline{E}_B \tag{3.8}$$

The diagonal matrices $\overline{y}_{ij}^{III}$ are like $\overline{y}_{ij}^{I}$, but they are inherent properties of region III.

The field at the intermediate region II must be matched in the spatial domain at both interfaces A and B in conjunction with the other fields resulted from the lower layer I and upper layer III.

In Electromagnetic theory, it is known that the tengential electric field vanishes within the perfect conductor like the tengential magnetic field. Indeed, for infinite conductivity the field in the conductor must be zero, since the flux lines of B are continuous, and in addition because the tengential component of E is continuous across the boundary, then, it is necessary that

$$\begin{aligned} n \cdot B &= 0 \\ E_t &= n \times E = 0 \end{aligned} \tag{3.9}$$

at the surface of a perfect conductor where n is a unit vector. However, for the tengential components of H the situation is different because a surface current J_s will exist on the surface in the limit $\sigma \to \infty$.

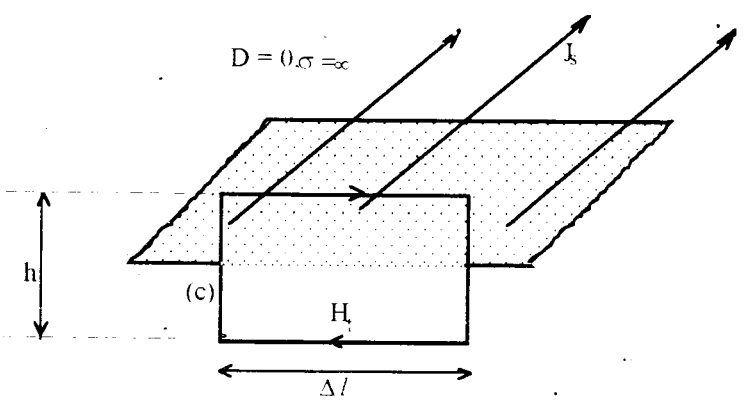

Fig. 3.3 Boundary of a perfect conductor

Applying Maxwell's equation to the countour C as illustrated in Fig. 3.3 [8], we get

$$\oint H \cdot dl = j\omega \int D \cdot dS + \int J \cdot dS$$

$$\oint H \cdot dl = H_t \Delta l = \lim_{h \to 0} \int j\omega D \cdot dS + \lim_{h \to 0} \int J \cdot dS$$

$$= \lim_{h \to 0} h J \cdot \Delta l = J_s \Delta l$$

or in vector form, as

$$n \times H = J_s \tag{3.10}$$

Here H is the magnetic field component at the metallic interface. It is worth to note that, both B and H vanishe within a perfect conductor.

Applying now the last result in eq. (3.10) to the actual studied case of finite conductor thickness. For the situation where the strip conductor is on the dielectic layer, and when neglecting the current J_y component, we get

$$\begin{aligned} H_x^- &= J_z \\ H_z^- &= -J_x \end{aligned} \tag{3.11}$$

Field matching at the interfaces A and B, as shown in Fig. 3.2, must be done in the spatial domain by means of eq. (3.10) for metallic regions by using the continuity condition of the tengential electric field within the regions of dielectric medium at the [illegible]. For instance at interface A, we have

$$E_{xA}^I = \begin{bmatrix} 0 \\ E_{xA}^{II1} \\ 0 \\ E_{xA}^{II2} \\ \vdots \end{bmatrix} ; \; E_{ZA}^I = \begin{bmatrix} 0 \\ E_{zA}^{II1} \\ 0 \\ E_{zA}^{II2} \\ \vdots \end{bmatrix} ; \; H_{xA}^I = \begin{bmatrix} J_{zA}^1 \\ H_{xA}^{II1} \\ J_{zA}^2 \\ H_{xA}^{II2} \\ \vdots \end{bmatrix} ; \; H_{ZA}^I = \begin{bmatrix} -J_{xA}^1 \\ H_{zA}^{II1} \\ -J_{xA}^2 \\ H_{zA}^{II2} \\ \vdots \end{bmatrix} \tag{3.12}$$

and similarly at interface B we get

$$E_{xB}^{III} = \begin{bmatrix} 0 \\ E_{xB}^{II1} \\ 0 \\ E_{xB}^{II2} \\ \vdots \end{bmatrix} ; \; E_{ZB}^{III} = \begin{bmatrix} 0 \\ E_{zB}^{II1} \\ 0 \\ E_{zB}^{II2} \\ \vdots \end{bmatrix} ; \; H_{xB}^{III} = \begin{bmatrix} -J_{zB}^1 \\ H_{xB}^{II1} \\ J_{zB}^2 \\ H_{xB}^{II2} \\ \vdots \end{bmatrix} ; \; H_{ZB}^{III} = \begin{bmatrix} J_{xB}^1 \\ H_{zB}^{II1} \\ -J_{xB}^2 \\ H_{zB}^{II2} \\ \vdots \end{bmatrix} \tag{3.13}$$

In these equations (3.12) and (3.13) the superscripts 1,2,... of the currents J and field components E, denote the 1st,2nd, ... strip conductors and intermediate regions respectively.

The back transformation of eq. (3.5) to the original domain for the case of boundary condition presented in Fig. 3.2, is performed by inverse transformation as

$$\begin{bmatrix} -jH_{zA} \\ H_{xA} \end{bmatrix} = \begin{bmatrix} T_{DN} & \\ & T_{ND} \end{bmatrix} \begin{bmatrix} \bar{y}_{11}^{I} & \bar{y}_{12}^{I} \\ \bar{y}_{21}^{I} & \bar{y}_{22}^{I} \end{bmatrix} \begin{bmatrix} T_{DN}^{t} & \\ & T_{ND}^{t} \end{bmatrix} \begin{bmatrix} \bar{E}_{xA} \\ -j\bar{E}_{zA} \end{bmatrix} \tag{3.14}$$

Substitution of eq. (3.12) into eq. (3.14) gives

$$\begin{bmatrix} jJ_{xA}^{1} \\ -jH_{zA}^{II1} \\ jJ_{xA}^{2} \\ -jH_{zA}^{II1} \\ \vdots \\ J_{zA}^{1} \\ H_{xA}^{II1} \\ J_{zA}^{2} \\ H_{xA}^{II1} \\ \vdots \end{bmatrix} = \begin{bmatrix} T_{DN} & \\ & T_{ND} \end{bmatrix} \begin{bmatrix} \bar{y}_{11}^{I} & \bar{y}_{12}^{I} \\ \bar{y}_{21}^{I} & \bar{y}_{22}^{I} \end{bmatrix} \begin{bmatrix} T_{DN}^{t} & \\ & T_{ND}^{t} \end{bmatrix} \begin{bmatrix} 0 \\ E_{xA}^{II1} \\ 0 \\ E_{xA}^{II2} \\ \vdots \\ 0 \\ -jE_{zA}^{II1} \\ 0 \\ -jE_{zA}^{II2} \\ \vdots \end{bmatrix} \tag{3.15}$$

This sytem of equations may be splited into two independent systems, where one of them establishes the relation between only the field components. In order to accomplish this decomposition, we first introduce the following abbreviations

$$H_A^{II} = \begin{bmatrix} -jH_{zA}^{II1} \\ -jH_{zA}^{II2} \\ \vdots \\ H_{xA}^{II1} \\ H_{xA}^{II2} \\ \vdots \end{bmatrix}; \; E_A^{II} = \begin{bmatrix} E_{xA}^{II1} \\ E_{xA}^{II2} \\ \vdots \\ -jE_{zA}^{II1} \\ -jE_{zA}^{II2} \\ \vdots \end{bmatrix}; \; J_A = \begin{bmatrix} jJ_{xA}^{1} \\ jJ_{xA}^{2} \\ \vdots \\ J_{zA}^{1} \\ J_{zA}^{2} \\ \vdots \end{bmatrix} \tag{3.16}$$

and the reduced transformation matrix T^r superscripted by r, and its complement T^{rc} containing the remained elements of the full-matrix without the reduced transformation matrix T^r. These matrices may be represented as

$$T_I^r = \begin{bmatrix} T_{DN}^r & \\ & T_{ND}^r \end{bmatrix}, \quad T_I^{rc} = \begin{bmatrix} T_{DN}^{rc} & \\ & T_{ND}^{rc} \end{bmatrix} \tag{3.17}$$

The reduced transformation matrices are formed by gathering block matrices belonging to the lines in the slot or intermediate regions. This means that T^r is not necessary a square matrix. While the complementary matrix is the other part of the full matrix, and consists of rows which belong to the lines in the strip conductor as illustrated in Fig. 3.4.

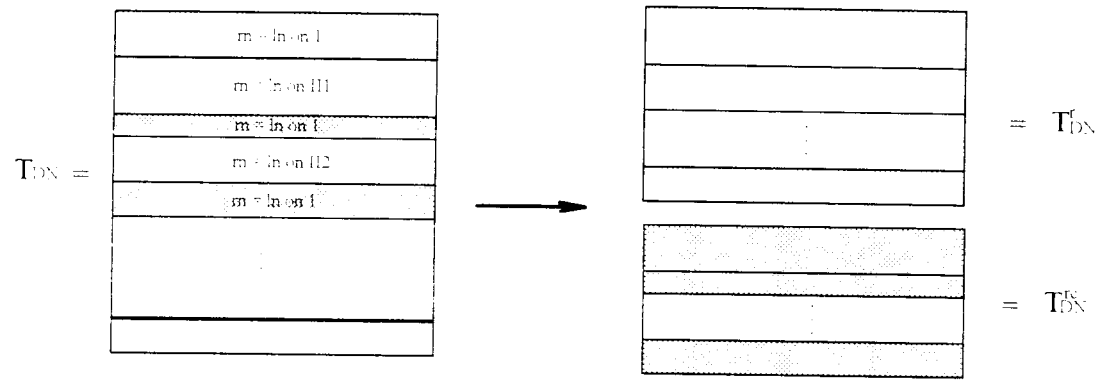

Fig. 3.4 Illustration of the reduction of the transformation matrices
rn : row numbers , ln : line numbers

Using these abbreviations, the system (3.10) is divided into two systems which are given by

$$H_A^{II} = T_I^r \bar{y}_1^I T_I^{rt} E_A^{II} \tag{3.18}$$

$$J_A = T_I^{rc} \bar{y}_1^I T_I^{rt} E_A^{II} \tag{3.19}$$

A complete analogue way may be developed for the interface B where the spatial component relationship can be performed by inverse transformation of eq. (3.7). After substituting eq. (3.13) the system established for the interface B' is given by

$$\begin{bmatrix} \\ jJ_{xB}^1 \\ jH_{zB}^{II1} \\ jJ_{xB}^2 \\ jH_{zB}^{II1} \\ \vdots \\ J_{zB}^1 \\ -H_{xB}^{II1} \\ J_{zB}^2 \\ -H_{xB}^{II1} \\ \vdots \end{bmatrix} = \begin{bmatrix} T_{DN} & \\ & T_{ND} \end{bmatrix} \begin{bmatrix} \bar{y}_{11}^{III} & \bar{y}_{12}^{III} \\ \bar{y}_{21}^{III} & \bar{y}_{22}^{III} \end{bmatrix} \begin{bmatrix} T_{DN}^t & \\ & T_{ND}^t \end{bmatrix} \begin{bmatrix} 0 \\ E_{xB}^{II1} \\ 0 \\ E_{xB}^{II2} \\ \vdots \\ 0 \\ -jE_{zB}^{II1} \\ 0 \\ -jE_{zB}^{II2} \\ \vdots \end{bmatrix} \tag{3.20}$$

and when inserting again the abbreviations

$$H_B^{II} = \begin{bmatrix} -jH_{zB}^{II1} \\ -jH_{zB}^{II2} \\ \vdots \\ H_{xB}^{II1} \\ H_{xB}^{II2} \\ \vdots \end{bmatrix} \quad ; \quad E_B^{II} = \begin{bmatrix} E_{xB}^{II1} \\ E_{xB}^{II2} \\ \vdots \\ -jE_{zB}^{II1} \\ -jE_{zB}^{II2} \\ \vdots \end{bmatrix} \quad ; \quad J_B = \begin{bmatrix} jJ_{xB}^{1} \\ jJ_{xB}^{2} \\ \vdots \\ J_{zB}^{1} \\ J_{zB}^{2} \\ \vdots \end{bmatrix} \tag{3.21}$$

then, the system (3.20) may be divided to

$$-H_B^{II} = T_{III}^{r} \bar{y}_1^{III} T_{III}^{rt} E_B^{II} \tag{3.22}$$

$$J_B = T_{III}^{rc} \bar{y}_1^{III} T_{III}^{rt} E_B^{II} \tag{3.23}$$

where y_1^{III} represents the block matrix of the $\bar{y}_{ij}^{III}$ and $T_{III} = T_I$ for the case of Fig. 3.2.
Transformation of eq. (3.3) to the spatial domain for all the intermediate regions yields

$$\begin{bmatrix} H_A^{IIi} \\ H_B^{IIi} \end{bmatrix} = \begin{bmatrix} T_{II}^{i} & \\ & T_{II}^{i} \end{bmatrix} \begin{bmatrix} \bar{y}_1^{IIi} & \bar{y}_2^{IIi} \\ \bar{y}_2^{IIi} & \bar{y}_1^{IIi} \end{bmatrix} \begin{bmatrix} T_{II}^{it} & \\ & T_{II}^{it} \end{bmatrix} \begin{bmatrix} E_A^{IIi} \\ -E_B^{IIi} \end{bmatrix} \qquad i = 1,2,\ldots \tag{3.24}$$

with

$$T_{II}^{i} = \begin{bmatrix} T_{NN}^{i} & \\ & T_{DD}^{i} \end{bmatrix} \tag{3.25}$$

where the matrices T_{NN}^{i} and T_{DD}^{i} are appropriate transformation matrices for each slot or intermediate region.

The systems (3.18), (3.22) and (3.24) established for each region (e.g. I, II, III) are enforced with continuity condition of the tengential electrical field at the interfaces A and B. In order to satisfy the continuity condition, the equations of all slot regions II^i must be combined to form one equation. In addition, the vectors E^{IIi} and H^{IIi} must be splitted into x and z parts and must be represented in the arrangement as the components in the vectors of eqs. (3.16) and (3.21). To achieve this combination, block matrices are formed for sub matrices of $\bar{y}_1^{IIi}$ and $\bar{y}_2^{IIi}$ according to

$$
\begin{aligned}
\bar{\bar{y}}^{II}_{k,11} &= diag\left\{\bar{y}^{II_i}_{k,11}\right\} \\
\bar{\bar{y}}^{II}_{k,22} &= diag\left\{\bar{y}^{II_i}_{k,22}\right\} \\
\bar{\bar{y}}^{II}_{k,12} &= quasidiag\left\{\bar{y}^{II_i}_{k,12}\right\} \\
\bar{\bar{y}}^{II}_{k,21} &= quasidiag\left\{\bar{y}^{II_i}_{k,21}\right\}
\end{aligned}
\tag{3.26}
$$

with $k = 1$ and $k = 2$, and $i = 1,2,\ldots$. These matrices are now combined to one block matrix

$$
\bar{\bar{y}}^{II}_{k} = \begin{bmatrix} \bar{\bar{y}}^{II}_{k,11} & \bar{\bar{y}}^{II}_{k,12} \\ \bar{\bar{y}}^{II}_{k,21} & \bar{\bar{y}}^{II}_{k,22} \end{bmatrix} \qquad k = 1,2 \tag{3.27}
$$

A corresponding transformation of the vectors of each slot region can be constructed according to

$$
\bar{T}_{NN} = diag\left\{T^{i}_{NN}\right\} \tag{3.28}
$$

$$
\bar{T}_{DD} = diag\left\{T^{i}_{DD}\right\} \tag{3.29}
$$

and by grouping these transformation matrices $\bar{T}_{NN}$ and $\bar{T}_{DD}$ to one block matrix, then the following transformation matrix corresponding to the field dimension according to that of eq. (3.16) and (3.21) is given by

$$
\bar{\bar{T}}_{II} = \begin{bmatrix} \bar{T}_{NN} & \\ & \bar{T}_{DD} \end{bmatrix} \tag{3.30}
$$

Now the system (3.24) is applied to all the slot regions of interfaces A and B and then putting together the obtained systems in such a way that the arrangement of the field vector is in the same order as in eq. (3.16). The collected sytem for the intermediate regions can now be established by

$$
\begin{bmatrix} H^{II}_{A} \\ H^{II}_{B} \end{bmatrix} = \begin{bmatrix} \bar{\bar{T}}_{II} & \\ & \bar{\bar{T}}_{II} \end{bmatrix} \begin{bmatrix} \bar{\bar{y}}^{II}_{1} & \bar{\bar{y}}^{II}_{2} \\ \bar{\bar{y}}^{II}_{2} & \bar{\bar{y}}^{II}_{1} \end{bmatrix} \begin{bmatrix} \bar{\bar{T}}^{t}_{II} & \\ & \bar{\bar{T}}^{t}_{II} \end{bmatrix} \begin{bmatrix} E^{II}_{A} \\ -E^{II}_{B} \end{bmatrix} \tag{3.31}
$$

where

$$H_{A,B}^{II} = \left[\left(H_{A,B}^{II1} \right)^t \quad \left(H_{A,B}^{II2} \right)^t \quad \ldots \right]^t$$
$$E_{A,B}^{II} = \left[\left(E_{A,B}^{II1} \right)^t \quad \left(E_{A,B}^{II2} \right)^t \quad \ldots \right]^t \tag{3.32}$$

In the other hand, in order to match the field at the interfaces A and B, equations (3.18) and (3. 22) must be combined to a single system so that its components are put in the order as that of eq.(3.31). This combination can be satisfied by

$$\begin{bmatrix} H_A^{II} \\ H_B^{II} \end{bmatrix} = \begin{bmatrix} T_I^r & \\ & T_I^r \end{bmatrix} \begin{bmatrix} \bar{y}^I & \\ & \bar{y}^{III} \end{bmatrix} \begin{bmatrix} T_I^{rt} & \\ & T_I^{rt} \end{bmatrix} \begin{bmatrix} E_A^{II} \\ -E_B^{II} \end{bmatrix} \tag{3.33}$$

Finally, substituting the left hand side of eq. (3.31) with the right hand side of eq. (3.33) then the indirect eigenvalue system is achieved

$$\left(\begin{bmatrix} \bar{\bar{T}}_{II} & \\ & \bar{\bar{T}}_{II} \end{bmatrix} \begin{bmatrix} \bar{y}_1^{II} & \bar{y}_2^{II} \\ \bar{y}_2^{II} & \bar{y}_1^{II} \end{bmatrix} \begin{bmatrix} \bar{\bar{T}}_{II} & \\ & \bar{\bar{T}}_{II} \end{bmatrix}^t - \begin{bmatrix} T_I^r & \\ & T_I^r \end{bmatrix} \begin{bmatrix} \bar{y}^I & \\ & \bar{y}^{III} \end{bmatrix} \begin{bmatrix} T_I^r & \\ & T_I^r \end{bmatrix}^t \right) \begin{bmatrix} E_A^{II} \\ -E_B^{II} \end{bmatrix} = 0. \tag{3.34}$$

or it can be abbreviated by

$$\left[Y(k_z, \omega) \right]_{red} \begin{bmatrix} E_A \\ -E_B \end{bmatrix} = 0 \tag{3.35}$$

This is the caracteristic equation for the analysed structure where the solution is obtained by solving the following determinental equation

$$\det \left(\left[Y(k_z, \omega) \right]_{red} \right) = 0 \tag{3.36}$$

From this system the propagation constant k_z can be determined in the same way as that done so far in chapter 2. Therefore the field vectors $E_{A,B}$ at the metallization interfaces are determined as eigenvectors by means of eq. (3.34). Consequently, all the other electric and magnetic field components can be derived, including the currents J_A and J_B which can be computed by using eqs. (3.19) and (3.23) respectively.

However, the established sytem of equation (3.34) is suitable for a large strip width, since the size of $[Y]_{red}$ is fixed by the number of lines that do not cross the metallic strip.

Note that the size of $[Y]_{red}$ becomes significant for situations where the strip width is smaller than the slot width. It is important in this situation to develop a system for the currents on the metallization instead of the electric fields as in eq. (3.34).
Indeed, from eqs. (3.6) and (3.8), similarly to eqs. (3.19) and (3.22),the electric fields E_A and E_B can be written as

$$E_A^{II} = T_I^r \left(y^I\right)^{-1} \left(T_I^{rc}\right)^t J_A + T_I^r \left(y^I\right)^{-1} T_I^{rt} H_A^{II} \tag{3.37}$$

$$E_B^{II} = T_I^r \left(y^{III}\right)^{-1} \left(T_I^{rc}\right)^t J_B - T_I^r \left(y^{III}\right)^{-1} T_I^{rt} H_B^{II} \tag{3.38}$$

Substituting equations (3.18) and (3.22) into eqs. (3.36) and (3.37) respectively, we get

$$E_A^{II} = z^I J_A \tag{3.39}$$

$$E_B^{II} = -z^{III} J_B \tag{3.40}$$

where

$$z^I = \left[I - T_I^r \left(y^I\right)^{-1} T_I^{rt} T_I^r y^I T_I^{rt} \right]^{-1} T_I^r \left(y^I\right)^{-1} \left(T_I^{rc}\right)^t$$

and

$$z^{III} = \left[I + T_I^r \left(y^{III}\right)^{-1} T_I^{rt} T_I^r y^{III} T_I^{rt} \right]^{-1} T_I^r \left(y^{III}\right)^{-1} \left(T_I^{rc}\right)^t$$

Replacing equations (3.38) and (3.39) into system (3.34) yields the following characteristic equations :

$$[\, Y \,] \begin{bmatrix} z^I & \\ & z^{III} \end{bmatrix} \begin{bmatrix} J_A \\ J_B \end{bmatrix} = 0 \tag{3.41}$$

The solution of this system is acheived by solving the following determinental equation

$$\det \left[\, Z(k_z, \omega) \,\right] = 0 \tag{3.42}$$

where

$$Z = [\, Y \,] \begin{bmatrix} z^I & \\ & z^{III} \end{bmatrix} \tag{3.43}$$

3.3 Non Uniform Discretization

For the analysis of multiconductor structure configuration for MICs and MMICs with finite metallization thickness, the discretization lines should coincide exactly with each conductor edge. The uniform discretization can not easily fit this last condition without dicreasing the discretization interval to an unpractical small value. This leads consequently to increase memory space and computing time as well. This difficulty can be solved by using the non uniform discretization scheme, which satisfies the condition of adjusting the discretization lines to each conductor edge. Moreover, it can be noted that the edge condition discussed so far does not apply here, since the analysis was only valid for zero strip metallization thickness. The edge condition must be violated in the current situation, but the convergence is always assured as argued in chapter 2. Whereas, the accuracy may be inproved as long as the discretization interval is decreased near singularities occuring at the edge of the metal conductor.

The former uniform discretization procedure that have been used in chapter 2, for the analysis of planar structures with zero metallization thickness, is still valid for the present analysis except that slight modifications are introduced. Thus, we only emphasize on particular points where changes must appear.
The discretization lines are sinusoidally spaced and the positions are determined according to

$$x_i = \frac{x_{na} + x_{nb}}{2} + \frac{x_{na} - x_{nb}}{2} \sin\left(\frac{2i - M_n}{2M_n}\pi\right); \quad i = 0,1,2,\ldots,M_n \qquad (3.44)$$

The smallest interval size $h_i = x_{M_n} - x_{M_{n-1}}$ on the conductor or on the slot, must be the same and determined for the smallest region. This is satisfied when M_n is given according to

$$M_n = INT\left(\frac{2\pi}{\pi - 2arc\,1 - 2\Delta\,(x_{nb} - x_{na})}\right) \qquad (3.45)$$

There is no correction on the interval sizes on the slot as shown in Fig. 3.5 in contrast to that used in chapter 2.

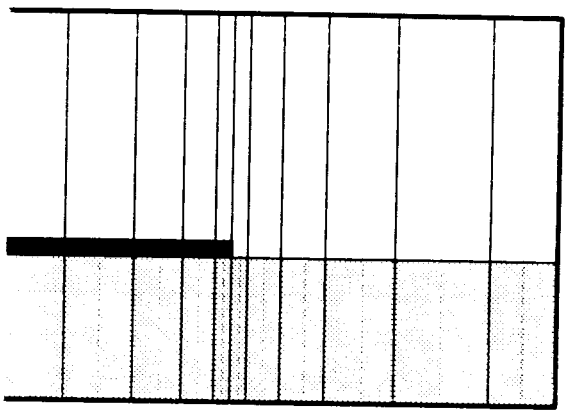

—— Electric field lines

Magnetic field lines

Fig. 3.5 Illustration of the discretization lines positions

3.4 Numerical Results and Discussions

To verify the performance of the described method, numerical data for selected microwave structures are presented. In the first step, the convergence behaviour when using both the uniform and nonuniform discretization, of the dielectric constant $\varepsilon_{eff} = \left(\frac{k_z}{k_o}\right)^2$ and the characterstic impedance Zc for a unilateral finline structure with finite metallization thickness t is studied. These convergence behaviours are represented as function of normalized discretization width $(a\ d)\ (n-1)\ \ h\ d$ (n is the total number of discretization lines), which are shown in Fig. 3.6 for d/λo=0.0102 and d/λo=0.0296. It can be seen that if the discretization width decreases to zero the calculated ε_{eff} and Zc converges always, and then an extrapolation to the exact value is possible. $\varepsilon_{eff\,o}$, Zco are the extrapolated value for $h \rightarrow 0$.

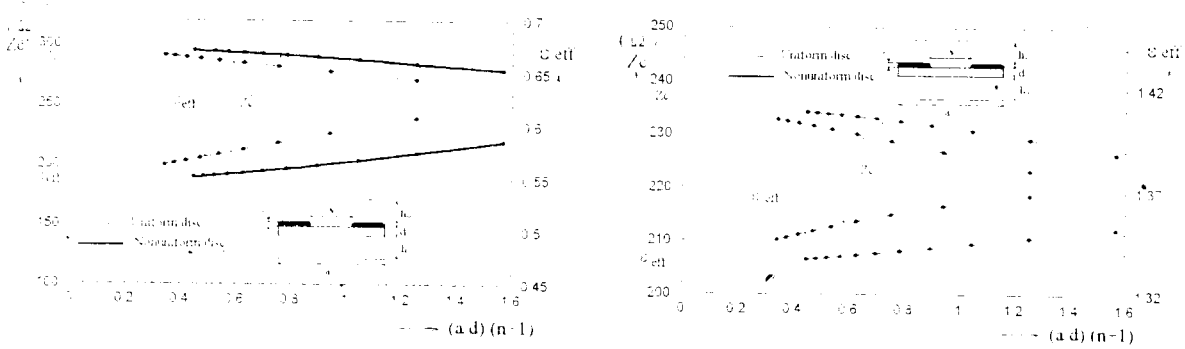

d/λo=0.0102 d/λo=0.0296

Fig. 3.6 Convergence behavior of ε_{eff} and Zc for unilateral finline structure using the uniform and nonuniform discretization as function of $(a\ d)\ (n-1)$, a/d=18.8, h1/d=18.8, h2/d=17.8, s/d=3.76, t/d=0.79, εr=3.8.

Although, as figure 3.6 shows, the nonuniform discretization assure in all cases better convergence than the uniform discretization for the same number of discretization lines. This minimizes both memory space and computing time.

Fig. 3.7 shows the dispersion of the dielectric constant ε_{eff} as function of d/λo for the microstrip line with finite and zero strip thickness. The comparison curves were determined with mode matching technique MMT [1,5].

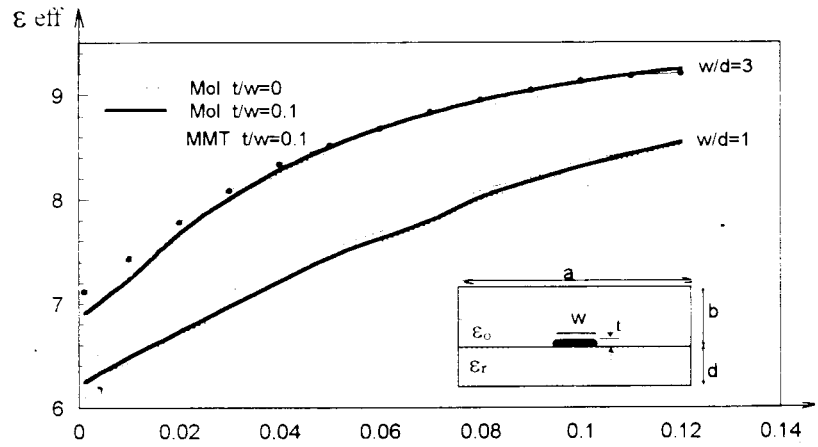

Fig. 3.7 Dispersion Characteristics ε_{eff} as function of d/λo for a microstrip line with finite metallization thickness a/d=16, b/d=8, εr=9.7.

It should be noted that dispersion curve for thick-strip cases is lower than that for thin case (t = 0). Moreover, the effect of strip metallization thickness is more significant at low frequencies and it becomes smaller at the higher frequencies. This is because at higher frequencies the electromagnetic fields are concentrated in the region of the substrate between the strip and the lower ground conductor. This minimizes the strip conductor effect at higher frequencies.

Figure 3.8 shows the effective dielectric constant ε_{eff} and the characteristic impedance Zc versus the normalized frequency d/λo for the unilateral finline with different slot widths and for metallization thicknesses t/d=0 and t/d=0.79. Our results are in excellent agreement, to within the accuracy that data can be read from the graph, with those obtained by Kitazawa and Mittra [3] utilizing the network analytical method and also with those obtained by Mansour and Macphie [9] employing the conservation of complex power technique.

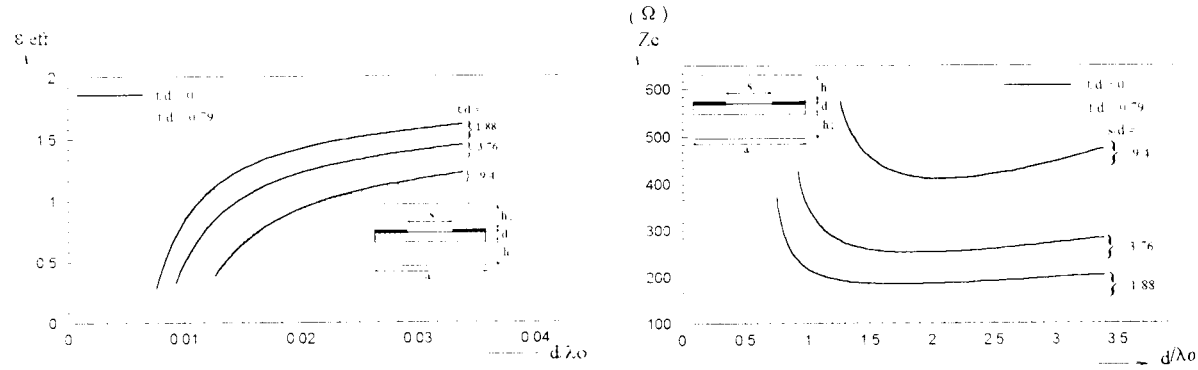

Fig. 3.8 Dispersion of the dielectric constant ε_{eff} and characteristic impedance Zc as function of d/λ_o a/d=18.8,h1/d=18.8, h2/d=17.8, εr=3.8.

The results indicate that the metallization thickness has a significant effect on the characteristic impedance [9]. Its effect, however, on the effective dielectric constant depends strongly on the slot width to the substrate thickness ratio s/d and is more pronounced for small s/d and for higher frequencies $k_o d$.

Figure 3.9 shows the dispersion of the effective permittivity ε_{eff} and the characteristic impedance Zc versus the normalized frequency d/λo for bilateral finline structure with different slot widths and for metallization thicknesses t/d=0 and t/d=0.96.

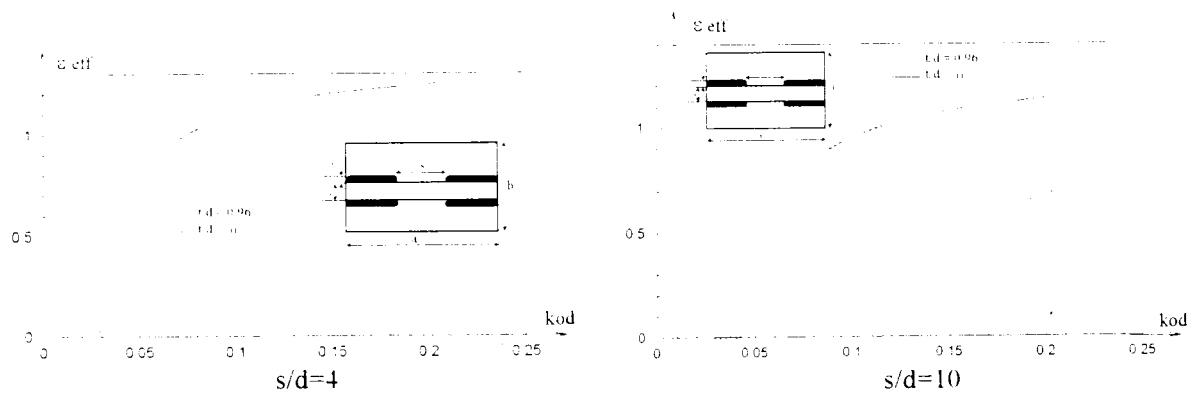

Fig. 3.9 The Effective dielectric constant as function of the normalized frequency d/λ_o for the bilateral finline structure a/d=28, b/d=56

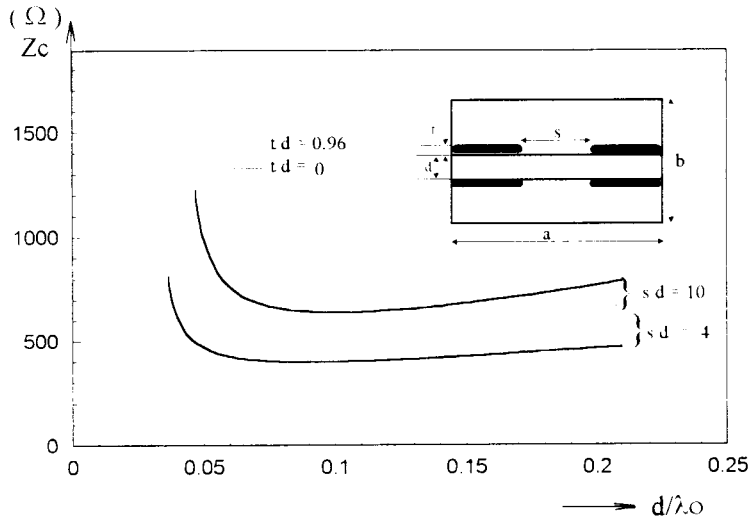

Fig. 3.10 Characteristic impedance Zc as function of d/λ_o for the bilateral finline strcucture a/d=28. b/d=56

For thin metallization (t/d=0) our results agree well with those published by Shmidt and Itoh [10] using the spectral domain technique for both ε_{eff} and Zc. In the other hand, for thick metallization thickness (t/d≠0) our data are compared to those published in [9]. where good agreement is observed for both the propagation constant and the characteristic impedance.

The results show that unilateral and bilateral finlines have identical behaviours for both ε_{eff} and Zc as far as the effect of the metallization thickness is concerned.

The effect of metallization thickness for the E-plane structures, e.g. the unilateral and bilateral finline structures, act in opposition to the effect of metallization thickness for the microstrip line. This can be explained by the fact that in the higher frequency range, the electromagnetic fields are concentrated near the line conductor edge (in the slot region) which increases the effect of the strip conductor thickness [6].

It is informative to plot the electric field Ex and Ez distribution for different metallization thicknesses. Fig. 3.9 shows the distribution of the electric field component for the bilateral finline structure for a particular choice of a physical dimension at a certain normalized frequency d/λo for two strip metallization thicknesses $t/d=10^{-2}$ and t/d=0.96.

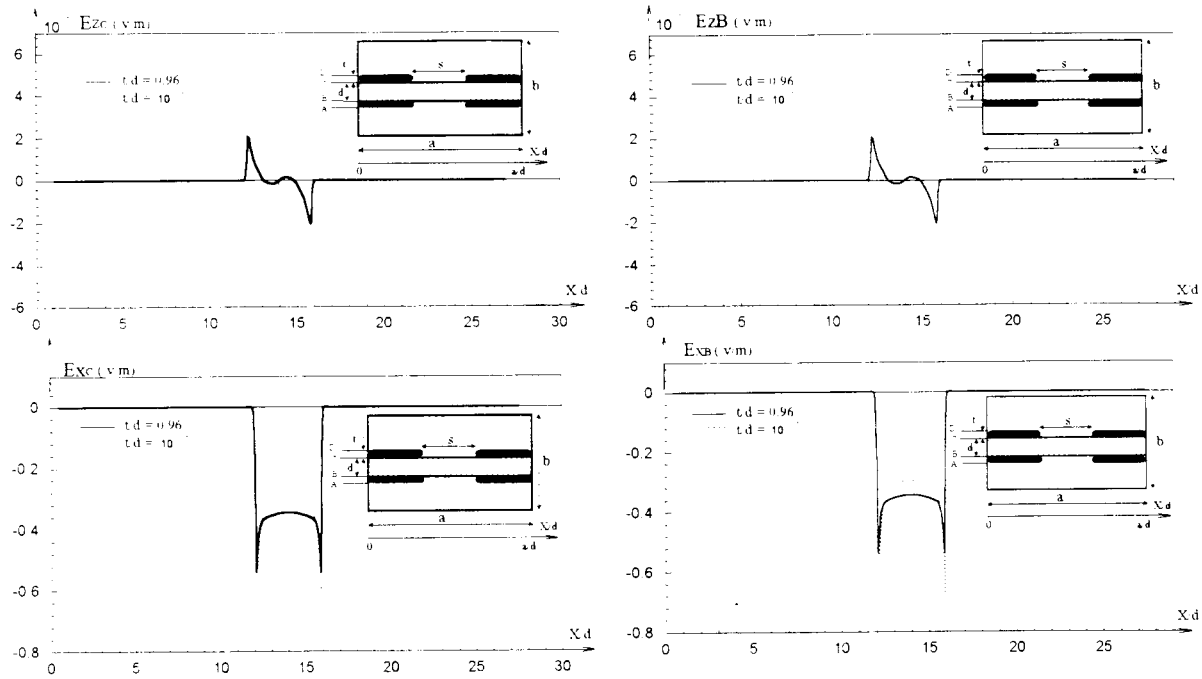

Fig. 3.9 Electric field Ez and Ex distribution at the interfaces B and C along the normalized structure width for the bilateral finline structure for a/d=28, b/d=56,s/d=4, at the normalized frequency $d/\lambda o=1/3.10^{-2}$.

3.5 Conclusion

The presented analysis within this chapter as well as in chapter 2 demonstrates that the MoL is a versatile and effecient technique to characterize MICs and MMICs structures, including certain technological parameters such as substrate anisotropy and metallization thickness. The numerical results obtained using this technique agree with other published data. This confirms the validity of the developed algorithm and its applicability to other untreated microwave structures.

It can be concluded from the numerical results that the effects of metallization thickness has to be taken into account if accurate and reliable analyses of MICs and MMICs structures are required.

References

[1] G. Kowalski and R. Pregla, " Dispersion characteristics of sheilded microstrips with finite thickness, with finite thickness, " *AEÜ*, Band25, pp.193-196, 1971.

[2] A. Beyer, " Analysis of the characteristics of an earthed Fin line," *IEEE Trans. Microwave Theory and Tech.*, Vol. MTT-29, pp.676-680, July 1981.

[3] T. Kitazawa and R. Mittra, " Analysis of finline with finite metallization thickness, " *IEEE Trans. Microwave Theory and Tech.*, Vol. MTT-32, pp. 1484-1487, Nov. 1984.

[4] R. Vahldieck, " Accurate hybrid-mode analysis of various finline configurations including multilayer dielectrics, finite metallization thickness, and substrate holding grooves, " *IEEE Trans. Microwave Theory and Tech.*, Vol. MTT-32, pp.1454-1460, Nov. 1984.

[5] R. Pregla and F. J. Scmükle, " The method of lines for the analysis of planar wave structures with finite metallization thickness, " (in German), *Kleinheubacher Berichte*, Vol.31, 431-438, 1988.

[6] T. Kitazawa, " Metallization thickness effect of striplines with anisotropic media :quasi-static and hybrid-mode analysis, " *IEEE Trans. Microwave Theory and Tech.*, Vol. MTT-37, pp.769-775, Apr. 1989.

[7] C. J. Railtdn and J. P. Mcgeehan, " An analysis of microstrip with rectangular and trapezoidal conductor cross sections, " *IEEE Trans. Microwave Theory and Tech.*, Vol. MTT-38, pp.1017-1022, August 1990.

[8] R. E. Collin, *Foundation for microwave engineering*, McGraw-Hill, pp. 34-37, 1966.

[9] R. R. Mansour and R. H. Macphie, " A unified hybrid-mode analysis for planar transmission lines with multilayer isotropic/anisotropic substrates, " *IEEE Trans. Microwave Theory and Tech.*, Vol. MTT-35, pp.1382-1391, Dec. 1987.

[10] L. P. Shmidt and T. Itoh, " Spectral domain analysis of dominant and higher order modes in fin-lines, " *IEEE Trans. Microwave Theory and Tech.*, Vol. MTT-28..pp.981-985, sept. 1980.

[11] J. Gerdes, K. H. Helf and R. Pregla, " Full-wave analysis of traveling-wave electrodes with finite thickness for electro-optic modulators by the method of lines, " *IEEE Trans. Microwave Theory and Tech.*, Vol. MTT-9, pp.461-467, April 1991.

Chapter 4

Analysis of Finline structures with Special Considerations

4.1 Introduction:

The ideal transmission line for millimeter wave integrated circuits is one which avoids miniaturization and yet offers the potential for low-cost production through the batch processing techniques. Many practical transmission lines are proposed to overcome the common transmission lines liability and associated problems at higher frequencies. This led Shneider to the proposal of suspended substrate microstrip lines [1] and Meier [2] to that of finlines.

With growing interest from the components designer, there has been increasing activity concerning the theoretical foundations of these structures. During the past several years, divers papers have been published by several authors [3,6-11] using various numerical techniques on the determination of the propagation characteristics of finline structures. However, most published analysis do not take into account the effect of finite metallization thickness and supporting grooves.

The metallization thickness has been taken into account by Beyer [8] and Vahldieck [9] using the mode-matching method and by Kitazawa [10] using the network analytical method and also by R. Mansour et al. employing the conservation of complex power technique [11]. Furthermore, the effects of side wall grooves, which have been employed in an actual realisation of finlines or generally used in E-plane circuits that support the substrate mechanically, has been considered as well in [9-11]. The effect of the metal strip thickness on the propagation characteristics of multiconductor planar transmission line structures has been taken into consideration by Saad and Schunemann [15], in which the approximation involved is only valid for structures with large slot width, and recently using accurate analysis [12]-[15].

In the present analysis, the hybrid-mode approach is used for evaluating the effective dielectric constant for the dominant and higher modes as well as the characteristic impedance for specially a unilateral finline structure. The analysis can also be applied to a wide variety of planar and quasi-planar transmission line structures with multiconductor and multilayer isotropic/anisotropic substrates.

Besides the versatility and the flexibility of this approach in treating complicated structures, it is numerically efficient and includes in addition, practical considerations such as metallization thickness and substrate mounting grooves. In addition, another important parameter disregarded by the overall published analysis has to be taken into consideration. Particularly for quasi-planar E-printed transmission line structures which do not support TEM-wave propagation, as that of the finline structures, have to be either isolated from the metallic housing at dc, or directly connected to the waveguide housing.

4.2 formulation of the Problem

To present the analysis, we consider a realistic finline structure of interest, which has been used by Meier [2] as shown in Fig. 4.1. For a better description of the analysis, the cross section of this practical structure is represented in a more unencumbered configuration as shown in Fig. 4.2. This integrated finline structure was developed to operate at millimeter wavelength where its cross section is suitable for mounting semiconductor devices.

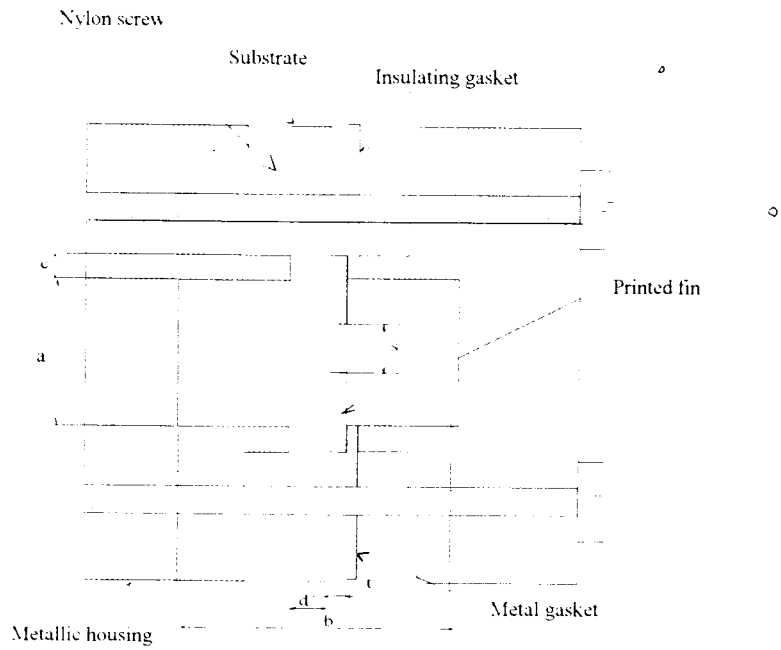

Fig. 4.1 Real unilateral finline structure and illustration of its fixation

In this structure (Fig. 4.1), the upper fin is insulated from the housing at dc by a dielectric gasket, where, according to Meier [2], it is grounded at RF by choosing the thickness of the broadwalls to be a quarter wavelength in the dielectric medium. The lower fin is grounded directly by a metal gasket to provide a dc return in solid-state applications. The typical realistic structure presented in Fig. 4.1 may have symmetric or unsymmetric fins.

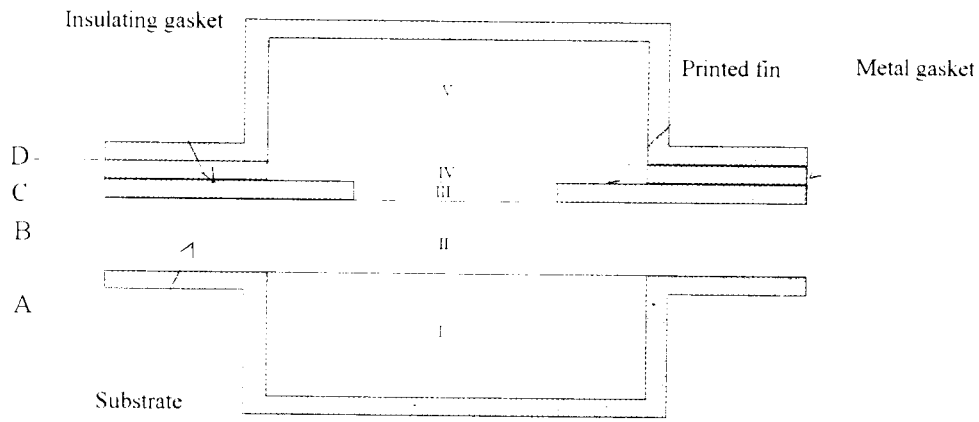

Fig 4.2 Unilateral finline structure with mounting grooves and using gasket insulator

For the analysis of this structures (Fig. 4.2), it is worth to note that the regions I, II, III and V are homogeneous isotropic or anisotropic dielectric layers, where in each region the wave equations have to be solved. The tangential field relationships needed for the matching are then directly exploited from previous appropriate established relations. However, the treatment of inhomogeneous layers, such as region IV, has not yet been achieved and therefore, is now recommended. This is the purpose of the following section.

4.3 Analysis of inhomogeneous dielectric layers

4.3-1 Discretization description of inhomogeneous dielectric

The homogeneous layer consists of an abrupt transition of two or more dielectric regions aligned in the same layer. In order to analyse microwave structures formed by either homogeneous and inhomogeneous dielectric layers, the problem of inhomogeneous layer should be solved first, and the resulted analysis must be mixed with that done so far for homogeneous layers. For this purpose we consider an inhomogeneous layer which consists of two dielectric abrupt transition as illustrated in Fig. 4.3 It can be noted that

the dielectric constant of each region is function of x. In this way, the problem of more than two transitions can be undertaken without difficulty.

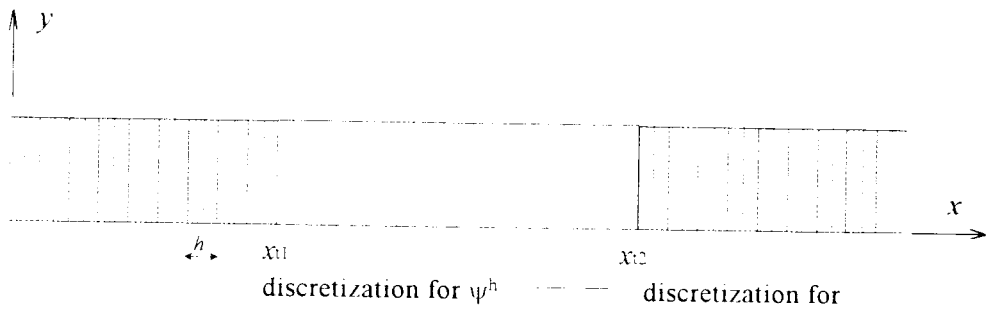

fig. 4.3 Uniform discretization of homogeneous dielectric layer

For reasons previously indicated in chapter 2, and following Collin [16-18] the wave field in this inhomogeneous layer can be determined from two vector potentials π_e and π_h , which have only one component in the dielectric of transition, namely the x-direction . The electromagnetic field is related to these potentials according to

$$E = \varepsilon_r(x)^{-1} \nabla \times \nabla \times \pi_e - jk_o \nabla \times \pi_h \qquad (4.1\text{-a}))$$

$$\eta_o H = jk_o \nabla \times \pi_e + \nabla \times \nabla \times \pi_h \qquad (4.1\text{-b})$$

with $k_o = \omega \sqrt{\varepsilon_o \mu_o}$ and $\eta_o = \sqrt{\mu_o / \varepsilon_o}$. For the vector potentials π_e and π_h , which are x-directed (unit $\hat{a}_x$) and propagating over a cross-section of waveguiding structure along the z-direction, may be written as

$$\pi_e(x,y) = \psi^e(x,y)\, e^{-jk_z z} k_o^{-2} \hat{a}_x \qquad (4.2\text{-a})$$

$$\pi_h(x,y) = \psi^h(x,y)\, e^{-jk_z z} k_o^{-2} \hat{a}_x \qquad (4.2\text{-b})$$

The potential functions ψ^e and ψ^h must fulfil the Helmotz equation (4.3-a) and the Sturm-Liouville differential equation (4.3-b) respectively :

$$\frac{\partial^2 \psi^h}{\partial x^2} + \frac{\partial^2 \psi^h}{\partial x^2} + \left(\varepsilon_r(x) k_o^2 - k_z^2 \right) \psi^h = 0 \qquad (4.3\text{-a})$$

$$\varepsilon_r(x) \frac{\partial}{\partial x} \left(\frac{1}{\varepsilon_r(x)} \frac{\partial \psi^e}{\partial x} \right) + \frac{\partial^2 \psi^e}{\partial x^2} + \left(\varepsilon_r(x) k_o^2 - k_z^2 \right) \psi^e = 0 \qquad (4.3\text{-b})$$

associated together with the following boundary conditions

Electric walls $\psi^h = 0 \quad ; \quad \frac{\partial \psi^e}{\partial x} = 0$ (4.4-a)

Magnetic walls $\psi^e = 0 \quad ; \quad \frac{\partial \psi^h}{\partial x} = 0$ (4.4-b)

Referring to the previous analysis, we note that the boundary conditions for ψ^h are the same as for e_z or the electric potential function in homogeneous layers, and those for ψ^e are the same for h_z or the magnetic potential function. This means that the quantities λ_e, λ_h, ky_e and ky_h associated to the potential functions ψ^e and ψ^h of this case, have dual properties to the quantities previously defined or named in the foregoing chapters.

In order to solve the PDE equations (4.3), both the potentials and dielectric constant must be discretized with respect to the x-variable. A two line systems are used for the full-wave analysis so that the lateral boundary conditions of the potentials are satisfied, as shown in Fig. 4.3 for the uniform discretization. Then two different discretized dielectric constants are then obtained for each potential function as.

for ψ^e : $\varepsilon_r(x) \longrightarrow diag(\varepsilon_r(x_e) = \varepsilon_e$ (4.5-a)

for ψ^h : $\varepsilon_r(x) \longrightarrow diag(\varepsilon_r(x_h) = \varepsilon_h$ (4.5-b)

In general the values of ε_h at the discretization lines x_t (transition) positioned at the interfaces where dielectric constant changes abruptly, we must take into account, for reason indicated in [17,18], special considerations $\varepsilon_r(x_t) = \left(\varepsilon_r(x_t^-) - \varepsilon_r(x_t^-)\right)/2$. Thus the first and the second differential operators with respect to x-direction can be approximated by finite difference approximation, and may be written as

$$h \frac{\partial \psi^h}{\partial x} \longrightarrow D\, \psi^h \qquad (4.6\text{-a})$$

$$h \frac{\partial \psi^e}{\partial x} \longrightarrow -D^t\, \psi^e \qquad (4.6\text{-b})$$

$$h^2 \frac{\partial^2 \psi^h}{\partial x^2} \longrightarrow -D^t D\, \psi^h = -P_h^{\varepsilon} \psi^h \qquad (4.6\text{-c})$$

$$h^2\,\varepsilon_r(x)\,\frac{\partial}{\partial x}\left(\frac{1}{\varepsilon_r(x)}\,\frac{\partial \psi^e}{\partial x}\right) \longrightarrow -\,\varepsilon_e\,D\,\varepsilon_h^{-1}\,D^t\,\psi^h = -P_e^{\varepsilon}\,\psi^e \qquad (4.6\text{-b})$$

where ψ^e and ψ^h are the column vectors of the discretized potentials, and D is the difference operator depending on the lateral boundaries. The two PDEs (4.3) can now be written in a unified form as follows :

$$\left\{-h^{-2}P^{\varepsilon}+k_o^2\varepsilon+\left(\frac{d^2}{dy^2}-k_z^2\right)\right\}\Psi=0 \qquad (4.7)$$

Where to the matrix quantities P^{ε}, ε and the vector potential function Ψ, have to be added either a subscript e or h.

In order to decouple the system (4.7), it is necessary to perform a suitable transformation as

$$\Psi = R\,\tilde{\Psi} \qquad (4.8)$$

Where $\tilde{\Psi}$ is the transformed column vector of the discretized potential functions, and S the transformation matrix that is obtained from the following eigenvalue problem

$$\left(h^{-2}k_o^{-2}P^{\varepsilon}-\varepsilon\right)R = R\,\lambda \qquad (4.9)$$

where λ is a diagonal matrix of distinct eigenvalues. To solve eq. (4.9), it is necessary to replace P^{ε} by its corresponding values P_e^{ε} and P_h^{ε}. Then, this leads then to λ_e, λ_h and S_e, S_h. The eigenvalue problem becomes

$$\left(h^{-2}\,k_o^{-2}\,\varepsilon_e\,D\,\varepsilon_h^{-1}\,D^t-\varepsilon_e\right)\mathrm{R}_e = R_e\,\lambda_e \qquad (4.10\text{-a})$$

$$\left(h^{-2}\,k_o^{-2}\,D^t\,D-\varepsilon_h\right)R_h = R_h\,\lambda_h \qquad (4.10\text{-b})$$

However, it is possible to split each of the transformations S_e and S_h into two independent transformations. Indeed, let

$$R_e = T_e\,S_e \qquad (4.11\text{-a})$$

$$R_h = T_h\,R_h \qquad (4.11\text{-b})$$

Then eq. (4.10) becomes

$$Q_e S_e = S_e \tilde{\lambda} \tag{4.12-a}$$

$$Q_h S_h = S_h \tilde{\lambda}_h \tag{4.12-b}$$

and

$$Q_e = \bar{\varepsilon}_e \bar{\delta} \varepsilon_h^{-1} \bar{\delta}^t - \bar{\varepsilon}_e \tag{4.13-a}$$

$$Q_h = \bar{\lambda}_h^2 - \bar{\varepsilon}_h \tag{4.13-b}$$

where $\bar{\delta} = (k_o h)^{-1} \delta$; $\delta = T_e^t D T_e$; $\bar{\lambda}_h^2 = \bar{\delta}^t \bar{\delta}$; $\bar{\varepsilon}_e = T_e^t \varepsilon_e T_e$; $\bar{\varepsilon}_h = T_h^t \varepsilon_h T_h$

The transformation matrices T_e and T_h are the matrices used for homogeneous layers and S_e and S_h are supplementary matrices to account for the inhomogeneous (dielectric slab) layers. Solving the eigenvalue problems of eq. (4.12), the diagonal matrices $\tilde{\lambda}_e$ and $\tilde{\lambda}_h$ of real and distinct eigenvalues, and the transformations matrices S_e and S_h are also derived numerically.

Then, the yielded system of uncoupled ODEs for $\tilde{\Psi}_e$ and $\tilde{\Psi}_h$ becomes,

$$\left(I \frac{1}{k_o^2} \frac{d^2}{dy^2} - k_z^2 \right) \tilde{\Psi}_{e,h} = 0 \tag{4.14}$$

where $ky_{e,h}(y) = diag\left(ky_{ie,h}/k_o\right)$, with $ky_{ie,h} = \left(\tilde{\lambda}_{ie,h} + \varepsilon_{re}\right) k_o^2$

The general solution of eq. (4.14) for the i-th component of $\tilde{\Psi}_{e,h}$ is given by

$$\tilde{\Psi}_i(y) = A_{ie,h} \cos\left(ky_{ie,h}\, y\right) + B_{ie,h}\, sin\left(ky_{ie,h}\, y\right) \tag{4.15}$$

The elimination of the constants $A_{ie,h}$ and $B_{ie,h}$ leads to the following solution for an arbitrary layer with thickness d, where A and B are its bottom and top interfaces where

$$\begin{bmatrix} \frac{d}{dy}\tilde{\Psi}_A \\ \frac{d}{dy}\tilde{\Psi}_B \end{bmatrix} = k_o k_{y'}^2 \begin{bmatrix} \gamma & \alpha \\ \alpha & \gamma \end{bmatrix} \begin{bmatrix} -\tilde{\Psi}_A \\ \tilde{\Psi}_B \end{bmatrix} \tag{4.16}$$

$$\alpha = diag\left(\frac{ky_i}{k_o} \sinh(ky_i\, d) \right)^{-1}$$

$$\gamma = diag\left(\frac{ky_i}{k_o} \tanh(ky_i\, d) \right)^{-1} \qquad (4.17)$$

$$k_{yy} = diag\left(\frac{k_{y_i}}{k_o} \right)$$

Note that in eq. (4.16), which is similar to eq. (2.15), the superscript γ has to be substituted by either e or h to denote the corresponding potential vector.

4.3-2 Calculations for the field components

The electromagnetic field components are calculated from the potentials ψ^e and ψ^h according to eqs. (4.1) and (4.2). After discretization and transformation of the fields T_e and T_h and approximating the derivatives with respect to x by differential operator , we get the transformed field components necessary for the matching on the interfaces

$$\overline{E}_x = -\overline{\varepsilon}_e^{-1} \underline{Q}_e S_e \tilde{\Psi}_e \qquad (4.18)$$

$$\eta_o \overline{H}_x = -\underline{Q}_h S_h \tilde{\Psi}_h \qquad (4.19)$$

$$j\overline{E}_z = -\frac{1}{k_o} S_h \frac{d}{dy} \tilde{\Psi}_h - \varepsilon_h^{-1}\, \tilde{\delta}^t S_e \tilde{\Psi}_e \qquad (4.20)$$

$$j\eta_o \overline{H}_z = -\frac{1}{k_o} S_e \frac{d}{dy} \tilde{\Psi}_e + \tilde{\delta} S_h \tilde{\Psi}_h \qquad (4.21)$$

with $\tilde{\delta} = \sqrt{\varepsilon_{re}}\, \overline{\delta}$

Whereas for the y- field component, necessary for the power computation, it is given by

$$\overline{E}_y = -\overline{\varepsilon}_h^{-1} \overline{\delta}^t S_e \left(\frac{1}{k_o} \frac{d}{dy} \tilde{\Psi}_e \right) - \sqrt{\varepsilon_{re}}\, S_h \tilde{\Psi}_h \qquad (4.22)$$

$$\eta_o \overline{H}_y = \overline{\delta} S_h \left(\frac{1}{k_o} \frac{d}{dy} \tilde{\Psi}_e \right) + \sqrt{\varepsilon_{re}}\, S_e \tilde{\Psi}_e \qquad (4.23)$$

The corresponding transformation of the field are performed by

$$\begin{aligned} E_y &= T_h \overline{E}_y \; ; \; E_z = T_h \overline{E}_z \; ; \; H_x = T_h \overline{H}_x \\ E_x &= T_e \overline{E}_x \; ; \; H_y = T_e \overline{H}_y \; ; \; H_z = T_e \overline{H}_z \end{aligned} \tag{4.24}$$

The set of equations (4.15)-(4.21) must be used for both interfaces A and B and when substituting $\frac{1}{k_o}\frac{d}{dy}\tilde{\Psi}$ by means of eq.(4.16), we get :

$$\begin{bmatrix} \overline{E}_{xA} \\ \overline{E}_{xB} \end{bmatrix} = -\overline{\varepsilon}_e^{-1} Q_e S_e \begin{bmatrix} \tilde{\Psi}_{eA} \\ \tilde{\Psi}_{eA} \end{bmatrix} = -\left(\overline{\delta}\,\overline{\varepsilon}_h^{-1}\,\overline{\delta}^t - I_e\right) S_e \begin{bmatrix} \tilde{\Psi}_{eA} \\ \tilde{\Psi}_{eA} \end{bmatrix} \tag{4.25}$$

$$\eta_o \begin{bmatrix} \overline{H}_{xA} \\ \overline{H}_{xB} \end{bmatrix} = -Q_h S_h \begin{bmatrix} \tilde{\Psi}_{hA} \\ \tilde{\Psi}_{hA} \end{bmatrix} = -\left(\overline{\lambda}_h - \overline{\varepsilon}_h\right) S_h \begin{bmatrix} \tilde{\Psi}_{hA} \\ \tilde{\Psi}_{hA} \end{bmatrix} \tag{4.26}$$

$$\begin{bmatrix} j\overline{E}_{zA} \\ j\overline{E}_{zB} \end{bmatrix} = -S_h\, ky_h^2 \begin{bmatrix} -\gamma_h & \alpha_h \\ -\alpha_h & \gamma_h \end{bmatrix} \begin{bmatrix} \tilde{\Psi}_{hA} \\ \tilde{\Psi}_{hA} \end{bmatrix} - \overline{\varepsilon}_h^{-1}\,\tilde{\delta}^t S_e \begin{bmatrix} \tilde{\Psi}_{eA} \\ \tilde{\Psi}_{eA} \end{bmatrix} \tag{4.27}$$

$$\eta_o \begin{bmatrix} j\overline{H}_{zA} \\ j\overline{H}_{zB} \end{bmatrix} = -S_e\, ky_e^2 \begin{bmatrix} -\gamma_e & \alpha_e \\ -\alpha_e & \gamma_e \end{bmatrix} \begin{bmatrix} \tilde{\Psi}_{eA} \\ \tilde{\Psi}_{eA} \end{bmatrix} + \tilde{\delta} S_h \begin{bmatrix} \tilde{\Psi}_{hA} \\ \tilde{\Psi}_{hA} \end{bmatrix} \tag{4.28}$$

For the field component in y-direction

$$\begin{bmatrix} \overline{E}_{yA} \\ \overline{E}_{yB} \end{bmatrix} = -\overline{\varepsilon}_h^{-1}\,\overline{\delta}^t S_e\, ky_e^2 \begin{bmatrix} -\gamma_e & \alpha_e \\ -\alpha_e & \gamma_e \end{bmatrix} \begin{bmatrix} \tilde{\Psi}_{eA} \\ \tilde{\Psi}_{eA} \end{bmatrix} + \sqrt{\varepsilon_{re}}\, S_h \begin{bmatrix} \tilde{\Psi}_{hA} \\ \tilde{\Psi}_{hA} \end{bmatrix} \tag{4.29}$$

$$\eta_o \begin{bmatrix} \overline{H}_{yA} \\ \overline{H}_{yB} \end{bmatrix} = -\overline{\delta} S_h\, ky_h^2 \begin{bmatrix} -\gamma_h & \alpha_h \\ -\alpha_h & \gamma_h \end{bmatrix} \begin{bmatrix} \tilde{\Psi}_{hA} \\ \tilde{\Psi}_{hA} \end{bmatrix} + \sqrt{\varepsilon_{re}}\, S_e \begin{bmatrix} \tilde{\Psi}_{eA} \\ \tilde{\Psi}_{eA} \end{bmatrix} \tag{4.30}$$

After discarding the potentials $\tilde{\Psi}_e$ and $\tilde{\Psi}_h$ by means of eqs. (4.25) and (4.26) respectively, we finally get a relation between the tangential components in interface A and interface B.

$$\begin{bmatrix} j\overline{E}_{zA} \\ j\overline{E}_{zB} \end{bmatrix} = -\eta_o\, S_h\, ky_h^2 \begin{bmatrix} -\gamma_h & \alpha_h \\ -\alpha_h & \gamma_h \end{bmatrix} S_h^{-1} Q_h^{-1} \begin{bmatrix} \overline{H}_{xA} \\ \overline{H}_{xB} \end{bmatrix} + \overline{\varepsilon}_h^{-1}\,\tilde{\delta}^t Q_e^{-1} \overline{\varepsilon}_e \begin{bmatrix} \overline{E}_{xA} \\ \overline{E}_{xB} \end{bmatrix} \tag{4.31}$$

$$\eta_o \begin{bmatrix} j\overline{H}_{zA} \\ j\overline{H}_{zB} \end{bmatrix} = -S_e\, ky_e^2 \begin{bmatrix} -\gamma_e & \alpha_e \\ -\alpha_e & \gamma_e \end{bmatrix} S_e^{-1} Q_e^{-1} \overline{\varepsilon}_e \begin{bmatrix} \overline{E}_{xA} \\ \overline{E}_{xB} \end{bmatrix} + \eta_o\, \tilde{\delta} Q_h^{-1} \begin{bmatrix} \overline{H}_{xA} \\ \overline{H}_{xB} \end{bmatrix} \tag{4.32}$$

For the field component in y-direction

$$\begin{bmatrix} \bar{E}_{yA} \\ \bar{E}_{yB} \end{bmatrix} = -\bar{\varepsilon}_h^{-1}\bar{\delta}^t S_e\, ky_e^{-2} \begin{bmatrix} -\gamma_e & \alpha_e \\ -\alpha_e & \gamma_e \end{bmatrix} S_e^{-1} Q_e^{-1}\bar{\varepsilon}_e \begin{bmatrix} \bar{E}_{xA} \\ \bar{E}_{xB} \end{bmatrix} + \eta_o \sqrt{\varepsilon_{re}}\, Q_h^{-1} \begin{bmatrix} \bar{H}_{xA} \\ \bar{H}_{xB} \end{bmatrix} \quad (4.33)$$

$$\eta_o \begin{bmatrix} \bar{H}_{yA} \\ \bar{H}_{yB} \end{bmatrix} = -\eta_o \bar{\delta}\, S_h\, ky_h^{-2} \begin{bmatrix} -\gamma_h & \alpha_h \\ -\alpha_h & \gamma_h \end{bmatrix} S_h^{-1} Q_h^{-1} \begin{bmatrix} \bar{H}_{xA} \\ \bar{H}_{xB} \end{bmatrix} - \sqrt{\varepsilon_{re}}\, Q_e^{-1}\bar{\varepsilon}_e \begin{bmatrix} \bar{E}_{xA} \\ \bar{E}_{xB} \end{bmatrix} \quad (4.34)$$

Using eq. (4.12) the two systems of equations (4.31) and (4.32) are converted to

$$\eta_o \begin{bmatrix} \bar{H}_{xA} \\ \bar{H}_{xB} \end{bmatrix} = B_h \tilde{\lambda}_h \begin{bmatrix} \gamma_h & \alpha_h \\ \alpha_h & \gamma_h \end{bmatrix} B_h^{-1} \begin{bmatrix} -j\bar{E}_{zA} \\ j\bar{E}_{zB} \end{bmatrix} + B_h \begin{bmatrix} \gamma_h & \alpha_h \\ \alpha_h & \gamma_h \end{bmatrix} \tilde{\lambda}_h B_h^{-1} \bar{\varepsilon}_h^{-1} \tilde{\delta}^t Q_e^{-1}\bar{\varepsilon}_e \begin{bmatrix} \bar{E}_{xA} \\ -\bar{E}_{xB} \end{bmatrix} \quad (4.35)$$

$$\eta_o \begin{bmatrix} -j\bar{H}_{xA} \\ -j\bar{H}_{xB} \end{bmatrix} = S_h \tilde{\lambda}_h \begin{bmatrix} \gamma_h & \alpha_h \\ \alpha_h & \gamma_h \end{bmatrix} S_h^{-1} \begin{bmatrix} -j\bar{E}_{zA} \\ j\bar{E}_{zB} \end{bmatrix} - \left(S_e\, ky_e^{-2} \begin{bmatrix} \gamma_e & \alpha_e \\ \alpha_e & \gamma_e \end{bmatrix} \tilde{\lambda}_e S_e^{-1} Q_e^{-1}\bar{\varepsilon}_e - \tilde{\delta} S_h \begin{bmatrix} \gamma_h & \alpha_h \\ \alpha_h & \gamma_h \end{bmatrix} S_h^{-1} \bar{\varepsilon}_h^{-1} \tilde{\delta}^t Q_e^{-1}\bar{\varepsilon}_e \right) \begin{bmatrix} \bar{E}_{xA} \\ -\bar{E}_{xB} \end{bmatrix} \quad (4.36)$$

Using $S^{-1}Q^{-1} = \lambda^{-1}S^{-1}$ derived from eq. (4.12), we finally obtain for the y-field components

$$\begin{bmatrix} \bar{E}_{yA} \\ \bar{E}_{yB} \end{bmatrix} = \bar{\varepsilon}_h^{-1}\bar{\delta}^t S_e\, ky_e^{-2} \begin{bmatrix} \gamma_e & \alpha_e \\ \alpha_e & \gamma_e \end{bmatrix} \tilde{\lambda}_e^{-1} S_e^{-1}\bar{\varepsilon}_e \begin{bmatrix} \bar{E}_{xA} \\ -\bar{E}_{xB} \end{bmatrix} - \eta_o \sqrt{\varepsilon_{re}}\, Q_h^{-1} \begin{bmatrix} \bar{H}_{xA} \\ \bar{H}_{xB} \end{bmatrix} \quad (4.37)$$

$$\eta_o \begin{bmatrix} \bar{H}_{yA} \\ \bar{H}_{yB} \end{bmatrix} = \eta_o \bar{\delta}\, S_h\, ky_h^{-2} \begin{bmatrix} \gamma_h & \alpha_h \\ \alpha_h & \gamma_h \end{bmatrix} \tilde{\lambda}_h^{-1} S_h^{-1} \begin{bmatrix} \bar{H}_{xA} \\ -\bar{H}_{xB} \end{bmatrix} - \sqrt{\varepsilon_{re}}\, Q_e^{-1}\bar{\varepsilon}_e \begin{bmatrix} \bar{E}_{xA} \\ \bar{E}_{xB} \end{bmatrix} \quad (4.38)$$

The equations (4.35) and (4.36) can be collated using the definition of the field vector as

$$H_{A,B} = \eta_o \begin{bmatrix} -jH_{zA,B} \\ H_{xA,B} \end{bmatrix} \quad ; \quad E_{A,B} = \begin{bmatrix} E_{xA,B} \\ -jE_{zA,B} \end{bmatrix}$$

and

$$\bar{y}_1 = \begin{bmatrix} \tilde{\gamma}_H \rho_e & \tilde{\delta}\tilde{\gamma}_h \\ \tilde{\gamma}_h \rho & \tilde{\gamma}_E \end{bmatrix} \quad ; \quad \bar{y}_2 = \begin{bmatrix} \tilde{\alpha}_H \rho_e & \tilde{\delta}\tilde{\alpha}_h \\ \tilde{\alpha}_h \rho & \tilde{\alpha}_E \end{bmatrix} \quad (4.3$$

in the form

$$\begin{bmatrix} \overline{H}_A \\ \overline{H}_B \end{bmatrix} = \begin{bmatrix} \overline{y}_1 & \overline{y}_2 \\ \overline{y}_2 & \overline{y}_1 \end{bmatrix} \begin{bmatrix} \overline{E}_A \\ -\overline{E}_B \end{bmatrix} \tag{4.40-a}$$

Where the following abbreviations must hold :

$$\begin{aligned}
&\tilde{\gamma}_h = S_h \gamma_h S_h^{-1} \quad ; && \tilde{\alpha}_h = S_h \alpha_h S_h^{-1} \\
&\tilde{\gamma}_E = S_h \tilde{\lambda}_h \gamma_h S_h^{-1} \quad ; && \tilde{\alpha}_E = S_h \tilde{\lambda}_h \alpha_h S_h^{-1} \\
&\tilde{\gamma}_e = S_e k y_e^2 \gamma_e S_e^{-1} \quad ; && \tilde{\alpha}_e = S_e k y_e^2 \alpha_e S_e^{-1} \\
&\rho_e = Q_e^{-1} \overline{\varepsilon}_e = \left(\overline{\delta} \overline{\varepsilon}_h^{-1} \overline{\delta}^t - I_e \right)^{-1} \quad ; && \rho_h = Q_h^{-1} \overline{\varepsilon}_h^{-1} = \overline{\lambda}_h \overline{\varepsilon}_h^{-1} - I_h \\
&\rho_e = \rho_e \tilde{\delta}^t \rho_e
\end{aligned} \tag{4.40-b}$$

with the help of eq. (4.40), which is formally arranged and can in this way, be easily adapted or used together with the representation given in chapters 2 and 3. As a remark, we note that the matrices $\overline{y}_1, \overline{y}_2$ are not diagonal matrices as compared to those previously determined in chapters 2 and 3.

4.4 Matching Equations

The wave equations are solved separately in each region of the considered structure, using appropriate potential functions or directly utilizing the electromagnetic field components, according to homogeneous/inhomogenuous regions as well as isotropic/anisotropic dielectric substrates. It is worth also to note that for all chosen related potential functions, the electromagnetic field component should coincide with each other; This means that each electric field component, say *Ex*, must be aligned with the same electric field component of its neighbourhood regions. Hence a special care has to be taken, if the boundary conditions change from region to another.

It has been shown in previous chapters that for a region of thickness *d*, a relation-ship between the transformed electromagnetic field components, that are necessary for the matching on the interfaces, can be established. That is for a region which has a top and bottom interfaces denoted respectively by (+) and (-), this relation can be written in a shorter way as

$$\begin{bmatrix} \overline{H}_+ \\ \overline{H}_- \end{bmatrix} = \begin{bmatrix} \overline{y}_1^R & \overline{y}_2^R \\ \overline{y}_2^R & \overline{y}_1^R \end{bmatrix} \begin{bmatrix} \overline{E}_+ \\ \overline{E}_- \end{bmatrix} \tag{4.4 }$$

$\bar{y}_k^R$ $\{k=1,2\}$ are summerized hereafter, from previous calculation, according to each region properties. First, for an isotropic homogeneous region, it is given by

$$\bar{y}_1^R = \begin{bmatrix} -\varepsilon_d \gamma_h & \gamma_h \tilde{\delta} \\ \tilde{\delta}' \gamma_h & \gamma_E \end{bmatrix}_R \quad ; \quad \bar{y}_2^R = \begin{bmatrix} -\varepsilon_d \alpha_h & \alpha_h \tilde{\delta} \\ \tilde{\delta}' \alpha_h & \alpha_E \end{bmatrix}_R \tag{4.42}$$

with the following abbreviations :

$$\tilde{\delta} = \sqrt{\varepsilon_{re}}\,\bar{\delta} \quad ; \quad \begin{Bmatrix} \alpha_E \\ \gamma_E \end{Bmatrix} = (\bar{\lambda}_e - \varepsilon_r) \begin{Bmatrix} \alpha_e \\ \gamma_e \end{Bmatrix} \tag{4.42-b}$$

In the other hand for the uniaxial anisotropic substrate with homogeneous region, this relation becomes

$$\bar{y}_1 = \begin{bmatrix} -\tilde{\gamma}_H & \tilde{\delta}\bar{\gamma}_e + \tilde{\gamma}_h \tilde{\delta} \\ \bar{\gamma}_e \tilde{\delta}' + \tilde{\delta}' \tilde{\gamma}_h & \tilde{\gamma}_E \end{bmatrix} \; ; \; \bar{y}_2 = \begin{bmatrix} -\tilde{\alpha}_H & \tilde{\delta}\bar{\alpha}_e + \bar{\alpha}_h \tilde{\delta} \\ \bar{\alpha}_e \tilde{\delta}' + \tilde{\delta}' \bar{\alpha}_h & \tilde{\alpha}_E \end{bmatrix} \tag{4.43-a}$$

with the following abbreviations

$$\begin{aligned}
\bar{\alpha}_e &= \varepsilon_- (\bar{\lambda}_e + \varepsilon_{re} I)^{-1} \alpha_e \; ; & \tilde{\alpha}_E &= \bar{\delta}' \bar{\alpha}_h \bar{\delta} - \varepsilon_{re} \bar{\alpha}_e \\
\bar{\gamma}_e &= \varepsilon_- (\bar{\lambda}_e + \varepsilon_{re} I)^{-1} \gamma_e \; ; & \tilde{\gamma}_E &= \bar{\delta}' \tilde{\gamma}_h \bar{\delta} - \varepsilon_{re} \bar{\gamma} \\
\bar{\alpha}_h &= k_{y_h}^2 \alpha_h (\bar{\lambda}_h + \varepsilon_{re} I)^{-1} \; ; & \tilde{\alpha}_H &= \bar{\delta} \bar{\alpha}_e \bar{\delta}' - \varepsilon_{re} \bar{\alpha}_h \\
\bar{\gamma}_h &= k_{y_h}^2 \gamma_h (\bar{\lambda}_h + \varepsilon_{re} I)^{-1} \; ; & \tilde{\gamma}_H &= \bar{\delta} \bar{\gamma}_e \bar{\delta}' - \varepsilon_{re} \tilde{\gamma}_h
\end{aligned} \tag{4.43-b}$$

For an isotropic inhomogeneous layer, it is given by

$$\bar{y}_1 = \begin{bmatrix} \tilde{\gamma}_H \rho_e & \tilde{\delta} \tilde{\gamma}_h \\ \tilde{\gamma}_h \rho & \tilde{\gamma}_E \end{bmatrix} \quad ; \quad \bar{y}_2 = \begin{bmatrix} \tilde{\alpha}_H \rho_e & \tilde{\delta} \tilde{\alpha}_h \\ \tilde{\alpha}_h \rho & \tilde{\alpha}_E \end{bmatrix} \tag{4.44}$$

Where the components of $\bar{y}_k^R$ $\{k=1,2\}$ are specified in eq. (4.40-b).

Generally the matrices λ, ky, α, γ, δ and T are inherent to each region and depend upon the number of discretization lines in each region and its associated boundaries.

The relation-ship between the transformed tangential field components at the interfaces A is given by

$$\begin{bmatrix} -j\overline{H}^{I}_{xA} \\ \overline{H}^{I}_{zA} \end{bmatrix} = -\begin{bmatrix} \overline{y}^{I}_{11} & \overline{y}^{I}_{12} \\ \overline{y}^{I}_{21} & \overline{y}^{I}_{22} \end{bmatrix}\begin{bmatrix} \overline{E}^{I}_{xA} \\ -j\overline{E}^{I}_{zA} \end{bmatrix} \tag{4.45-a}$$

or in shorter form as

$$\overline{H}^{I}_{A} = -\overline{y}^{I}_{1}\,\overline{E}^{I}_{A} \tag{4.45-b}$$

and for the region V at the interface D, the established relation can be written as

$$\begin{bmatrix} -j\overline{H}^{V}_{xD} \\ \overline{H}^{V}_{zD} \end{bmatrix} = \begin{bmatrix} \overline{y}^{V}_{11} & \overline{y}^{V}_{12} \\ \overline{y}^{V}_{21} & \overline{y}^{V}_{22} \end{bmatrix}\begin{bmatrix} \overline{E}^{V}_{xD} \\ -j\overline{E}^{V}_{zD} \end{bmatrix} \tag{4.46-a}$$

which can also be written in compacted form as

$$\overline{H}^{V}_{D} = \overline{y}^{V}_{1}\,\overline{E}^{V}_{D} \tag{4.46-b}$$

For the inhomogeneous region IV it has two interfaces C and D. The connection of the tangential electromagnetic field components at the interfaces C and D are related with the following reduced form

$$\begin{bmatrix} \overline{H}^{IV}_{C} \\ \overline{H}^{IV}_{D} \end{bmatrix} = \begin{bmatrix} \overline{y}^{IV}_{1} & \overline{y}^{IV}_{2} \\ \overline{y}^{IV}_{2} & \overline{y}^{IV}_{1} \end{bmatrix}\begin{bmatrix} \overline{E}^{IV}_{C} \\ -\overline{E}^{IV}_{D} \end{bmatrix} \tag{4.47}$$

Although the regions II and III have also two interfaces each, which are B-C and A-B. The relation-ship of the tangential field components for these two regions at their corresponding interfaces are given by

$$\begin{bmatrix} \overline{H}^{II}_{A} \\ \overline{H}^{II}_{B} \end{bmatrix} = \begin{bmatrix} \overline{y}^{II}_{1} & \overline{y}^{II}_{2} \\ \overline{y}^{II}_{2} & \overline{y}^{II}_{1} \end{bmatrix}\begin{bmatrix} \overline{E}^{II}_{A} \\ -\overline{E}^{II}_{B} \end{bmatrix} \tag{4.48}$$

$$\begin{bmatrix} \overline{H}^{III}_{B} \\ \overline{H}^{III}_{C} \end{bmatrix} = \begin{bmatrix} \overline{y}^{III}_{1} & \overline{y}^{III}_{2} \\ \overline{y}^{III}_{2} & \overline{y}^{III}_{1} \end{bmatrix}\begin{bmatrix} \overline{E}^{III}_{B} \\ -\overline{E}^{III}_{C} \end{bmatrix} \tag{4.49}$$

Field matching at the interfaces A, B, C and D has to be done in spatial domain. At the interfaces A and D, we have

$$\overline{E}^{II}_{xA} = \begin{bmatrix} 0 \\ E^{I}_{xA} \\ 0 \end{bmatrix}, \quad \overline{E}^{II}_{zA} = \begin{bmatrix} 0 \\ E^{I}_{zA} \\ 0 \end{bmatrix}, \quad \overline{H}^{II}_{xA} = \begin{bmatrix} H^{II}_{xAM1} \\ H^{I}_{xA} \\ H^{II}_{xAM2} \end{bmatrix}, \quad \overline{H}^{II}_{zA} = \begin{bmatrix} H^{II}_{zAM1} \\ H^{I}_{zA} \\ H^{II}_{zAM2} \end{bmatrix} \tag{4.50}$$

$$\overline{E}^{IV}_{xD} = \begin{bmatrix} 0 \\ E^{V}_{xD} \\ 0 \end{bmatrix}, \quad \overline{E}^{IV}_{zD} = \begin{bmatrix} 0 \\ E^{V}_{zD} \\ 0 \end{bmatrix}, \quad \overline{H}^{IV}_{xD} = \begin{bmatrix} H^{IV}_{xDM1} \\ H^{V}_{xD} \\ H^{IV}_{xAM2} \end{bmatrix}, \quad \overline{H}^{IV}_{zD} = \begin{bmatrix} H^{IV}_{zDM1} \\ H^{I}_{zD} \\ H^{II}_{zAM2} \end{bmatrix} \tag{4.51}$$

M1 and M2 are subscripts used in the fields components to describe the metallization component parts laying along the groove depth. However for the interfaces B and C, the component of interest are given by

$$\overline{E}^{II}_{xB} = \begin{bmatrix} 0 \\ E^{III}_{xB} \\ 0 \end{bmatrix}, \quad \overline{E}^{II}_{zB} = \begin{bmatrix} 0 \\ E^{III}_{zB} \\ 0 \end{bmatrix}, \quad \overline{H}^{II}_{xB} = \begin{bmatrix} J^{1}_{zB} \\ H^{III}_{xB} \\ J^{2}_{zB} \end{bmatrix}, \quad \overline{H}^{II}_{zB} = \begin{bmatrix} -J^{1}_{xB} \\ H^{III}_{zB} \\ -J^{2}_{xB} \end{bmatrix} \tag{4.52}$$

$$\overline{E}^{II}_{xC} = \begin{bmatrix} 0 \\ E^{III}_{xC} \\ 0 \end{bmatrix}, \quad \overline{E}^{II}_{zC} = \begin{bmatrix} 0 \\ E^{III}_{zC} \\ 0 \end{bmatrix}, \quad \overline{H}^{II}_{xC} = \begin{bmatrix} -J^{1}_{zC} \\ H^{III}_{xC} \\ -J^{2}_{zC} \end{bmatrix}, \quad \overline{H}^{II}_{zB} = \begin{bmatrix} J^{1}_{xC} \\ H^{III}_{zC} \\ -J^{2}_{xC} \end{bmatrix} \tag{4.53}$$

In the last two equations (4.52) and (4.53) the superscript in the current J mark the 1st and 2nd conductor at the metallization interface.

In order to represent the tangential electromagnetic field in spatial domain, equations (4.45)–(4.49) must be back transformed to the original domain. These inverse transformations must be performed in the same manner as described in chapters 2 and 3, and according to the field subvectors of interest represented in eqs. (4.50)–(4.53).

Collating the subvectors of the field components of the same kind and the same interface i according to

$$E_i = \begin{bmatrix} E_{xi} \\ -jE_{zi} \end{bmatrix} \quad ; \quad H_i = \eta_0 \begin{bmatrix} -jH_{zi} \\ H_{xi} \end{bmatrix} \tag{4.54}$$

The tangential electromagnetic field components of the layers I and III in the original domain, after inverse transformation, are given by

$$H^{I}_{A} = y^{I}_{1}\, E^{I}_{A} \tag{4.55}$$

and

$$H^{V}_{D} = -\, y^{V}_{1}\, E^{V}_{D} \tag{4.56}$$

However for layers II and IV, the subvector fields relation-ship that are necessary for the field matching are given in the spatial domain by

$$\begin{bmatrix} H_A^I \\ H_B^{III} \end{bmatrix} = \begin{bmatrix} M_{11}^{II} & M_{12}^{II} \\ M_{21}^{II} & M_{22}^{II} \end{bmatrix} \begin{bmatrix} E_A^I \\ -E_B^{III} \end{bmatrix} \tag{4.57}$$

for layer II, and for layer IV they are given by :

$$\begin{bmatrix} H_C^{III} \\ H_D^{V} \end{bmatrix} = \begin{bmatrix} M_{11}^{IV} & M_{12}^{IV} \\ M_{21}^{IV} & M_{22}^{IV} \end{bmatrix} \begin{bmatrix} E_C^{III} \\ -E_D^{V} \end{bmatrix} \tag{4.58}$$

In these equations (4.57) and (4.58) $M_{ij}^{II,IV}$ $\{ i,j = 1,2 \}$ are the reduced matrices obtained by inverse transformation, which are of appropriate size following the corresponding dimensions of the tangential field components of the field vectors E and H at each metallization interface.

From equations (4.54)¬(4.58) the following matching field equations are established :

$$y_1^I E_A^I = M_{11}^{II} E_A^I - M_{12}^{II} E_B^{III} \tag{4.59-a}$$

$$-y_1^V E_D^V = M_{21}^{IV} E_C^{III} - M_{22}^{IV} E_D^V \tag{4.59-b}$$

$$y_1^{III} E_B^{III} - y_2^{III} E_C^{III} = M_{21}^{II} E_A^I - M_{22}^{II} E_B^{III} \tag{4.59-c}$$

$$y_2^{III} E_B^{III} - y_1^{III} E_C^{III} = M_{11}^{IV} E_C^{III} - M_{12}^{IV} E_D^V \tag{4.59-d}$$

Form eq.(4.59-c), the field E_C can be expressed in terms of E_B^{III} and E_A^I as

$$E_C^{III} = -M_{CA} E_A^I + M_{CB} E_B^{III} \tag{4.60}$$

where

$$M_{CA} = \left(y_2^{III}\right)^{-1} M_{21}^{II}$$

$$M_{CB} = \left(y_2^{III}\right)^{-1} \left(y_1^{III} + M_{22}^{II}\right)$$

It is important to note that the inversion of y_2^{III} can be performed analytically.

Substituting now E_C^{III} of eq.(4.60) into eqs.(4.59-a)–(4.59-c), then the following eigenvalue system (ε_{eff} as eigenvalue) is achieved as

$$\begin{bmatrix} M_{11}^{II} - y_1^I & M_{12}^{II} & 0 \\ M_{21}^{IV} M_{CA} & M_{21}^{IV} M_{CB} & M_{22}^{IV} - y_1^V \\ (y_1^{III} + M_{11}^{IV}) M_{CA} & (y_1^{III} + M_{11}^{IV}) M_{CB} - y_2^{III} & M_{12}^{IV} \end{bmatrix} \begin{bmatrix} E_A^I \\ -E_B^{III} \\ E_D^V \end{bmatrix} = 0 \tag{4.61}$$

or in the form

$$\left[M_{red}(\varepsilon_{eff}) \right] \begin{bmatrix} E_A^I \\ -E_B^{III} \\ E_D^V \end{bmatrix} = 0 \tag{4.62}$$

This system (4.62) possesses a non trivial solution if its determinant vanishes

$$\det \left\{ \left[M_{red}(\varepsilon_{eff}) \right] \right\} = 0 \tag{4.63}$$

4.5 Numerical results and discussion

The influence of the substrate mounting groove depth wg on the normalised propagation constant and characteristic impedance is demonstrated for both unilateral and bilateral finline structure centred in the waveguide housing. Figure 4.4 shows the normalised propagation constant ε_{eff} of the dominant and First higher order odd mode for the groove depth $wg\ d = 0$ and $wg\ d \neq 0$ (Fig. 4.4-a and Fig. 4.4-b) and the metallization thickness $t\ d \approx 0.05$. Our results agree well with those published in [11] employing the conservation of complex power technique.

In these figures, it is observed that when the mounting groove depth is taken into account, the propagation constant is increased while the cut-off frequency is decreased. This changes are then due to the dielectric slab part considered in the mounting groove depth wg. It can be noted that, particularly when the first higher mode starts to propagate the dominant mode is considerably affected. Moreover, the cut-off frequency of the first higher order mode, which limits practically the most interesting monomode range, is largely reduced, unlike that of the dominant mode [11]. Then the monomode bandwidth is greatly narrowed when the mounting grooves is used.

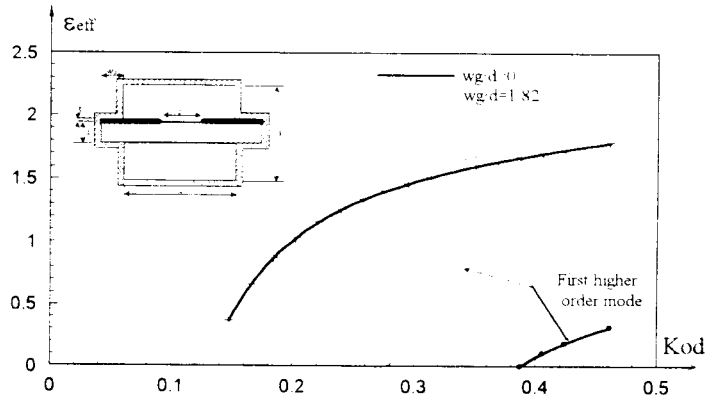

(a)

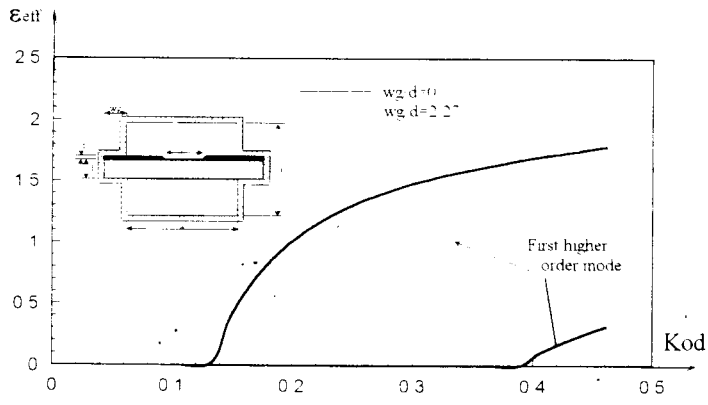

(b)

Fig. 4.4 Hybrid-mode and higher order mode versus normalised frequency in unilateral finline structure with a/d= 7.5, b/d=15 , s/d=2.72 , t/d=0.045 , (a) : wg/d=1.82 ; (b) :wg/d=2.27.

The effect of the mounting groove depth *wg* on the characteristic impedance Zc for the unilateral finline is illustrated in Fig. 4.5. The computed results confirm those published by Mansour and Macphie [11]. It can be observed that the deviations of the characteristic impedance from the ideal case (*wg* =0) are more pronounced when the first higher order mode starts to propagate.

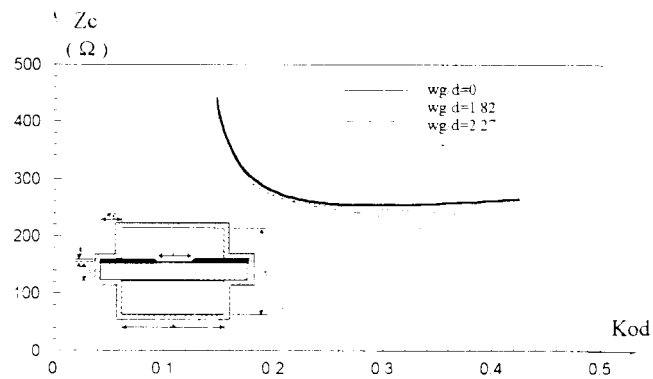

Fig. 4.5 Characteristic impedance versus normalised frequency in unilateral finline structure with a/d= 7.5,b/d=15 , s/d=2.72 , t/d=0.045 ; for different groove depths : wg/d=0; wg/d=1.82 ; wg/d=2.27.

Figures 4.6 shows the effect of the groove depth *wg* on the propagation constant ε_{eff} versus the normalised frequency d/λo for the bilateral finline structure with fixed finite metal thickness *t=0.04*.

It is observed that for the different groove depths *wg d=1.6* (Fig. 4.6-a), *wg d=4.8* (Fig. 4.6-b) and *wg d=8* (Fig. 4.6-c), the hybrid mode and the first higher mode are not considerably affected when the mounting groove depth is taken into account.

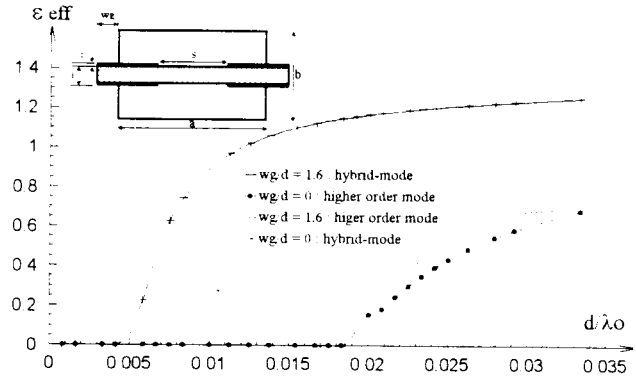

(a)

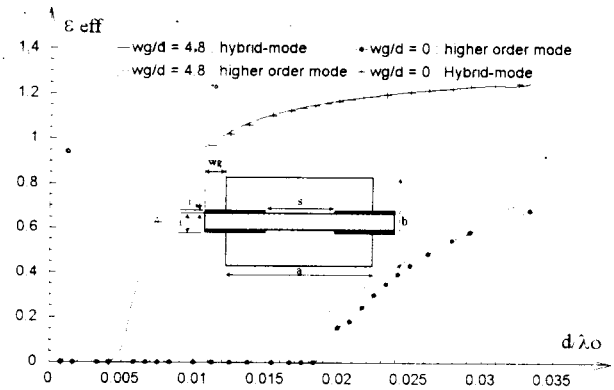

(b)

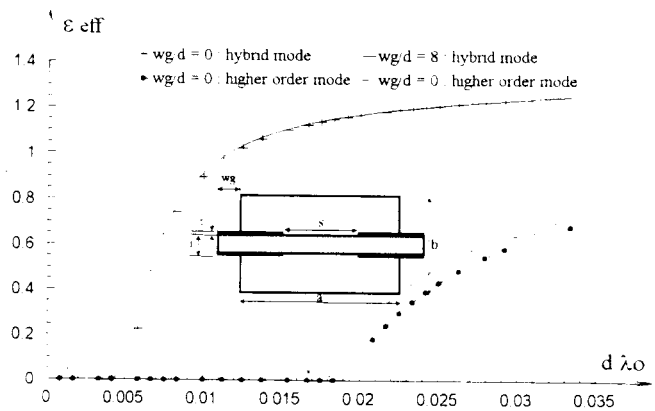

(c)

Fig. 4.6

The hybrid-mode and higher modes dispersion characteristics versus the normalized frequency or the bilateral finline structure for various groove depths with : a/d= 56.9, b/d=28.45, s/d=2.72, t/d=0.04, ε_r=3 ; for different groove depths : (a) - wg/d=1.6; (b), - wg/d=4.8 ;(c) - wg/d=8.

Also shown in Fig. 4.7 is the characteristic impedance versus the normalised frequency d/λo with various groove depths. It can be noted that only a small deviation between the results when the groove depth is considered and that when it is neglected.

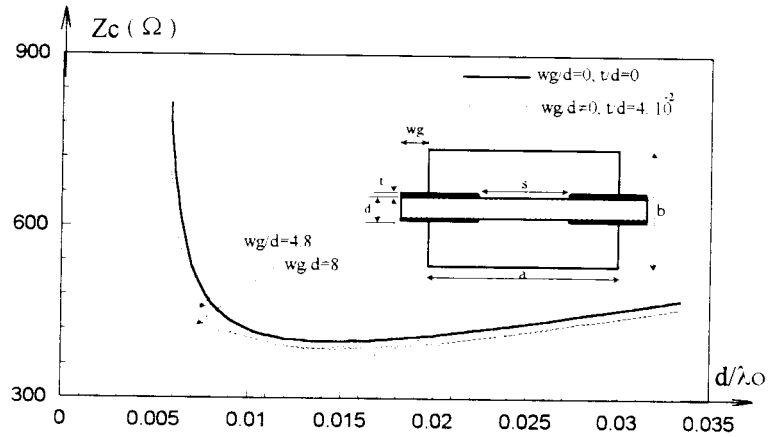

Fig. 4.7

Characteristic impedance versus the normalised frequency for the bilateral finline structure for various groove depths with : a/d= 56.9. b/d=28.45 . s/d=2.72 .t/d=0.04. ε_r=3 ; for different groove depths : wg/d=0; wg/d=4.8 ; wg/d=8.

For practical applications when the unilateral finline structure is used along with active components, one or both fins are insulated by a gasket which allows a dc voltage to be developed across the fins.

The dispersion curves of the propagation constant for the so called " isolated finline " are presented in Fig. 4.8. It is shown in this Figure, the effect of various gasket heights *gh d* ($\varepsilon_r = 1$ is assumed for the gasket insulation dielectric layer) for different mounting groove depths *wg d* and fixed metallization thickness *t d*, on the frequency dependent dominant mode of isolated unilateral finline structure. It is also observed that, the dispersion characteristics ε_{eff} versus the normalised frequency *d λo* is greatly influenced when the insulation gasket is used. This influence becomes more important as the insulation gasket height increases. Moreover , the effective dielectric constant has no cut-off frequency when insulation gasket is used since the dominant mode propagating at low frequencies is Quasi-TEM.

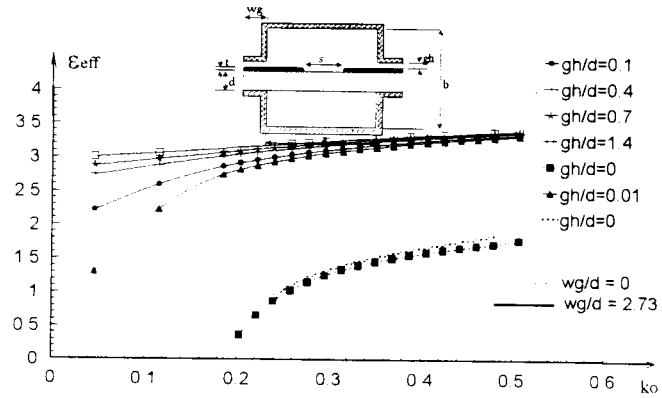

(a)

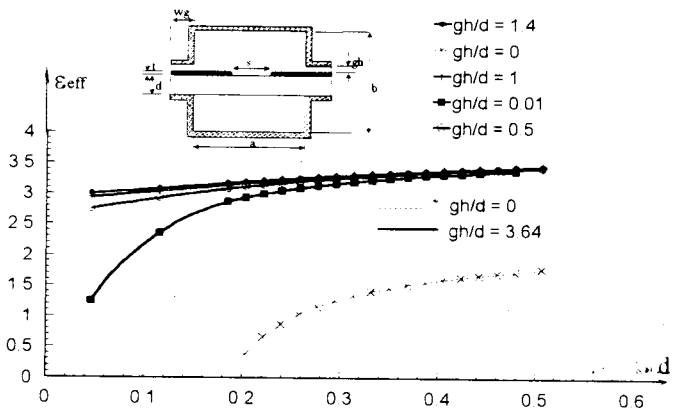

(b)

Fig. 4.8
The effect of gasket insulator on the dispersion
dielectric constant ε_{eff} for fixed metallization thickness
and various goove depths of unilateral finline structure
with a/d=6.82 , b/d=14.1 , s/d=1.82 t/d=0.023,
ε_r=3.75.(a) : wg/d=2.72, - (b) : wg/d=3.64

It is observed that the dispersion characteristics of the effective dielectric constant ε_{eff} versus the normalised frequency d/λo is greatly influenced when the dielectric gasket is used.

Figure 4.9 illustrates the effect of using the insulating gasket in a finline structure on the characteristic impedance. The impedance follows the same behaviour as that of the effective dielectric constant. It is characterized by low values at low frequencies because the dominant propagating mode is a quasi-TEM. Whereas for higher frequencies the impedance becomes higher and closer to that of the ideal structure. This can be explained by the fact that beyond a certain range of frequencies, the strip conductor becomes short-circuited to the metallic housing and, hence, behaves as an ideal finline structure.

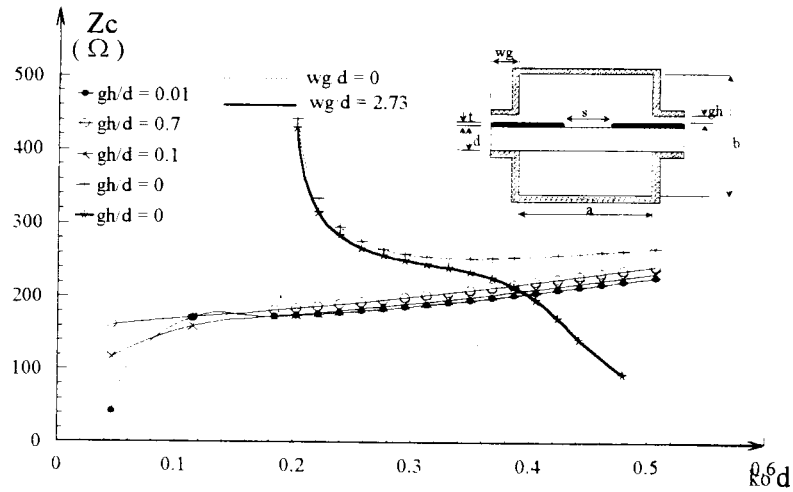

(a)

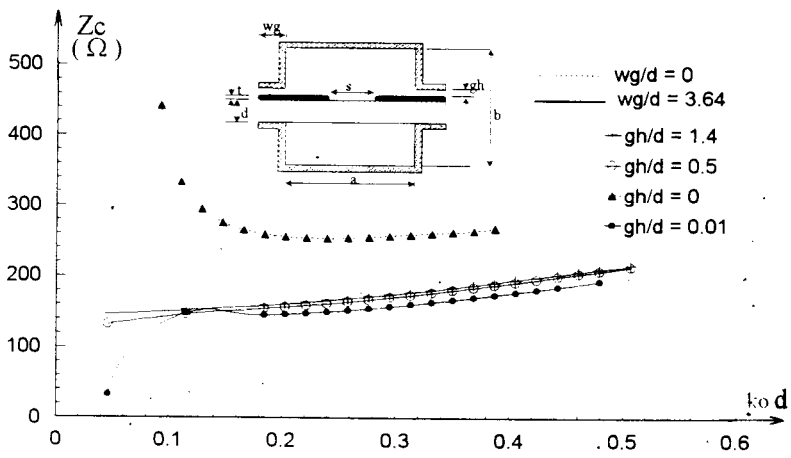

(b)

Fig. 4.9 The effect of gasket insulator on the characteristic impedance Zc with fixed metallization thickness and various goove depths of unilateral finline structure with a/d=6.82 , b/d=14.1 , s/d=1.82 , t/d=0.023, ε_r=3.75, - (a) : wg/d=2.72, - (b) : wg/d=3.64

4.6 Conclusion

The numerical results presented in this chapter which are compared with other published data provide a further confirmation of the validity of the used technique and show its simplicity for treating different planar structures. The characterization of finline structures with more complicated practical configuration are of particular interest, but the analysis can easily be extended to characterize other E-plane transmission structures of similar configurations.

The unilateral and bilateral finline structures including all important and practical parameters, such as metallization thickness and groove depth, have been investigated.

The effect of this realistic parameters have been discussed and show that, at higher frequencies, the grooves supporting the substrate cannot be neglected and, in addition, their influence is more significant than the effect of the finite metallization thickness.

Another unilateral finline structure, particularly the " isolated finline " with complicated configuration necessary in practical applications for active components, was also analysed. This real structure supports TEM mode and do not have a cut-off frequency as the ideal finline structure. The derived results confirm the practical results predicted by Meier [2].

References

[1] M. V. Schneider. "Microstrip lines for microwave integrated circuits." Bell syst. Tech. J., Vol. 48. pp. 1421-1444. 1969.

[2] P. J. Meier. " Integrated finline millimeter components." *IEEE trans. Microwave theory and Tech.*, Vol. MTT-22. pp. 1209-1216. Dec. 1974

[3] L. P. Schmidt and T. Itoh. " Spectral domain analysis of dominant and higher order modes in finlines." *IEEE trans. Microwave theory and Tech.*, Vol. MTT-28. pp. 981-985. Sept. 1980.

[4] L. P. Schmidt. T. Itoh and H. Hofmann. " Characteristics of unilateral finline structures with arbitrarily located slots." *IEEE trans. Microwave theory and Tech.*, Vol. MTT-29. pp. 352-355. 1981.

[5] A. K. Saad and K. Schunemann. " Efficient eigenmode analysis for planar transmission lines." *IEEE trans. Microwave theory and Tech.*, Vol. MTT-30. pp. 2125-2132. Dec. 1982.

[6] —. " A simple method for analysing fin-line structure." *IEEE trans. Microwave theory and Tech.*, Vol. MTT-26. pp. 1002-1007. Dec. 1978.

[7] B. M. Sheall and N. Alexopoulos. " The method of lines applied to a finline/strip configuration on an anisotropic substrate." *IEEE trans. Microwave theory and Tech.*, Vol. MTT-35. pp. 568-575. 1987.

[8] A. Bayer. " Analysis of the characteristics of an earthed finline." *IEEE trans. Microwave theory and Tech.*, Vol. MTT-29. pp. 676-680. July 1981.

[9] R. Vahldieck. " Accurate hybrid-mode analysis of various finline configurations including multilayered dielectric's. finite metallization thickness. and substrate holding grooves." *IEEE trans. Microwave theory and Tech.*, Vol. MTT-32. pp. 1454-1460. Nov. 1984.

[10] T. Kitazawa and R. Mittra. " Analysis of finline with finite metallization thickness." *IEEE trans. Microwave theory and Tech.*, Vol. MTT-32. pp. 1484-1487. Nov. 1984.

[11] R. R. Mansour and R. H. Macphie. " A unified hybrid-mode analysis for planar transmission line with multilayer isotropic/anisotropic substrates." *IEEE trans. Microwave theory and Tech.*, Vol. MTT-35. pp. 1382-1391. Dec. 1987.

[12] R. Pregla and F. J. Schmückle. " The method of lines for the analysis of planar waveguide structures with finite metallization thickness. " (in German). *kleinheubacher Ber.*, Vol.31. pp. 431-438. 1988.

[13] T. Kitazawa. " Metallization thickness effect of striplines with anisotropic media : quasi-static and hybrid-mode analysis." *IEEE trans. Microwave theory and Tech.*, Vol. MTT-35. pp. 769-775. April 1989.

[14] C. J. Railton and J. Mc Geehan. " An analysis of microstrip with rectangular and trapezoidal conductor cross-section." *IEEE trans. Microwave theory and Tech.*, Vol. MTT-38. pp. 1017-1022. Aug. 1990.

[15] J. Gerdes. K. Heiz Helf and R. Pregla. " Full-wave analysis of travelling-wave electrodes with finite thickness for electro-optic modulators by the method of lines. " *Journal of light Tech.*, Vol. 9. pp. 461-467. April 1991.

[16] R.E. Collin . Field Theory of Guided Waves. pp. 224-234. Mc Graw-Hill. New-York. 1960.

The effect of this realistic parameters have been discussed and show that, at higher frequencies, the grooves supporting the substrate cannot be neglected and, in addition, their influence is more significant than the effect of the finite metallization thickness. Another unilateral finline structure, particularly the " isolated finline " with complicated configuration necessary in practical applications for active components, was also analysed. This real structure supports TEM mode and do not have a cut-off frequency as the ideal finline structure. The derived results confirm the practical results predicted by Meier [2].

References

[1] M. V. Schneider. "Microstrip lines for microwave integrated circuits." Bell syst. Tech. J., Vol. 48. pp. 1421-1444. 1969.

[2] P. J. Meier, " Integrated finline millimeter components." *IEEE trans. Microwave theory and Tech.*, Vol. MTT-22, pp. 1209-1216, Dec. 1974

[3] L. P. Schmidt and T. Itoh, " Spectral domain analysis of dominant and higher order modes in finlines." *IEEE trans. Microwave theory and Tech.*, Vol. MTT-28, pp. 981-985, Sept. 1980.

[4] L. P. Schmidt, T. Itoh and H. Hofmann, " Characteristics of unilateral finline structures with arbitrarily located slots." *IEEE trans. Microwave theory and Tech.*, Vol. MTT-29, pp. 352-355, 1981.

[5] A. K. Saad and K. Schunemann, " Efficient eigenmode analysis for planar transmission lines." *IEEE trans. Microwave theory and Tech.*, Vol. MTT-30, pp. 2125-2132, Dec. 1982.

[6] —, " A simple method for analysing fin-line structure." *IEEE trans. Microwave theory and Tech.*, Vol. MTT-26, pp. 1002-1007, Dec. 1978.

[7] B. M. Sheall and N. Alexopoulos, " The method of lines applied to a finline/strip configuration on an anisotropic substrate." *IEEE trans. Microwave theory and Tech.*, Vol. MTT-35, pp. 568-575, 1987.

[8] A. Bayer, " Analysis of the characteristics of an earthed finline." *IEEE trans. Microwave theory and Tech.*, Vol. MTT-29, pp. 676-680, July 1981.

[9] R. Vahldieck, " Accurate hybrid-mode analysis of various finline configurations including multilayered dielectric's, finite metallization thickness, and substrate holding grooves." *IEEE trans. Microwave theory and Tech.*, Vol. MTT-32, pp. 1454-1460, Nov. 1984.

[10] T. Kitazawa and R. Mittra, " Analysis of finline with finite metallization thickness." *IEEE trans. Microwave theory and Tech.*, Vol. MTT-32, pp. 1484-1487, Nov. 1984.

[11] R. R. Mansour and R. H. Macphie, " A unified hybrid-mode analysis for planar transmission line with multilayer isotropic/anisotropic substrates." *IEEE trans. Microwave theory and Tech.*, Vol. MTT-35, pp. 1382-1391, Dec. 1987.

[12] R. Pregla and F. J. Schmückle, " The method of lines for the analysis of planar waveguide structures with finite metallization thickness. " (in German), *kleinheubacher Ber.*, Vol.31, pp 431-438, 1988.

[13] T. Kitazawa, " Metallization thickness effect of striplines with anisotropic media : quasi-static and hybrid-mode analysis." *IEEE trans. Microwave theory and Tech.*, Vol. MTT-35, pp. 769-775, April 1989.

[14] C. J. Railton and J. Mc Geehan, " An analysis of microstrip with rectangular and trapezoidal conductor cross-section." *IEEE trans. Microwave theory and Tech.*, Vol. MTT-38, pp. 1017-1022, Aug. 1990.

[15] J. Gerdes, K. Heiz Helf and R. Pregla, " Full-wave analysis of travelling-wave electrodes with finite thickness for electro-optic modulators by the method of lines. " *Journal of light Tech.*, Vol. 9, pp. 461-467, April 1991.

[16] R.E. Collin , Field Theory of Guided Waves, pp. 224-234, Mc Graw-Hill, New-York, 1960.

The effect of this realistic parameters have been discussed and show that, at higher frequencies, the grooves supporting the substrate cannot be neglected and, in addition, their influence is more significant than the effect of the finite metallization thickness.
Another unilateral finline structure, particularly the " isolated finline " with complicated configuration necessary in practical applications for active components, was also analysed. This real structure supports TEM mode and do not have a cut-off frequency as the ideal finline structure. The derived results confirm the practical results predicted by Meier [2].

References

[1] M. V. Schneider. "Microstrip lines for microwave integrated circuits." Bell syst. Tech. J., Vol. 48. pp. 1421-1444. 1969.

[2] P. J. Meier, " Integrated finline millimeter components." *IEEE trans. Microwave theory and Tech.*, Vol. MTT-22. pp. 1209-1216. Dec. 1974

[3] L. P. Schmidt and T. Itoh. " Spectral domain analysis of dominant and higher order modes in finlines." *IEEE trans. Microwave theory and Tech.*, Vol. MTT-28. pp. 981-985. Sept. 1980.

[4] L. P. Schmidt. T. Itoh and H. Hofmann. " Characteristics of unilateral finline structures with arbitrarily located slots." *IEEE trans. Microwave theory and Tech.*, Vol. MTT-29. pp. 352-355. 1981.

[5] A. K. Saad and K. Schunemann, " Efficient eigenmode analysis for planar transmission lines." *IEEE trans. Microwave theory and Tech.*, Vol. MTT-30. pp. 2125-2132. Dec. 1982.

[6] —. " A simple method for analysing fin-line structure." *IEEE trans. Microwave theory and Tech.*, Vol. MTT-26. pp. 1002-1007. Dec. 1978.

[7] B. M. Sheall and N. Alexopoulos. " The method of lines applied to a finline/strip configuration on an anisotropic substrate." *IEEE trans. Microwave theory and Tech.*, Vol. MTT-35. pp. 568-575. 1987.

[8] A. Bayer. " Analysis of the characteristics of an earthed finline." *IEEE trans. Microwave theory and Tech.*, Vol. MTT-29. pp. 676-680. July 1981.

[9] R. Vahldieck. " Accurate hybrid-mode analysis of various finline configurations including multilayered dielectric's. finite metallization thickness. and substrate holding grooves." *IEEE trans. Microwave theory and Tech.*, Vol. MTT-32. pp. 1454-1460. Nov. 1984.

[10] T. Kitazawa and R. Mittra, " Analysis of finline with finite metallization thickness." *IEEE trans. Microwave theory and Tech.*, Vol. MTT-32. pp. 1484-1487. Nov. 1984.

[11] R. R. Mansour and R. H. Macphie, " A unified hybrid-mode analysis for planar transmission line with multilayer isotropic/anisotropic substrates." *IEEE trans. Microwave theory and Tech.*, Vol. MTT-35. pp. 1382-1391. Dec. 1987.

[12] R. Pregla and F. J. Schmückle. " The method of lines for the analysis of planar waveguide structures with finite metallization thickness. " (in German). *kleinheubacher Ber.*, Vol.31. pp 431-438. 1988.

[13] T. Kitazawa. " Metallization thickness effect of striplines with anisotropic media : quasi-static and hybrid-mode analysis." *IEEE trans. Microwave theory and Tech.*, Vol. MTT-35. pp. 769-775. April 1989.

[14] C. J. Railton and J. Mc Geehan. " An analysis of microstrip with rectangular and trapezoidal conductor cross-section." *IEEE trans. Microwave theory and Tech.*, Vol. MTT-38. pp. 1017 1022. Aug. 1990.

[15] J. Gerdes. K. Heiz Helf and R. Pregla. " Full-wave analysis of travelling-wave electrodes with finite thickness for electro-optic modulators by the method of lines. " *Journal of light Tech.*, Vol. 9. pp. 461-467. April 1991.

[16] R.E. Collin . Field Theory of Guided Waves. pp. 224-234. Mc Graw-Hill. New-York. 1960.

The effect of this realistic parameters have been discussed and show that, at higher frequencies, the grooves supporting the substrate cannot be neglected and, in addition, their influence is more significant than the effect of the finite metallization thickness.
Another unilateral finline structure, particularly the " isolated finline " with complicated configuration necessary in practical applications for active components, was also analysed. This real structure supports TEM mode and do not have a cut-off frequency as the ideal finline structure. The derived results confirm the practical results predicted by Meier [2].

References

[1] M. V. Schneider. "Microstrip lines for microwave integrated circuits." Bell syst. Tech. J., Vol. 48. pp. 1421-1444. 1969.

[2] P. J. Meier. " Integrated finline millimeter components." *IEEE trans. Microwave theory and Tech.*, Vol. MTT-22. pp. 1209-1216. Dec. 1974

[3] L. P. Schmidt and T. Itoh. " Spectral domain analysis of dominant and higher order modes in finlines." *IEEE trans. Microwave theory and Tech.*, Vol. MTT-28. pp. 981-985. Sept. 1980.

[4] L. P. Schmidt. T. Itoh and H. Hofmann. " Characteristics of unilateral finline structures with arbitrarily located slots." *IEEE trans. Microwave theory and Tech.*, Vol. MTT-29. pp. 352-355. 1981.

[5] A. K. Saad and K. Schunemann. " Efficient eigenmode analysis for planar transmission lines." *IEEE trans. Microwave theory and Tech.*, Vol. MTT-30. pp. 2125-2132. Dec. 1982.

[6] —. " A simple method for analysing fin-line structure." *IEEE trans. Microwave theory and Tech.*, Vol. MTT-26. pp. 1002-1007. Dec. 1978.

[7] B. M. Sheall and N. Alexopoulos. " The method of lines applied to a finline/strip configuration on an anisotropic substrate." *IEEE trans. Microwave theory and Tech.*, Vol. MTT-35. pp. 568-575. 1987.

[8] A. Bayer. " Analysis of the characteristics of an earthed finline." *IEEE trans. Microwave theory and Tech.*, Vol. MTT-29. pp. 676-680. July 1981.

[9] R. Vahldieck. " Accurate hybrid-mode analysis of various finline configurations including multilayered dielectric's. finite metallization thickness. and substrate holding grooves." *IEEE trans. Microwave theory and Tech.*, Vol. MTT-32. pp. 1454-1460. Nov. 1984.

[10] T. Kitazawa and R. Mittra. " Analysis of finline with finite metallization thickness." *IEEE trans. Microwave theory and Tech.*, Vol. MTT-32. pp. 1484-1487. Nov. 1984.

[11] R. R. Mansour and R. H. Macphie. " A unified hybrid-mode analysis for planar transmission line with multilayer isotropic/anisotropic substrates." *IEEE trans. Microwave theory and Tech.*, Vol. MTT-35. pp. 1382-1391. Dec. 1987.

[12] R. Pregla and F. J. Schmückle. " The method of lines for the analysis of planar waveguide structures with finite metallization thickness. " (in German). *kleinheubacher Ber.*, Vol.31. pp. 431-438. 1988.

[13] T. Kitazawa. " Metallization thickness effect of striplines with anisotropic media : quasi-static and hybrid-mode analysis." *IEEE trans. Microwave theory and Tech.*, Vol. MTT-35. pp. 769-775. April 1989.

[14] C. J. Railton and J. Mc Geehan. " An analysis of microstrip with rectangular and trapezoidal conductor cross-section." *IEEE trans. Microwave theory and Tech.*, Vol. MTT-38. pp. 1017-1022. Aug. 1990.

[15] J. Gerdes. K. Heiz Helf and R. Pregla. " Full-wave analysis of travelling-wave electrodes with finite thickness for electro-optic modulators by the method of lines. " *Journal of light Tech.*, Vol. 9. pp. 461-467. April 1991.

[16] R.E. Collin . Field Theory of Guided Waves. pp. 224-234. Mc Graw-Hill. New-York. 1960.

[17] U. Rogge and R. Pregla, " The method of lines for the analysis of strip-loaded optical waveguides", to be published ; private communication
[18] R. Pregla and W. Pasher, " The method of lines " in Numerical Techniques for Microwave and Millimeter wave Passif Structures, T. Itoh, Ed. New-York : Wiley, 1989, pp. 381-446.

CONCLUSION

Throughout this investigation, the full-wave analysis of planar and quasi-planar MICs and MMICs has been used to achieve an accurate characterization dictated by the actual trend of complex configurations and miniaturization of microwave circuits, leading to a first time design success with optimized cost and reduced size. The hybrid-mode analysis covers a wide class of waveguiding structures, ranging from the habitual transmission line structures to the more intricate ones, such as the multilayer multi-metallization waveguiding systems, including some realistic geometrical and physical circuit parameters.

The Method of Lines, is the mathematical tool used to solve the associated value problems for modelling the dispersive properties of the aforementioned structures. This technique has proved to be very efficient for the analysis of distributed circuit elements in a rectangular waveguide. The MoL has distinct properties with respect to some other techniques. Among them, is that the solution is obtained without requiring the choice of arbitrary functions, the mathematical problem can be easily formulated and the resulting computer algorithm can be adapted on a personal computer, since only a relatively small memory space is required.

In the first part of this dissertation, a generalized full-wave approach using the MoL has been established for the frequency dependent characteirization of multilayer multiconductor waveguiding structures based on isotropic and/or anisotropic substrates. The resulted algorithm uses the uniform or non uniform discretization approach where both of them converge always to the right solution. In this way, the exact solution can be attained easily by extrapolation. In addition, it has been found that the non uniform discretization procedure is advantageous over the uniform approach, since it reduces the memory space and the computing time as well.

Divers transmission line structures have been analysed using this technique, and good agreement is obtained between our results and those published in literature. This shows the reliability of our implemented numerical algorithm and, hence its applicability to the full range of other planar circuit structures. It has been also shown, from the various studied planar structures, that when anisotropy is neglected in the computation of the dispersion characteristics, an error is incurred which increases for higher frequencies and/or for larger metallic strip width .

Besides the determination of frequency dependent characteristics for different planar microwave structures, this technique allows the determination of relative strip-currents (Jx and Jz) slot-fields (Ex, Ey, Ez, Hx, Hy, Hz) distribution at the metallic interface. For a particular choice of the physical dimensions of the transmission line structure, these distributions depends upon the frequency and the mode number. Moreover, the distribution of the electromagnetic field components over the entire cross-section of the waveguiding structure may also be represented in three-dimensional plots.

In the second part of the present work, the MoL is used to treat planar circuit structures with finite metallization thickness in order to improve the characterization of MIC and MMIC structures of reduced size and operating at higher frequencies. The numerical results obtained for some structures using this technique agree with other given published data. This confirms also the validity of the implemented computer algorithm and its ability to analyse other planar structures not yet treated. The numerical results have shown that the effect of metallization thickness has to be considered if accurate and reliable dispersion characteristics of MIC and MMIC structures are required.

In the last part, the E-plane quasi-planar transmission line structures have been analysed with special consideration claimed for practical design purposes. Indeed, in addition to the finite metallization thickness and the substrate anisotropy, the groove depth and the insulating dielectric gasket are accounted for in computating of the dispersion characteristics of the structure under consideration. The effect of the groove depth is more pronounced for the unilateral finline than for bilateral finline structure. In addition, it has been shown that when insulating gasket is introduced with the holding groove depth, the wave mode propagation in the structure becomes quasi-TEM. The derived results show also that the structure do not possess a cut-off frequency as the ideal structure. The obtained results confirms the practical predictions stated by Meier.

Because of the successful numerical results obtained with the developed algorithms using the presented efficient technique, the implemented programs can be used to elaborate a 2D field theoritical microwave simulator tool involved in current Computer Aided design packages of modern MICs and MMICs design.

APPENDIX 1

	D	λ	T
D-N	$\begin{bmatrix} 1 & & & \\ -1 & \ddots & & \\ & \ddots & \ddots & \\ & & -1 & 1 \end{bmatrix}$	$\lambda_k = 4\sin^2\left(\frac{k\pi}{2N+2}\right)$ $k = 0,1,2,\ldots,N$	$T_{ij} = \sqrt{\frac{2}{N+\frac{1}{2}}}\sin\frac{i(j-\frac{1}{2})\pi}{N+\frac{1}{2}}$ $i,j = 1,2,\ldots,N$
N-D	$\begin{bmatrix} 1 & -1 & & \\ & \ddots & \ddots & \\ & & \ddots & -1 \\ & & & 1 \end{bmatrix}$	$\lambda_k = 4\sin^2\left(\frac{k-\frac{1}{2}}{2N+1}\pi\right)$ $k = 1,2,\ldots,N$	$T_{ij} = \sqrt{\frac{2}{N+\frac{1}{2}}}\sin\frac{(i-\frac{1}{2})(j-\frac{1}{2})\pi}{N+\frac{1}{2}}$ $i,j = 1,2,\ldots,N$
D-D	$\begin{bmatrix} 1 & & & \\ -1 & \ddots & & \\ & \ddots & 1 & \\ & & -1 & \end{bmatrix}$	$\lambda_k = 4\sin^2\left(\frac{k\pi}{2N+2}\right)$ $k = 1,2,\ldots,N$	$T_{ij} = \sqrt{\frac{2}{N+1}}\sin\frac{ij\pi}{N+1}$ $i,j = 1,2,\ldots,N$
N-N	$\begin{bmatrix} 1 & -1 & & \\ & \ddots & \ddots & \\ & & \ddots & -1 \\ & & & 1 \end{bmatrix}$	$\lambda_k = 4\sin^2\left(\frac{k\pi}{2N+2}\right)$ $k = 0,1,2,\ldots,N$	$T_{i0} = \sqrt{\frac{1}{N+1}}$ $T_{ij} = \sqrt{\frac{2}{N+1}}\sin\frac{(i+\frac{1}{2})j\pi}{N+1}$ $i = 0,1,2,\ldots,N$ $j = 1,2,\ldots,N$

ANNEXE

Liste et composition du jury en vue de la soutenance de la these de magister en ***Ingenierie des Systèmes Electroniques.***
Par ***Mr OUADI Abderrahmane***

PRESIDENT/ Dr FARAH Aheene, Docteur d'Etat (Maitre de Conferences a L'E.N.P)

RAPPORTEUR/ Dr BOURDOUCEN Hadj, Docteur d'Etat (Maitre de Conferences a L'I.N.E.L.E.C)

EXAMINATEURS/ Dr DJEDDI Mohamed, Docteur d'Etat (Chargé de recherche a L'I.N.E.L.E.C)
Dr BENSEBTI, Docteur d'Etat (Charge de cours à l'U.BLIDA)
Mr B.BOUKNNA, Master (Chargé de cours à l'U.BLIDA), Invite